

**Modelling and simulation to improve the
mechanistic understanding of physiological
processes associated with the inhalation route of
drug administration**

Dissertation

to obtain the academic degree
Doctor rerum naturalium (Dr. rer. nat.)

submitted to the Department of Clinical Pharmacy,
Institute of Pharmacy,
Faculty of Mathematics, Informatics and Natural Sciences
University of Hamburg

by Anneke Himstedt

from Bremen

2024

This dissertation was conducted between February 2018 and October 2023 supervised by Prof. Dr. Sebastian G. Wicha at the Department of Clinical Pharmacy, Institute of Pharmacy, University of Hamburg.

1st Reviewer: Prof. Dr. Sebastian G. Wicha

2nd Reviewer: Prof. Dr. Georg Hempel

Thesis defense committee: Prof. Dr. Sebastian G. Wicha
Priv.-Doz. Dr. Claudia Langebrake
Prof. Dr. Wolfgang Maison

Date of thesis defense and approval: 06th May 2024

I. List of publications

Original articles included in the cumulative dissertation

A. Himstedt, C. Braun, S.G. Wicha, J.M. Borghardt, Towards a Quantitative Mechanistic Understanding of Localized Pulmonary Tissue Retention—A Combined In Vivo/In Silico Approach Based on Four Model Drugs, *Pharmaceutics*, 12 (2020) 408.

A. Himstedt, C. Braun, S.G. Wicha, J.M. Borghardt, Understanding the suitability of established antibiotics for oral inhalation from a pharmacokinetic perspective: an integrated model-based investigation based on rifampicin, ciprofloxacin and tigecycline in vivo data, *Journal of Antimicrobial Chemotherapy*, 77(11) (2022) 2922-2932.

A. Himstedt, J.M. Borghardt, S.G. Wicha, Inferring pulmonary exposure based on clinical PK data: accuracy and precision of model-based deconvolution methods. *Journal of pharmacokinetics and pharmacodynamics*, 49(2) (2022) 135-149.

Original articles - other

A. Dallmann, **A. Himstedt**, J. Solodenko, I. Ince, G. Hempel, T. Eissing, Integration of physiological changes during the postpartum period into a PBPK framework and prediction of amoxicillin disposition before and shortly after delivery. *Journal of pharmacokinetics and pharmacodynamics*, 47(4) (2020) 341-359.

Y. Cui, R. Lotz, H. Rapp, K. Klinder, **A. Himstedt**, A. Sauer, Muscle to Brain Partitioning as Measure of Transporter-Mediated Efflux at the Rat Blood–Brain Barrier and Its Implementation into Compound Optimization in Drug Discovery, *Pharmaceutics*, 11 (2019) 595.

Book contributions

A. Himstedt, P. Bäckman, J.M. Borghardt, Physiologically-based pharmacokinetic modeling after drug inhalation. In *Inhaled Medicines* (2021) 319-358. Academic Press.

Conference contributions (oral/posters)

A. Himstedt, J.M. Borghardt. Optimizing Drug Formulations for Oral Inhalation – Perspectives from integrative pharmacokinetic modeling. Formulation & Drug Delivery Congress, September 22, 2021.

(oral presentation)

A. Himstedt, S.G. Wicha, J.M. Borghardt, Model-Based Evaluation of Pulmonary PK Selectivity – Towards a Feasibility Assessment of Targeting the Lung by Oral Drug Inhalation. Respiratory Drug Delivery (Digital RDD 2020): Posters on the Podium. April 2020.

(oral presentation, invited talk, proceedings paper)

A. Himstedt, J.M. Borghardt, S.G. Wicha. Prediction of pulmonary exposure based on plasma pharmacokinetics: A comparison of different model-based approaches. Population Approach Group Europe Conference (PAGE 2019). Stockholm, Sweden. June 11-14, 2019.

(poster presentation)

A. Himstedt, C. Braun, J.M. Borghardt, S.G. Wicha. Using physiology-based pharmacokinetic modelling to investigate the distribution of drugs into different lung tissues in rats. German Pharmaceutical Society (DPhG 2018) Annual Meeting. Hamburg, Germany. October 3-5, 2018.

(poster presentation)

A. Dallmann, **A. Himstedt**, I. Ince, J. Solodenko, T. Eissing, G. Hempel. Extension of a pregnancy physiologically-based pharmacokinetic model for renally cleared drugs to the postpartum period. Population Approach Group Europe Conference (PAGE 2017). Budapest, Hungary. June 6-11, 2017.

(poster presentation, presenting author)

Presentations without abstract

A. Himstedt, J.M. Borghardt, S.G. Wicha. Modellierung der Pharmakokinetik von Arzneimitteln nach inhalativer Gabe. Tag der Pharmazie, Hamburg, Germany, June 20, 2018.

II. Contents

I.	List of publications	i
II.	Contents	iii
III.	List of abbreviations	v
	Zusammenfassung.....	vii
	Abstract.....	ix
1	Introduction.....	1
1.1	Oral inhalation – local delivery of drugs for pulmonary diseases.....	1
1.2	Pulmonary anatomy and physiology	1
1.3	Lung-specific PK processes	2
1.4	Applications of oral inhalation.....	3
1.5	Research and development process of orally inhaled drugs	4
1.6	Applications of pharmacometric approaches for oral inhalation	6
1.6.1	Modelling approaches for pulmonary distribution	7
2	Objectives	10
3	Cumulative part.....	12
3.1	Publication I: Developing a localized pulmonary tissue retention PBPK model.....	13
3.2	Publication II: Identifying favorable drug characteristics for potential oral inhalation drugs	35
3.3	Publication III: Evaluation of model-based approaches to infer pulmonary exposure	48
4	Discussion	65
4.1	Drug discovery and research	65
4.1.1	Published investigations of pulmonary distribution in drug discovery	66
4.1.2	Physicochemical optimization parameters for orally inhaled drugs	68
4.2	Preclinical development	69
4.3	Clinical development.....	70

4.3.1	Published investigations of pulmonary PK in humans	70
4.4	Learnings from PK models for oral inhalation.....	72
4.5	Challenges and outlook	73
5	Bibliography	75
6	Appendix.....	81
6.1	Hazardous material.....	81
6.2	Supplementary material publication I	82
6.3	Supplementary material publication II.....	95
6.4	Supplementary material publication III.....	104
7	Acknowledgements.....	117
8	Eidesstattliche Versicherung.....	119

III. List of abbreviations

AAFE	Average absolute fold error
AIC	Akaike information criterion
AUC	Area under the concentration-time curve
BALF	Bronchioalveolar lavage fluid
B_{\max}	Maximal bacterial concentration
C_{eff}	Concentration in the effect compartment
cfu	Colony forming units
CL	Clearance
CMT	Compartment
COPD	Chronic obstructive pulmonary disease
C_u	Unbound concentration
CV	Coefficient of variation
E	Effect
EC_{50}	Concentration needed to achieve half-maximal effect
Eff	Efflux ratio
ELF	Epithelial lining fluid
E_{\max}	Maximum attainable effect
F	Bioavailability
FOCE	First-order conditional estimation
FP	Fluticasone propionate
$F_{\text{slow/med/fast}}$	Fraction slow/intermediate/fast absorbed
f_u	Fraction unbound (plasma)
GMFE	Geometric mean fold error
i.t.	Intratracheal
i.v.	Intravenous
IND	Indomethacin
IPP	Individual PK parameters
$k_{a,\text{pul}}$	pulmonary absorption rate constant
k_{e0}	First-order equilibration rate constant
k_{growth}	Bacterial growth rate
k_{\max}	Maximum kill rate

K_p	Tissue partition coefficient
$k_{\text{slow/med/fast}}$	Slow/intermediate/fast (pulmonary) absorption rate constant
LABA	long-acting β_2 -agonist
LAMA	long-acting muscarinic receptor agonist
LIN	Linezolid
MAT	Mean absorption time
MCC	Mucociliary clearance
MRT	Mean residence time
NCA	Non-compartmental analysis
PAE	Post-antibiotic effect
P_{app}	Apparent permeability
PBPK	Physiologically-based pharmacokinetics
PD	Pharmacodynamics
PF	Proportionality factor
PK	Pharmacokinetics
PPB	Plasma protein binding
PPP	Population PK parameters
Q	Intercompartmental clearance
$Q_{\text{T/B/A}}$	Perfusion rate of the trachea/bronchi/alveolar region
SA	Surface area
SAL	Salmeterol
SSE	Stochastic simulation and estimation
$t_{1/2,\text{pul}}$	Pulmonary absorption half-life
V	Volume of distribution
$V_{\text{T/B/A}}$	Weight of the trachea/bronchi/alveolar region

Zusammenfassung

Orale Inhalation ist seit tausenden von Jahren Bestandteil der Behandlung von Krankheiten.^{1,2} Bis zum heutigen Tag ist Inhalation immer noch die relevanteste Administrationsroute für Lungenerkrankungen wie Asthma und die chronisch obstruktive Lungenerkrankung (COPD). Dennoch gibt es noch immer viel über die spezifischen Prozesse pulmonaler Administration und den Einfluss der Physiologie verschiedener Lungenbereiche auf die Pharmakokinetik (PK) von Arzneistoffen zu Lernen.

Obwohl die Lunge als einzelnes Organ gilt, gibt es große Unterschiede in der Physiologie zwischen den leitenden Atemwegen und dem Alveolarbereich in dem der Gasaustausch stattfindet. Pharmakometrie, und genauer Physiologie-basierte PK (PBPK) Modellierung, stellt einen wichtigen Ansatz zur quantitativen Beschreibung auch lokaler Gewebe-PK dar und ermöglicht die Abtrennung der relevanten Inhalations-assoziierten Prozesse auf physiologischer Basis. Das Ziel dieser Arbeit war es, ein verbessertes Verständnis der PK oraler Inhalativa zu ermöglichen. Der Fokus lag hier auf der Verteilung in Lungengewebe und der Beziehung zwischen lokaler pulmonaler PK und systemischen (Plasma-)Konzentrationen.

In Publikation I wurde ein semi-mechanistisches PK-Modell für vier Arzneistoffe nach intravenöser (i.v.) Gabe in Ratten entwickelt. Die zugrunde liegenden Daten wurden mit einer neuen Methode generiert, die die simultane Messung von Arzneistoffkonzentrationen in der Trachea, den oberen Bronchien, und dem Alveolarbereich im selben Tier zulässt. Das Modell war in der Lage, die lokalen Konzentrations-Zeit Profile in der Lunge basierend auf gemeinsamen Schätzwerten für Lungenblutfluss und Gewebegewichten für alle Substanzen zu beschreiben. Die einzigen Arzneistoff-spezifischen Parameter waren Gewebe-Plasma Partitionskoeffizienten (K_p) und die systemischen PK-Parameter. Diese Gewebe-spezifischen K_p Werte waren bis zu sechsfach höher im Alveolarbereich, verglichen mit der Trachea. Dies zeigt, dass sich das Verteilungsverhalten, abhängig von den physikochemischen Eigenschaften des Arzneistoffs, substantiell zwischen verschiedenen Lungenstrukturen unterscheiden kann.

Publikation II betraf die Eignung oraler Inhalation für etablierte Antibiotika. Hierfür wurde das existierende Modell um eine Unterscheidung zwischen Intra- und Extrazellulärem Raum, ein separates Kompartiment für die Epithelial-Flüssigkeit (ELF), und ein bakterielles Wachstumsmodell für pharmakodynamische (PD) Untersuchungen erweitert. Die Methode für die Erhebung von in vivo Daten wurde so verfeinert, dass sie zusätzlich die Messung von Konzentrationen in der ELF der Trachea und des Alveolarbereichs zuließ.

Eine Sensitivitätsanalyse wurde mit einer humanisierten Version des PBPK-Modells durchgeführt, um Arzneistoff-Charakteristika zu identifizieren, die auf Vorteile eines Wechsels von i.v. Administration zu oraler Inhalation hindeuten, und Anhaltspunkte für Optimierungsparameter bei der Entwicklung neuer inhalativer Antibiotika aufzeigen könnten. Die Analyse zeigte, dass niedrige Permeabilität, hoher Efflux und ein langer post-antibiotischer Effekt treibende Parameter für lokale Effektivität darstellen.

In Publikation III wurde eine post-hoc Analyse zur Untersuchung der Beziehung zwischen gemessenen Plasma-Konzentrationen und pulmonaler PK anhand publizierter klinischer PK-Modelle für orale Inhalation durchgeführt. Verschiedene Strukturen von Absorptionsmodellen wurden identifiziert und in Hinblick auf ihre Eignung untersucht, um mit oder ohne Variabilität auf Konzentrationen in der Lunge zurückzuschließen. In den meisten Fällen war die errechnete Lungenexposition und -Retentionszeit innerhalb des zweifachen Fehlerbereichs, solange das richtige Absorptionsmodell inklusive aller relevanten pulmonalen PK-Prozesse für die jeweilige Substanz ausgewählt wurde.

Abstract

Oral inhalation for the treatment of diseases has been around for thousands of years.^{1,2} To this day, it is still the most relevant route of administration for pulmonary diseases such as asthma and chronic obstructive pulmonary disease (COPD). However, there is still much to learn about the processes specific to pulmonary administration or even how the physiology of different lung regions affects the pharmacokinetics (PK) of drugs.

While the lungs are generally considered to be a single organ, there is quite a difference in physiology between the conducting airways and the respiratory (alveolar) region, where the gas-exchange takes place. Pharmacometrics, and specifically physiologically-based PK (PBPK) modeling, is an important approach to quantitatively describe even local tissue PK and can help separate the relevant processes associated with oral inhalation on a physiologically reasonable level. The aim of this thesis was to enhance the understanding of PK of orally inhaled drugs, with emphasis on the distribution into pulmonary tissues and the relationship between local pulmonary PK and systemic (plasma) concentrations.

In publication I, a semi-mechanistic PK model was developed for four model drugs after intravenous (i.v.) administration in rats. The underlying data was generated using a new methodology allowing for the measurement of tissue concentrations in the trachea, upper bronchial tree, and the alveolar region within the same animals. The model was able to describe the local pulmonary concentration-time profiles based on shared values of blood flows and tissue weights across drugs, with the only drug-specific parameters being tissue-to-plasma partition coefficients (K_p) and systemic PK parameters. Depending on the physicochemical characteristics of the drug, tissue-specific K_p values varied up to six-fold between the trachea and the alveolar parenchyma, showing that distribution behavior can differ substantially between pulmonary tissues.

Publication II focused on the suitability of inhaled administration for established antibiotics. To this end, the existing model was expanded to include a distinction between intra- and extracellular space, a separate compartment for the epithelial lining fluid (ELF), and a bacterial growth model for pharmacodynamic (PD) evaluation. The methodology for the generation of in vivo PK data was further refined to allow ELF concentration measurements in the trachea and alveolar region. A sensitivity analysis was carried out using a humanized version of the PBPK model to identify promising drug characteristics suggesting advantages of an i.v.-to-inhaled switch, as well as a point of reference for optimization parameters during the

development of inhaled antibiotics. Low permeability, a high epithelial efflux ratio, and long post-antibiotic effect were found to be driving parameters for local efficacy.

In publication III, a post-hoc analysis of published clinical PK models of oral inhalation was performed investigating the relationship between observed plasma concentrations and pulmonary PK. Different structures of absorption models were identified and tested regarding their suitability of inferring pulmonary exposure and retention time with and without added variability. In most cases, the inferred pulmonary exposure and retention metrics were within two-fold error range, given that an adequate absorption model including all relevant PK processes for a given drug was selected.

1 Introduction

1.1 Oral inhalation – local delivery of drugs for pulmonary diseases

Oral inhalation constitutes an attractive route of administration for the treatment of pulmonary diseases where the drug is directly administered into the lungs. The delivery of drugs directly to the target-site promises high initial concentrations to achieve a fast onset of action and provides the opportunity to increase pulmonary selectivity, leading to reduced side effects caused by systemic drug exposure.³ Even though there are also suggested benefits for non-pulmonary diseases, like needle-free administration of otherwise not bioavailable drugs such as insulin, this application of oral inhalation has not been reliably pursued in practice yet.⁴

However, even for pulmonary targets there is a difference to be made regarding the localization of the target within the lung. The exposure and distribution behavior of drugs may vary between different lung regions. Still, lung homogenate or bronchioalveolar lavage fluid (BALF) measurements are mainly used for the evaluation of target exposure.⁵⁻⁸

1.2 Pulmonary anatomy and physiology

While the lung is considered to be a single organ, it is highly heterogenous in nature. On the one hand, there are the conducting airways, sometimes called central lung. Starting with the trachea, which splits into left and right bronchus, the airways continually branch in a dichotomous fashion in human lungs. After about 16 bifurcations (generations), the bronchial tree leads into the terminal bronchioles that, together with the alveoli, form the respiratory or alveolar region.⁴

The physiology of the alveolar region is quite different compared with the conducting airways. As the alveolar vascular system is part of the pulmonary circulation, blood flow through this tissue is much higher than through the conducting airways, which are part of the systemic circulation.⁹⁻¹¹ The epithelial and endothelial surface areas are higher in the alveolar region, and finally also the constitution is different compared to the conducting airways.^{12,13} The vast surface area and short distance between epithelium and endothelium of the respiratory area results in an optimal air-blood interface for gas exchange. While this also shows some promise for rapid drug absorption into lung tissues, the high perfusion may also lead to fast absorptive clearance into the blood stream. In contrast, cartilage rings and smooth muscle are only present in the thicker conducting airways. Another discerning factor is the epithelial lining fluid (ELF).

While the epithelium in the alveolar region is coated by a very thin, surfactant-containing layer of ELF, the ELF layer in the conducting airways is thicker, mucus-like and is moved continually toward the mouth-throat area by ciliated epithelial cells.⁴ This process is called mucociliary clearance (MCC). A schematic representation of the lung and differences in epithelia can be found in Figure 1.

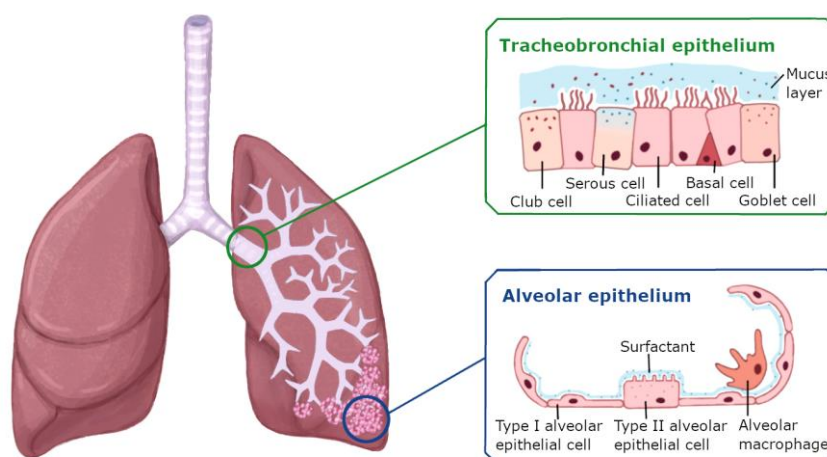


Figure 1. Schematic of the human lung and tracheobronchial and alveolar epithelial structure.

Depiction of epithelial cells was inspired by an image created by Enlo-Scott et al.¹⁴

1.3 Lung-specific PK processes

The before-mentioned differences in physiology may have a negligible impact on the systemic PK of intravenously or orally administered drugs. However, they can be expected to affect local pulmonary PK profiles. This is especially true for pulmonary drug administration, as there are several pulmonary PK processes, which are specific for oral inhalation. Figure 2 shows an overview of the relevant processes.

First, any droplet or particle that is released by the inhalation device and does not get caught in the mouth-throat area travels through the conducting airways until it impacts and deposits in the ELF, where solid particles will start to dissolve. Deposition patterns vary depending on airway anatomy, particle size and inhalation flow rate.¹⁵ When the deposition site is in the conducting airways, solid and dissolved drug alike is transported upwards by ciliated cells until it reaches the mouth-throat area to be subsequently swallowed. Particles in the alveolar region may be cleared by alveolar macrophages.¹⁶⁻¹⁸ Dissolved, unbound drug molecules are free to

permeate and distribute into the lung tissue, where (mostly basic) drugs can be trapped within lysosomes due to pH differences.¹⁹ From the tissue, they can be absorbed into the blood stream or metabolized within the lung.^{20–22} Due to the difference in perfusion rates, drug distribution to and absorption from the alveolar region is thought to be faster compared to other parts of the lung for specific drugs.²³ All these processes can occur in parallel. However, their relative impact on systemic and local PK and PD after oral inhalation depends on the properties of the investigated drug.

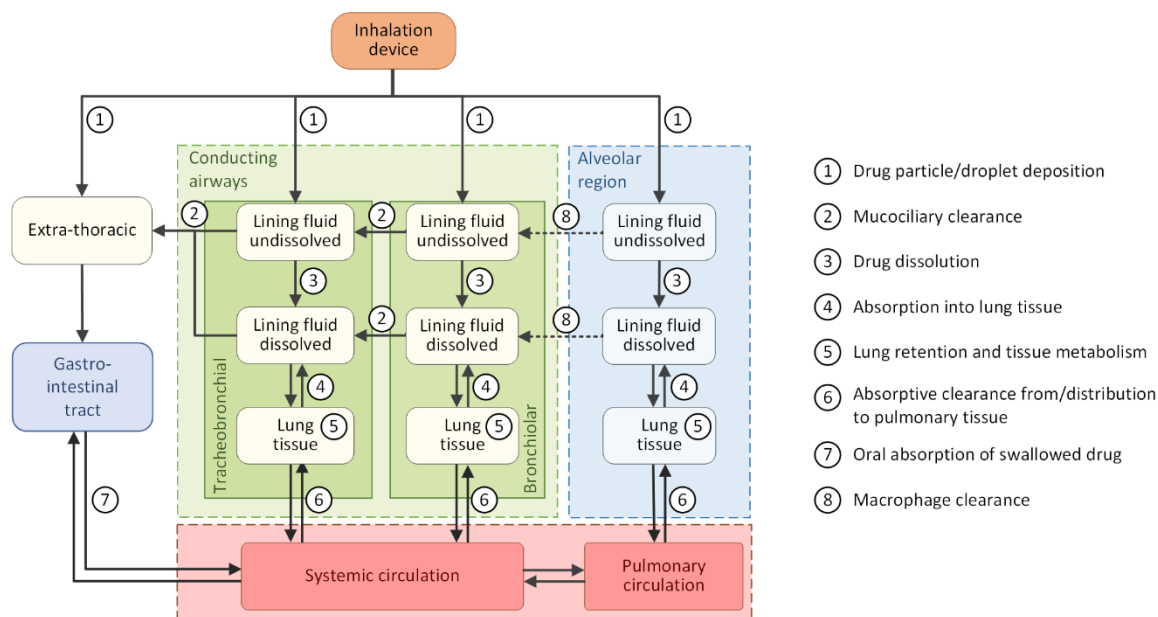


Figure 2. Overview of pulmonary PK processes including those specific for oral inhalation.

1.4 Applications of oral inhalation

The field where oral inhalation is typically applied are strictly pulmonary diseases such as asthma and COPD, both common and chronic lung conditions. One of the main symptoms – restricted breathing – is shared by both conditions, which can be alleviated by targeted treatment via oral inhalation. To reduce the frequency and severity of exacerbations, the obstruction of the airways can be treated with anti-inflammatory drugs (inhaled corticosteroids), bronchodilators (beta₂-agonistic drugs for both diseases and muscarinic antagonists for COPD), or a combination of both types.^{24,25}

The same arguments could also be made for the treatment of localized pulmonary infections, with the added benefit of potentially preventing and overcoming drug resistance due to the high initial concentrations.²⁶ While advantages and rationale for inhaled corticosteroids and

bronchodilators have been sufficiently shown,^{24,25} standardized and randomized studies are lacking for most antibiotics, and only few anti-infective drugs are approved for inhaled administration.²⁷ Exceptions are e.g., colistin, aztreonam, and tobramycin for the treatment of pulmonary infections associated with cystic fibrosis.²⁷ Nevertheless, off-label use of established i.v. antibiotics via nebulization is practiced frequently, especially in intensive care units.²⁷ However, contrary to asthma and COPD medications, these drugs have not been designed with oral inhalation in mind. Therefore, the impact of the change in administration route on the pulmonary pharmacokinetics and respective pharmacokinetic/ pharmacodynamic relationship of these re-purposed antibiotics has not been well studied, raising the question of adequate doses and dosing frequency.²⁸

1.5 Research and development process of orally inhaled drugs

Optimal physicochemical properties of inhaled drugs can vary depending on the target location (e.g., intra-, or extracellular) and depending on the desired efficacy (e.g., short- vs. long acting). Generally, inhaled drugs are structurally different compared to orally or intravenously administered drugs with a trend towards higher polar surface area and a higher molecular weight of inhaled drugs.^{29,30}

Designing new drugs for oral inhalation comes with unique challenges: As the administration site and the target site are identical, the target is upstream from plasma (i.e., the typical measurement site for drug exposure), requiring back-translation to infer on local effective concentrations. In addition, systemic exposure is desired to be as low as possible, sometimes even below quantification limits at efficacious doses, limiting quantitative investigations of PK/PD relations.^{31,32} High pulmonary exposure combined with low concentrations in plasma can be achieved by different means. In general, long lung retention (e.g., via binding to tissue components), slow dissolution, fast systemic clearance, and low oral bioavailability are beneficial for pulmonary selectivity. This is in stark contrast to the desired properties of orally administered drugs, which are often highly bioavailable and slowly cleared from the systemic circulation.

The differences in the research and development process already start as early as the lead-optimization stage, as some of the above-mentioned strategies can best be addressed by carefully designing the physicochemical properties of potential drug candidates. For instance, implementing basic centers within the drug molecules was shown to increase residence times

in the lung, which was attributed mostly to lysosomal trapping.^{19,33} Therefore, the influence of drug characteristics on local PK should be known to streamline lead optimization. Further down the line, non-clinical development plays an important role for orally inhaled drugs. Since the inhalation device and formulation properties hugely impact deposition patterns and dissolution behavior, these characteristics need to be investigated early on to enable well-founded translation from the preclinical to the clinical stage. The translation of inhaled PK and PK/PD characteristics to humans is challenging, even with extensive knowledge of the drug molecule. Animal models typically do not adequately depict the human lungs in either morphology or breathing behavior. While possible in rodents, local concentration measurements in clinical studies are rare, work intensive and present a considerable burden on the study participant. Unfortunately, inhaled administration in rats additionally shows challenging translatability to the human situation, due to physiological and anatomical differences (see Figure 3).³⁴

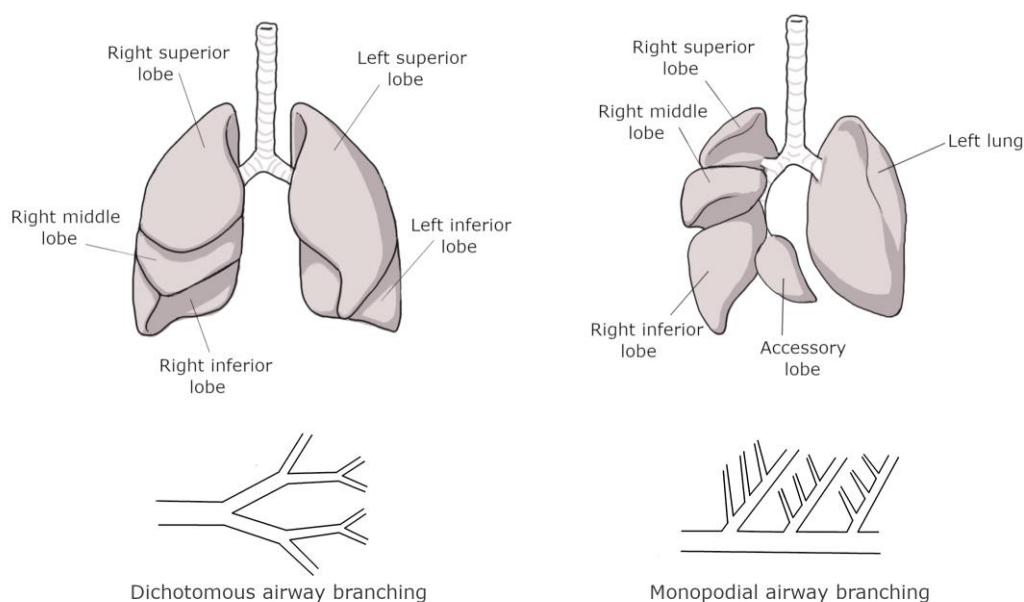


Figure 3. Lobar structure and branching type of human (left) and rat (right) lungs.

In addition to the overall size and airway branching structure being different, rats are obligatory nose-breathers. The result would be a major deposition in the nasal cavity and, depending on the experimental set-up (e.g., nebulization into the whole chamber), also in the fur of the animals which can then be taken up orally via grooming behavior. This would again lead most of the drug being distributed to the lungs via the systemic perfusion after oral and/or nasal absorption rather than via the direct deposition within the airways. Some of these difficulties

can be avoided by intratracheal (i.t.) administration. However, the deposition patterns for this administration route are also not well defined. In addition, the particle size distribution of the chosen formulation, which heavily impacts the deposition pattern, will behave and dissolve differently in the much smaller rat lung with narrower airways and lower fluid volumes.³⁴

To get closer to human physiology and breathing characteristics, it would be necessary to perform experiments in non-rodents, such as dogs, which can be trained to inhale via the mouth³⁵ This however might be challenging also for ethical reasons, as an adequate evaluation of the local PK after i.t. administration would require not only plasma sampling but potentially also additional tissue sampling, i.e., sacrificing of the non-rodents. In any case, an adequate translation is considered possible, if the impact of the individual PK processes associated with oral inhalation and the differences between animal and human are well understood.

The same might also hold true for the interpretation of clinical data. Oral inhalation relies on patients to follow specific instructions regarding the inhalation maneuver. Slight differences in inhalation flow rate may change the deposition pattern and even the dose reaching the lungs, increasing the PK variability in clinical studies further.³⁶ Local concentration measurements, typically from bronchioalveolar lavage or – in rare cases – biopsies can be difficult to interpret, especially if the samples do not represent the targeted area of the lung. Additionally, time-resolved pulmonary concentration measurements are rare. All of this makes it necessary to infer the pulmonary exposure from plasma concentrations. This can be difficult, as the systemic PK profile may not be representative of the local situation.³⁷

1.6 Applications of pharmacometric approaches for oral inhalation

Pharmacometrics, including PK modeling and simulation methods, allows to quantitatively describe the fate of drugs within the body. Owing to the increase in PK/PD related data generation, as well as access to computer-based mathematical modeling tools over the recent years, modeling methods have become more and more relevant across drug discovery and development.^{38–40} Today, pharmacometric approaches are widely applied to investigate PK/PD relationships, utilizing a range of empirical to more mechanistic models. Empirical models rely on measured data (e.g., plasma concentration-time profiles) to inform the relevant parameters of compartmental models, while mechanistic models are usually based on prior knowledge and mechanistic insight to mathematically describe specific PK processes. Oftentimes, however, modeling approaches are neither fully empiric nor mechanistic but contain elements of both,

depending on the purpose of the model. This allows, for instance, to focus on the impact of specific PK processes while keeping the overall complexity on a manageable level.

Mechanistic models to describe PK are typically referred to as physiologically-based PK (PBPK) models. These models combine relevant physiological characteristics, such as blood flows and organ weights, with drug and product attributes to be mechanistically linked to specific PK processes. Although they are frequently applied for oral, i.v., or subcutaneous drugs, for which unbound blood or plasma exposure is considered an adequate surrogate for the relevant unbound tissue concentrations to determine efficacy,^{41–43} fewer PBPK modeling approaches have been reported for local drug administration.

Reported application of pharmacometric approaches for orally inhaled drugs differ in the level of complexity and mechanistic implementation of processes depending on intended use. While there are *in silico* methodologies available to describe each of the various pulmonary PK processes, a lot of focus is laid on formulation properties, especially regarding bioequivalence testing. Mathematical models for the prediction of deposition patterns and dissolution profiles are quite distinguished and easily found, as extensive information about human airway geometry is publicly available. Artificial models of the mouth-throat area and the conducting airways are available to test the influence of particle or droplet size on fluid dynamics and deposition outside of clinical studies.^{44,45} However, few studies are dedicated to investigating absorption and distribution characteristics separately.^{6,46} While there are PBPK models for orally inhaled drugs ranging from a simple distinction between central and peripheral lung to accounting for each conducting airway generation separately, these models are seldom supported by actual exposure data with the same level of granularity.

1.6.1 Modelling approaches for pulmonary distribution

Pulmonary absorption as a process combines both the absorption from the ELF into lung tissue, distribution in these tissues, and the absorptive clearance into the systemic circulation. It is challenging to investigate these processes separately from deposition, MCC, and dissolution after oral inhalation, especially for poorly soluble drugs. However, they can be treated as the reverse of drug distribution into the lung from plasma, which can – given adequate experimental design – be studied after i.v. administration. Regarding distribution, there are different aspects to be considered: On the one hand, there is the classical distribution between

plasma and tissue. On the other hand, there is spatial distribution, with differences between different lung structures, such as trachea, bronchi, and alveolar region, or within these structures between different cell types or components.

Regarding pharmacometric approaches, there are several ways to implement pulmonary distribution into PK models for oral inhalation.

1.6.1.1 Empirical PK models

The simplest one is the implementation of empirical absorption processes, as seen in publication III (section 3.3). This approach requires the least amount of data, i.e., the model can be built relying on just plasma concentration data. However, these empirical processes typically represent a combination of all processes up to the absorption into the systemic circulation. For poorly soluble drugs, the absorption rates are more likely to describe the dissolution as the slowest process rather than pulmonary distribution, possibly resulting in flip-flop kinetics. Without the distinction between dissolved and undissolved drug, and missing the backflow from plasma to lung tissues, it therefore provides limited information about effective pulmonary concentrations.

1.6.1.2 PBPK models

In addition to physiological parameters like perfusion rates and organ volumes, tissue retention in PBPK models is typically governed by tissue-to-plasma partition coefficients (K_p) and the fraction unbound in plasma (f_u) (as applied in publications I and II, chapters 3.1 and 0, respectively). Plasma protein binding, which can be quantified through *in vitro* assays,⁴⁷ is considered as only unbound drug is assumed to be able to cross endothelial membranes and distribute into the tissues. K_p values on the other hand represent the concentration ratio between tissue and plasma at equilibrium, i.e., a metric for the magnitude of tissue retention which also influences the backflow of drug from tissue to plasma. Depending on the available data, these parameters can be based on different assumptions. A pulmonary K_p value can be predicted *in silico* based on published relationships between physicochemical drug properties and published tissue constituents like phospholipids and intracellular and extracellular water content.^{48–51} This method is typically applied by (commercial) whole-body PBPK models.^{52,53} Furthermore, *in vitro* and *ex vivo* assays may be used to investigate distribution into pulmonary tissues. This includes determining tissue binding ($f_{u,tissue}$) based on homogenized lung tissue, or an unbound volume of distribution based on lung slice experiments.⁵⁴ However, these methods only provide whole lung K_p values, disregarding potential differences between lung structures. *In vivo*

distribution studies require destructive sampling, where tissue and plasma concentrations are sampled and measured directly. In this case, K_p values are determined by either the concentration ratio between the concentrations in tissue and plasma when equilibrium is established, or the ratio of observed area under the concentration-time curves (AUC).⁵⁵ Another method of quantifying the K_p based on *in vivo* information is PK modeling, with the added advantage that it works with less samples than the AUC determination, while not depending on equilibrium being reached within the time frame of the experiment.

For more granular models including cellular compartments or models for low permeability drugs, effective permeability can be implemented as a parameter to describe permeation across cell membranes in addition to f_u and K_p . Permeability, which can be derived from *in vitro* permeability assays measuring cell-permeability (Caco-2 or Calu-3 cell lines)^{56,57} or – less often used – parallel artificial membrane permeability (PAMPA), is then scaled by the physiological surface area of the respective barrier (e.g., endothelial, or epithelial surface areas) to calculate permeation rates. This parameter may also be estimated from observed data, given a sufficient data basis.

2 Objectives

A good understanding of PK and PK/PD relationships is crucial across all stages of drug discovery and development. From the selection of the drug candidate with the best PK/PD properties during the discovery phase over formulation development to the determination of the right human dose and posology, careful planning of studies and knowledge of the relevant PK processes are critical for the success of any project. This is especially true for locally-acting drugs, as the measured concentrations in plasma may not be an adequate surrogate for the efficacious concentrations at the administration site.

Although deposition and dissolution behavior may be difficult to translate from rat to human (as discussed in section 1.5), tissue composition is assumed to be comparable across species.⁵⁵ Taking advantage of this, distribution into pulmonary tissues can be investigated in rodents. To bypass formulation dependent differences in exposure due to varying deposition patterns and dissolution rates, pulmonary tissue distribution can better be investigated via i.v. administration. As distribution from the systemic side and absorption from the lungs after oral inhalation are governed by the same principles, model-based analysis of i.v. administration experiments also allows for conclusions on absorption behavior and pulmonary retention.

The overall scope of the presented work was to elucidate local pulmonary PK based on *in vivo* exposure and PK/PD modeling, as well as to identify favorable drug characteristics for oral inhalation across the research and development process (see Figure 4). Special focus was placed on the influence of drug characteristics on absorption and distribution processes, while formulation-related aspects were intentionally not covered in the present work.

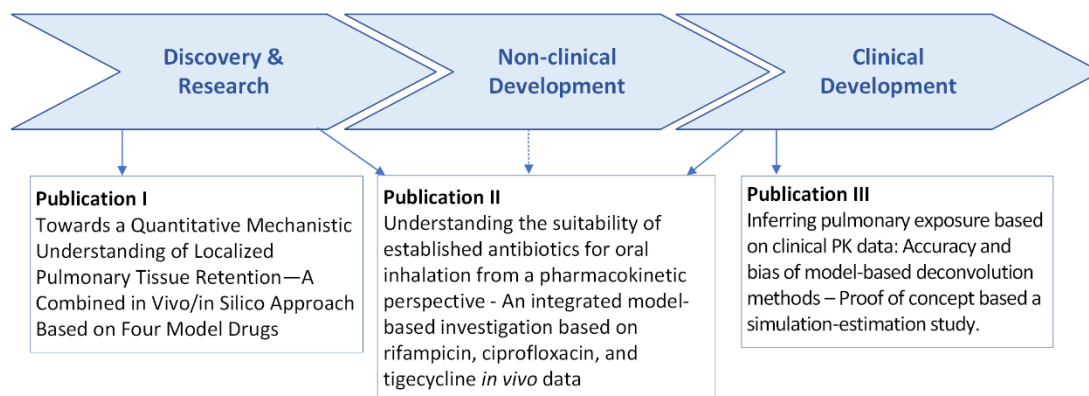


Figure 4. Stages of the drug discovery and development process and context of the original articles included in the cumulative dissertation.

The scope of the here included publications I, II, and III was as follows:

Publication I: Developing a localized pulmonary tissue retention PBPK model

- Development of a (rat) pulmonary PBPK model to quantitatively capture the local PK based on physiological differences between trachea, bronchi, and alveolar parenchyma
- Characterization of distribution processes between pulmonary tissues and the systemic circulation based on detailed *in vivo* tissue distribution data
- Relating changes in local exposure to physicochemical drug characteristics

Publication II: Identifying favorable drug characteristics for potential oral inhalation drugs

- Refinement of the initial pulmonary PBPK model in rats to include a differentiation between interstitium, intracellular space, and ELF
- Translation of the physiological model parameters from rat to human
- Identification of impactful drug characteristics for orally inhaled anti-infectives by performing a sensitivity analysis, assuming interchangeable deposition and dissolution behavior

Publication III: Evaluation of model-based approaches to infer on pulmonary exposure

- Meta-analysis of published empirical pulmonary absorption models
- Characterization of different empirical absorption processes based on clinical PK data after i.v. administration and oral inhalation
- Evaluation of empirical approaches to infer pulmonary PK from plasma concentrations

3 Cumulative part

Three publications are introduced and presented in the cumulative part of this work and represent the key results of this dissertation project. The focus lays on improving the understanding of local pulmonary PK by application of pharmacometric approaches across the research and development timeline of orally inhaled drugs.

The following articles were published in *Pharmaceutics*, *Journal of Antimicrobial Chemotherapy*, and *Journal of Pharmacokinetics and Pharmacodynamics*.⁵⁸⁻⁶⁰

3.1 Publication I: Developing a localized pulmonary tissue retention PBPK model

Towards a quantitative mechanistic understanding of localized pulmonary tissue retention – A combined in vivo/in silico approach based on four model drugs

Anneke Himstedt, Clemens Braun, Sebastian G. Wicha,
Jens M. Borghardt

Pharmaceutics, 12 (2020), 408

Impact factor: 6.321 (2020)

Synopsis:

One of the optimization strategies for orally inhaled drugs that needs to be implemented in the lead optimization phase during research consists of increasing tissue affinity to achieve pulmonary retention. Together with perfusion rates, tissue affinity represents a key parameter governing the distribution into pulmonary structures. However, knowledge about the exact target location within the lung is important, since (as outlined in Section 1.2) the lung is a heterogenous organ, which may impact local drug disposition. While optimization strategies for the lung as a whole have been established before, the impact of regional physiology on tissue affinity has not been investigated in as much detail.

A semi-mechanistic rat PBPK model was developed to quantitatively study regional distribution of four structurally diverse model drugs into the trachea, bronchi, and the alveolar region. The aim of the model was the characterization of regional blood flows and tissue K_p as a marker for tissue affinity. Detailed and time-resolved *in vivo* exposure data from each region after i.v. infusion was used for the parameterization of the model. The blood flow estimates for the lung perfusion were determined via a combined fit across data from all compounds. Localized disposition of the basic and neutral drugs (salmeterol, fluticasone propionate, and linezolid) could be successfully described, while the one acidic drug (indomethacin) showed diverting behavior. The results suggested a noticeable, up to six-fold, difference in regional K_p values between the trachea and alveolar parenchyma for individual drugs. A comparison to frequently used K_p prediction methods developed by Rodgers and Rowland showed closer agreement between the predicted values and the estimated values for the alveolar region than with the corresponding estimates for the conducting airways.


3 Cumulative part

These individually determined distribution parameters for trachea, bronchi, and alveolar region, apart from alveolar blood flow highlight the importance of understanding not only overall pulmonary kinetics, but also regional drug disposition.



Article

Towards a Quantitative Mechanistic Understanding of Localized Pulmonary Tissue Retention—A Combined In Vivo/In Silico Approach Based on Four Model Drugs

Anneke Himstedt ^{1,2}, Clemens Braun ², Sebastian Georg Wicha ^{1,*} and Jens Markus Borghardt ^{2,*} 

¹ Department of Clinical Pharmacy, Institute of Pharmacy, University of Hamburg, 20146 Hamburg, Germany; anneke.himstedt@uni-hamburg.de

² Drug Discovery Sciences, Boehringer Ingelheim Pharma GmbH & Co. KG, 88397 Biberach, Germany; clemens.braun@boehringer-ingelheim.com

* Correspondence: sebastian.wicha@uni-hamburg.de (S.G.W.); jens_markus.borghardt@boehringer-ingelheim.com (J.M.B.)

Received: 30 March 2020; Accepted: 27 April 2020; Published: 29 April 2020



Abstract: Increasing affinity to lung tissue is an important strategy to achieve pulmonary retention and to prolong the duration of effect in the lung. As the lung is a very heterogeneous organ, differences in structure and blood flow may influence local pulmonary disposition. Here, a novel lung preparation technique was employed to investigate regional lung distribution of four drugs (salmeterol, fluticasone propionate, linezolid, and indomethacin) after intravenous administration in rats. A semi-mechanistic model was used to describe the observed drug concentrations in the trachea, bronchi, and the alveolar parenchyma based on tissue specific affinities (K_p) and blood flows. The model-based analysis was able to explain the pulmonary pharmacokinetics (PK) of the two neutral and one basic model drugs, suggesting up to six-fold differences in K_p between trachea and alveolar parenchyma for salmeterol. Applying the same principles, it was not possible to predict the pulmonary PK of indomethacin, indicating that acidic drugs might show different pulmonary PK characteristics. The separate estimates for local K_p , tracheal and bronchial blood flow were reported for the first time. This work highlights the importance of lung physiology- and drug-specific parameters for regional pulmonary tissue retention. Its understanding is key to optimize inhaled drugs for lung diseases.

Keywords: lung retention; pharmacokinetics; pulmonary blood flow; tissue affinity; semi-mechanistic PK modelling; trachea; bronchi; alveolar; lung concentration

1. Introduction

Pulmonary drug delivery is the preferred administration route for treatment of respiratory disorders like asthma or chronic obstructive pulmonary disease. The reason is that oral drug inhalation can provide pulmonary selectivity for locally acting drugs and long-lasting pulmonary efficacy, as can be seen for long-acting β_2 -receptor agonists (LABAs) and long-acting muscarinic receptor agonists (LAMAs). To achieve long-lasting pulmonary efficacy, there are mainly two strategies applied to maintain pulmonary exposure over a long period of time, namely slow dissolution (e.g., inhaled fluticasone propionate [1]) or retention by high tissue affinity (postulated e.g., for the LABA salmeterol [2]). However, a recent publication suggested that retention due to high lung tissue

affinity is preferable over slow dissolution in terms of target exposure [3]. One reason is that slow dissolution may lead to noticeable drug loss in the conducting airways via the mucociliary clearance.

The lung is a very heterogeneous organ with various structural differences between the conducting airways and the alveolar region [4]. In addition, the alveolar region is stronger perfused compared to the conducting airways, as the alveolar region is perfused by the pulmonary circulation, whereas the conducting airways are perfused by the systemic circulation. All these physiological differences potentially influence drug pharmacokinetics (PK), raising the question if total lung concentrations are a valid surrogate for target-site concentrations. For example, β_2 -receptors are expressed in all lung regions [5], yet the relaxation of smooth muscle cells by inhaled sympathomimetics is driven by receptor activation in the conducting airways. This means that only the drug concentrations in the conducting airways elicit the desired effect. Therefore, it is key to understand the PK in the local tissues and not only for the complete lung.

The local pulmonary tissue PK and therefore the local tissue retention is determined by two aspects, first the tissue affinity and second the local perfusion. Due to experimental difficulties, investigations of pulmonary tissue retention have been mostly qualitative in nature [6,7] or were based on empirical estimation of tissue distribution or absorption rate constants [8,9]. A more mechanistic quantitative determination of pulmonary disposition kinetics remains challenging for various reasons: First, after inhalation the variability in the PK is typically much higher compared to other routes of administration, so that a larger data set is required to infer on the pulmonary tissue retention. Second, after inhalation or intratracheal administration, there are many interacting PK processes, such as pulmonary deposition or the mucociliary clearance. All these processes confound the identification of the characteristics of single processes—here the pulmonary tissue retention [4]. Furthermore, low solubility drugs provide the additional challenge that there is no convenient way of differentiating between undissolved and dissolved drug in the lung. All of this makes it challenging to quantitatively determine the extent of the pulmonary tissue retention. By switching to intravenous (i.v.) administration to study distribution into different lung tissues one avoids most of these challenges, i.e., reduces the variability in the PK and removes confounding pulmonary PK processes.

The objective of this work was to better understand pulmonary retention in different lung regions by combining well-designed *in vivo* tissue distribution studies with a PK model-based analysis of plasma and tissue concentration measurements. Finally, the aim was to provide accurate estimates for tissue affinity and perfusion for different regions of the lung.

To achieve this, four drugs with varying physicochemical properties, namely salmeterol (SAL), fluticasone propionate (FP), linezolid (LIN), and indomethacin (IND), were intravenously administered to rats and the concentrations in plasma, trachea, bronchi and alveolar parenchyma were measured. These model drugs were chosen based on tolerability and relevance while covering a range of physicochemical properties (one basic, two neutral, and one acidic drug). Both SAL and FP are used to treat lung diseases, and LIN is often used for the treatment of pulmonary infections. As there are only few acidic drugs on the market, which are targeting pulmonary structures, IND was chosen based on tolerability and ease of acquisition. The data from these *in vivo* PK studies was further investigated regarding their disposition in the different lung tissues using a semi-mechanistic model accounting for both physiological and drug-specific properties. Since to date, no separate quantification of blood flows in trachea and bronchi has been reported in the literature, pulmonary blood flows were estimated based on the available data of all four drugs. Finally, based on the resulting understanding of the local concentration–time profiles, current plasma concentration–based practices for determining pharmacodynamic (PD) parameters were evaluated.

2. Materials and Methods

2.1. Chemicals

FP, SAL, LIN, and IND were sourced from the in-house compound dispensary at Boehringer Ingelheim Pharma GmbH & Co. KG, (Biberach, Germany). Deuterated internal standards were purchased for IND (indomethacin-d4, Biomol GmbH, Hamburg, Germany), FP (fluticasone propionate-d5, Santa Cruz Biotechnology Inc., Dallas, TX, USA), and LIN (linezolid-d3, Biomol GmbH). Structures and key properties of the drugs are given in the supplementary material (Supplementary material 1, Figure S1, Table S1).

2.2. Study Design

The *in vivo* PK studies were designed based on concentration–time profiles from exploratory *i.v.* cocktail PK studies (data not shown). Model-based analyses were performed to ensure that (a) the dose is sufficient to achieve concentrations above the lower limit of quantification in plasma and tissues over the whole study period, and (b) the timing of tissue sampling allows for accurate estimation of partition coefficients and localized pulmonary blood flows and therefore adequately capturing the shape of tissue concentration–time profiles. For the latter analysis, a stochastic simulation and estimation approach (SSE) was used to evaluate identifiability, bias and imprecision of the model parameters prior to performing the *in vivo* studies (Supplementary Material 1, Section 2, Tables S2 and S3, Figures S2 and S3). In the final studies, the drugs were administered via intravenous infusion to reach near-steady state conditions in the study period and minimize residual variability due to potential imprecision of the sampling time.

2.3. Animal Studies

Male Han Wistar rats, weighing 250 to 332 g, purchased from Janvier Labs (Le Genest-Saint-Isle, France) were used for the *in vivo* studies. All animal care and experimental procedures at Boehringer Ingelheim were conducted in compliance with the German and European Animal Welfare Act (EU Directive 2010/63/EU) and were approved by the Regierungspräsidium Tübingen as the responsible local German authority (reference number 14-009-G).

The infusion studies were performed in anesthetized animals. Briefly, the rats were anesthetized via whole body exposure to anesthetic gas (2–5% Isoflurane, 2.5 L/min Oxygen). Following anaesthetization, rats were intubated, placed in supine position on a heated device (39 °C), and the spontaneously breathing rats were connected to an anesthetic gas supply (1.5–2.5% Isoflurane, 2–2.5 L/min O₂). Thereafter, rats received a subcutaneous bolus of metamizol (100 mg/kg). Body temperature was controlled. Placement of catheters for drug infusion and blood sampling was not started before a body temperature of at least 36.5 °C was reached. Unilaterally, the carotid artery and the jugular vein were prepared and catheters were placed. The carotid catheter was used for blood pressure monitoring to adjust anesthesia by changing isoflurane concentration as well as for collection of blood samples. The jugular catheter was used for constant infusion over one hour (infusion rate 10 mL/h/kg) using a standard infusion pump. Blood samples (volume 100 µL) were collected in EDTA-tubes at the assigned time points. Plasma samples were prepared and subsequently stored at –20 °C. At the end of the *in-life* part, rats were exsanguinated.

2.4. Tissue Preparation

Immediately after exsanguination, the lungs including trachea and larynx were removed en bloc, rinsed in saline, blotted dry, and weighed. The preparation of the lung was performed after placing the lung on weighed cellulose swabs to collect leaking fluid during preparation (Figure 1). The trachea including the larynx was cut just above the first airway bifurcation and transferred to a weighed vial. A small piece (30–60 mg) of parenchyma was cut with a scalpel from the lateral part of the left lung. For preparation of the bronchial sample, the remaining lung was held in place

with forceps at the bifurcation while the parenchyma was squished by gently knocking with the back part of curved forceps. Afterwards, the destroyed parenchyma was carefully stripped from the bronchi up to the third airway generation. Finally, the remaining tissue and the cellulose swabs were collected for further analysis. Having finished the preparation, all collected samples were weighed, transferred to 7 mL Precellys[®] tubes (Bertin Instruments, Montigny-le-Bretonneux, France), and 4 parts of acetonitrile/methanol (1:1) solution were added. Samples were homogenized using a Precellys[®] homogenizer. After centrifugation, supernatants were stored at $-20\text{ }^{\circ}\text{C}$.

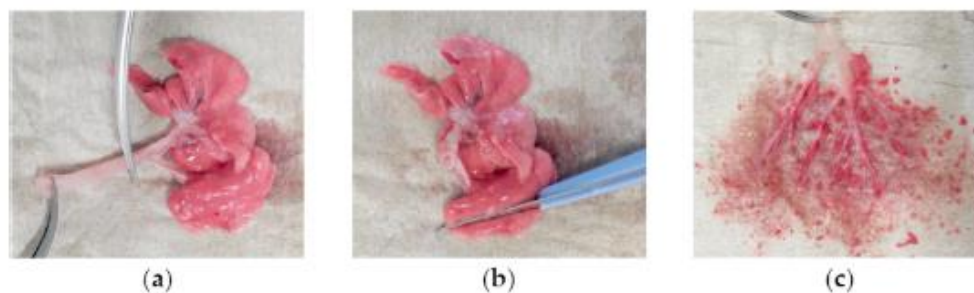


Figure 1. Preparation of tissue samples. (a) Sampling of the trachea from the intact lungs; (b) cutting a slice from the lateral part of the left lung; (c) bronchial sample after removal of the surrounding parenchyma.

2.5. Bioanalysis

Drug concentrations in plasma and tissue homogenates were determined by HPLC-MS/MS (reverse-phase HPLC coupled with a Thermo Scientific[™] TSQ Altis[™] triple quadrupole mass spectrometer (Thermo Fisher Scientific, Bremen, Germany) or a SCIEX QTRAP 6500 (AB Sciex, Darmstadt, Germany)). Prior to bioanalysis, plasma and tissue samples were spiked with internal standard solution and diluted with acetonitrile for protein precipitation. A more detailed description of analytical methods can be found in the supporting information (Supplementary Material 1, Section 5, Figures S4–S8).

2.6. Modelling and Simulation

The model-based PK analysis was carried out in Phoenix WinNonlin[™] 7.0 (Certara, L.P., Princeton, NJ, USA). PK parameters of the semi-mechanistic model (Figure 2) were estimated in a two-stage approach. As a first step, the systemic PK parameters were estimated based on the plasma concentration–time data, resulting in empirical one- or two-compartment models depending on the drug characteristics. In the second step, the tissue-specific parameters were estimated on top of the fixed systemic parameters using the tissue concentration–time profiles resulting from the four time points of tissue sampling.

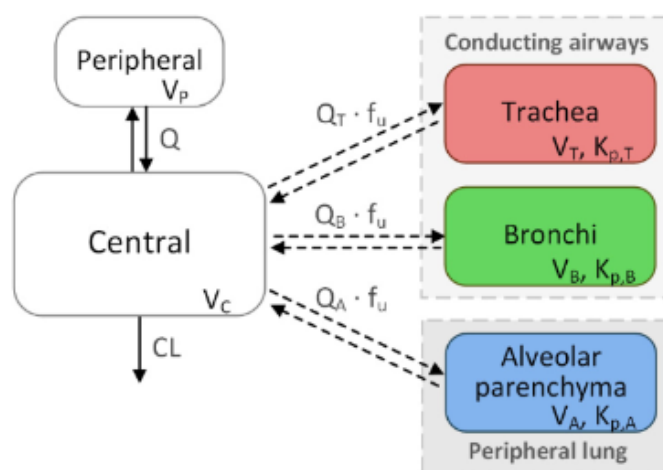


Figure 2. Structure of the pharmacokinetic (PK) model. CL: systemic clearance, V_C : central volume of distribution (Vd), Q : intercompartmental clearance, V_P : peripheral Vd; Q_T , Q_B , and Q_A represent the blood flow to the trachea, bronchi and alveolar parenchyma, respectively. f_u : fraction unbound in plasma, V_T : weight of the trachea, V_B : weight of the bronchi, V_A : weight of the alveolar parenchyma. $K_{p,T}$, $K_{p,B}$, and $K_{p,A}$ denote the tissue-to-plasma partition coefficients for the respective tissues.

As the systemic disposition model already constitutes distribution into the lung, the pulmonary compartments were implemented as “virtual” compartments, i.e., these compartments did not contribute to the mass flow of the systemic compartments. In contrast to the systemic disposition model, the parameters involving the tissue compartments were chosen based on the underlying physiology [10].

The volume of distribution (Vd) for each of the pulmonary compartments was fixed to the weight of each tissue in proportion to the bodyweight. The according weight for the alveolar parenchyma equated to 0.004 kg/kg bodyweight, assuming that the parenchyma represents approximately 80% of total lung tissue [11] (0.5% of bodyweight, [12]). The remaining 20% (0.001 kg/kg bodyweight) were assumed to represent the conducting airways including bronchi and trachea. For the trachea, the implemented weight corresponded to the individual sample weights (Supplementary Material, Table S4) in relation to the bodyweight (mean value, 0.0002 kg/kg bodyweight), and the bronchi corresponded to the remaining 0.0008 kg/kg bodyweight.

The blood flows to the lung tissues were estimated. As the blood flow should be independent of the infused drug, these parameters were estimated simultaneously with the combined data from all drugs. Plausible initial values for the estimation were calculated based on literature data on cardiac output (alveolar parenchyma) and bronchial circulation (bronchi and trachea, calculated proportional to tissue weight) [12]. The blood flows were scaled with the fraction unbound in plasma, i.e., it was assumed that only unbound drug is permeating into tissue. Tissue affinity was described by tissue-to-plasma partition coefficients (K_p), which were estimated separately for each of the three lung tissues. The model code is provided in the supporting information (Supplementary Material 2).

For comparison with common approaches that consider the lung as a single compartment [13–17], the same analysis was also carried out without separation of trachea, bronchi and alveolar parenchyma. To this end, full lung concentrations were calculated from the concentrations of all three lung tissues plus concentrations measured in the remaining lung tissue, weighted based on relative tissue size (Supplementary Material 1, Section 7), and subsequently used for estimation of lung-specific parameters. Model predictions of both variants were compared to the observed data using goodness-of-fit plots and the coefficients of determination.

Pulmonary absorption half-lives ($t_{1/2,pul}$) for each lung region were calculated from the resulting model parameters:

$$t_{1/2,pul} = \ln(2)/k_{a,pul} \quad (1)$$

with $k_{a,pul}$ being the absorption rate constant representing the unidirectional drug transfer from the lung tissue to the systemic circulation:

$$k_{a,pul} = (Q_{pul} \cdot f_{u,plasma}) / (V_{pul} \cdot K_{p,pul}), \quad (2)$$

Q_{pul} being the respective estimated pulmonary blood flow scaled with the fraction unbound in plasma ($f_{u,plasma}$). V_{pul} denotes the Vd of the respective lung region, and $K_{p,pul}$ is the respective estimated tissue-to-plasma partition coefficient. The ratio of $f_{u,plasma}/K_{p,pul}$ represents the free fraction in the respective pulmonary tissue.

Since rodent studies are typically performed to better predict the human situation and all four model drugs are designed for treatment of humans, allometric scaling to human was performed. This was done by the fixed exponent method, assuming an exponent of 0.75 for the blood flow:

$$Q_{pul,human} = Q_{pul,rat} \cdot SF \cdot (BW_{human}/BW_{rat})^{0.75}, \quad (3)$$

and 1 for the pulmonary volume of distribution:

$$V_{pul,human} = V_{pul,rat} \cdot SF \cdot (BW_{human}/BW_{rat})^1, \quad (4)$$

with BW_{rat} (0.28 kg, mean bodyweight of animals used in the studies, Supplementary material, Table S4) and BW_{human} (70 kg) as bodyweights for rats and humans, respectively. SF denotes a scaling factor (BW_{rat}/BW_{human}) to account for the bodyweight normalization. $K_{p,pul}$ was assumed to be conserved between species [18]. The respective extrapolated parameters were again used as input to Equation (2) to calculate the human absorption rate constant, which was used to calculate the human pulmonary absorption half-life according to Equation (1).

PK studies are often performed to infer on the expected efficacy by correlating the measured drug concentrations to the observed effect. As target-site concentrations in tissues are difficult to measure, plasma concentrations are typically used as a surrogate to quantify the concentration–response relationship. However, this approach does not consider potentially delayed concentration changes at the target site compared with plasma. To investigate the influence of this distributional delay, the developed PK model for SAL was further expanded by an E_{max} model, linking the predicted unbound concentration in the bronchi ($C_{u,bronchi}$) to the effect, assuming the bronchi to be the target tissue for SAL [19]:

$$E [\%] = (E_{max} \cdot C_{u,bronchi}) / (EC_{50,free} + C_{u,bronchi}). \quad (5)$$

Here, E denotes the effect associated with a given $C_{u,bronchi}$, E_{max} represents the maximum attainable effect (here 100%), and the $EC_{50,free}$ represents the unbound concentration needed to achieve half-maximal effect. To exemplify the impact for the example of SAL, the EC_{50} for SAL was taken from Hendrickx et al. [8], who measured the inhibition of methacholine-induced bronchoconstriction and found an EC_{50} of 36 nM (total lung concentration). This value was scaled to unbound concentrations using the fraction unbound in plasma ($f_{u,plasma}$) and the estimated K_p in bronchi ($K_{p,B}$):

$$f_{u,bronchi} = f_{u,plasma} / K_{p,B}, \quad (6)$$

assuming that unbound concentrations at equilibrium are the same in plasma and tissue.

Simulations were carried out to mimic the determination of unbound plasma EC_{50} ($EC_{50,free}$) of SAL by dose escalation at four different time points (0.25 h, 0.75 h, 2 h, and 4 h). This was done by simulating unbound plasma and tissue concentration–time profiles, as well as the effect over time for a wide dose range. The simulated effect for each dose at the selected time point was then correlated to the corresponding unbound plasma concentration. The resulting concentration–response relationship was then used to determine the plasma $EC_{50,free}$. For better illustration, the resulting parameter

estimates were normalized to the true $EC_{50,free}$. The determination of PD parameters was performed in R (version 3.3.2) [20].

3. Results

3.1. *In Vivo* PK Studies

Based on the results from the SSE analysis (Supplementary Material, Section 2), four time points were chosen for sampling of the lung tissues (three samples per time point and tissue), resulting in 12 samples per tissue and drug. The first samples were taken during the infusion (0.25 h and 0.75 h) to capture potential initial delayed increases in tissue concentrations. The two additional samples were taken at 2 h and 4 h after start of infusion, corresponding to 1 h and 3 h after the end of the infusion. Plasma was sampled until the end of the respective experiment, resulting in an average (range) of 67 (58–70) plasma samples per drug (see Supplementary Material, Table S4), which were mainly sampled within the first hour.

Plasma concentrations of SAL, FP, and LIN showed a bi-exponential decline after stopping the infusion, while IND showed mono-exponential decay (Figure 3). While pulmonary tissue concentrations of LIN were only slightly lower than plasma concentrations, for the acidic IND up to ten-fold lower tissue concentrations were measured. In contrast, tissue concentrations of both the neutral FP and the basic SAL were generally higher than the corresponding plasma concentration measurements.

IND concentrations were comparable in all pulmonary tissues. In contrast, the raw data of SAL, FP, and LIN indicated differences in magnitude and time-course of concentrations between trachea, upper bronchial tree, and alveolar parenchyma. This was most noticeable for SAL, which showed up to 20-fold higher concentrations in the alveolar parenchyma compared to the trachea. All drugs showed a distributional delay in the trachea.

3.2. Model-Based PK Analysis

The bi-exponential decline of plasma concentrations of SAL, FP and LIN was best described by an empirical two-compartment model. Since the plasma sampling of SAL shortly after stopping the infusion was not sufficient to support the estimation of all PK parameters of the systemic disposition model, additional data from another PK study was included in the analysis (Supplementary Material 1, Section 4). For IND, a one-compartment model was sufficient to capture the systemic PK.

In the second step, the tissue-specific parameters (K_p and tissue blood flows) were estimated on top of the fixed systemic disposition model. Estimates for K_p varied depending on both the investigated drug and tissue. In accordance with the raw data, K_p values for IND were comparable between all three lung tissues and estimated to range between 0.249–0.384, indicating lower tissue affinity compared to the affinity to plasma proteins. FP also showed similar affinity for all three pulmonary tissues (K_p between 5.21 and 6.64). While the K_p estimates for all tissues were higher for SAL compared to LIN, both drugs showed higher concentrations in the alveolar parenchyma compared to the conducting airways, with the lowest concentrations found in the trachea. SAL showed the strongest divergence in K_p values between tissues, with a six-fold higher affinity for the alveolar parenchyma than the trachea (39.3 vs. 6.52, respectively). Pulmonary blood flows could successfully be estimated (<22% CV) when data of all drugs was combined for simultaneous fitting. The tracheal blood flow was estimated to be 0.054 L/h/kg (14.3% CV), the bronchial blood flow amounted to 0.777 L/h/kg (21.5% CV). The parameter estimates for systemic and tissue PK can be found in Table 1.

Table 1. Model parameters (% CV).

Parameter	Unit	Salmeterol	Fluticasone Propionate	Linezolid	Indomethacin
CL	$L \cdot h^{-1} \cdot kg^{-1}$	3.86 (6.07)	3.37 (3.42)	0.279 (2.22)	0.0691 (11.0)
V_C	$L \cdot kg^{-1}$	0.123 (16.2)	0.223 (56.0)	0.320 (19.7)	0.154 (5.27)
Q	$L \cdot h^{-1} \cdot kg^{-1}$	3.24 (21.1)	4.72 (12.8)	2.79 (34.9)	-
V_P	$L \cdot kg^{-1}$	3.77 (14.6)	2.41 (8.18)	0.628 (9.96)	-
$K_{p,T}$	-	6.52 (7.04)	5.21 (16.9)	0.404 (11.2)	0.356 (20.2)
$K_{p,B}$	-	18.6 (12.2)	6.64 (13.2)	0.534 (6.52)	0.249 (16.0)
$K_{p,A}$	-	39.3 (8.10)	5.84 (10.6)	0.785 (5.11)	0.384 (35.5)
Q_T^{-1}	$L \cdot h^{-1} \cdot kg^{-1}$		0.054 (14.3)		
Q_B^{-1}	$L \cdot h^{-1} \cdot kg^{-1}$		0.777 (21.5)		
Q_A^{-1}	$L \cdot h^{-1} \cdot kg^{-1}$		10.6 (10.7)		

Abbreviations are provided in Figure 2. ¹ Blood flows were estimated simultaneously for all drugs.

The model-based analysis adequately explained the tissue-specific pulmonary disposition of the neutral and basic model drugs (SAL, FP, and LIN). However, applying the same principles, it was not possible to fully capture the pulmonary PK of the acidic drug IND. The model predictions suggested a much faster increase in pulmonary concentrations than observed in vivo, resulting in overestimation of tissue concentrations over the first two hours. Figure 3 shows the observed and predicted concentration–time profiles for all four drugs.

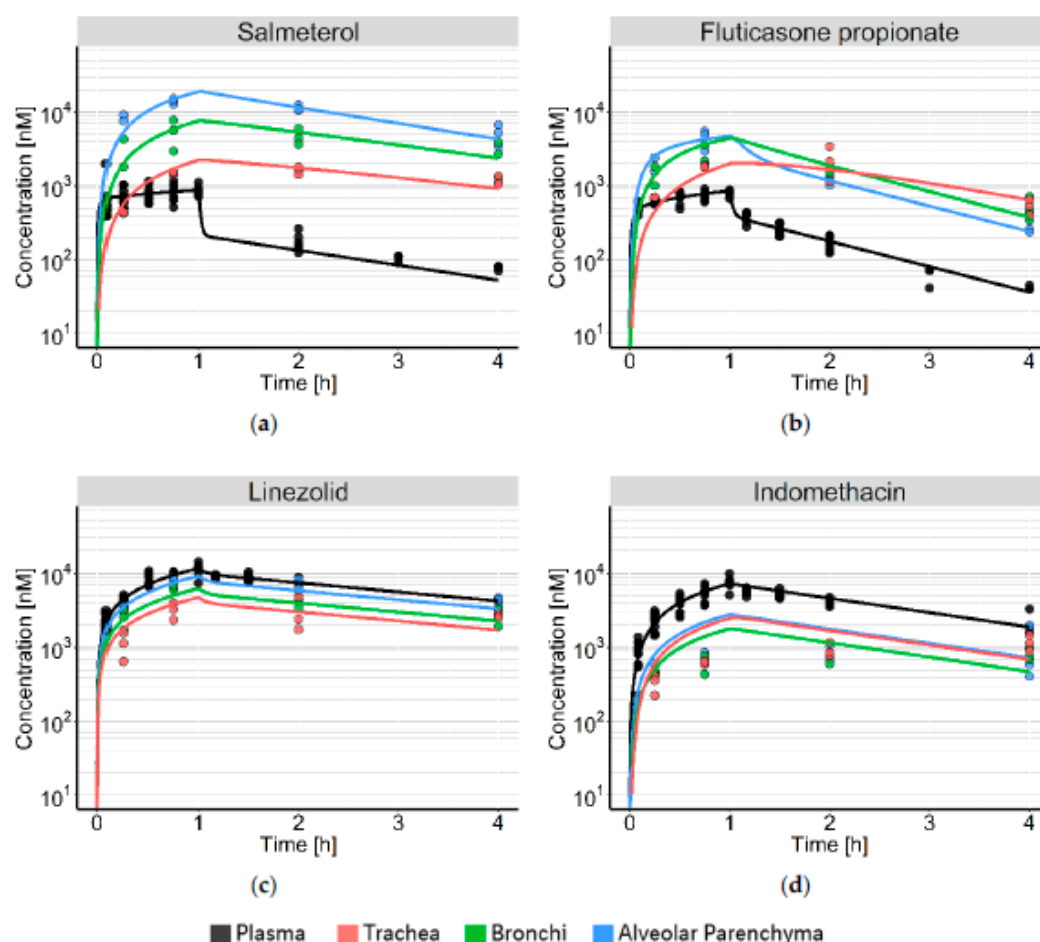


Figure 3. Concentration–time profiles of (a) salmeterol; (b) fluticasone propionate; (c) linezolid, and (d) indomethacin. Dots represent the observed concentrations; solid lines show the model-based prediction. Plasma concentrations are shown in black; concentrations in the trachea, bronchi, and alveolar parenchyma are shown in red, green and blue, respectively.

3.3. Comparison with Total Lung Concentrations

The K_p values estimated based on total lung concentrations were similar to those found for the alveolar parenchyma (37.7 ± 2.7 for SAL, 6.21 ± 0.727 for FP, 0.781 ± 0.035 for LIN, and 0.347 ± 0.086 for IND), which was also the case for the blood flow estimate (11.6 ± 1.39 L/h/kg). The “whole lung” model was therefore able to describe concentrations in the alveolar region quite well. However, the concentration–time profiles in bronchi and trachea were not captured adequately (Figure 4; Supplementary Material 1, Figure S9).

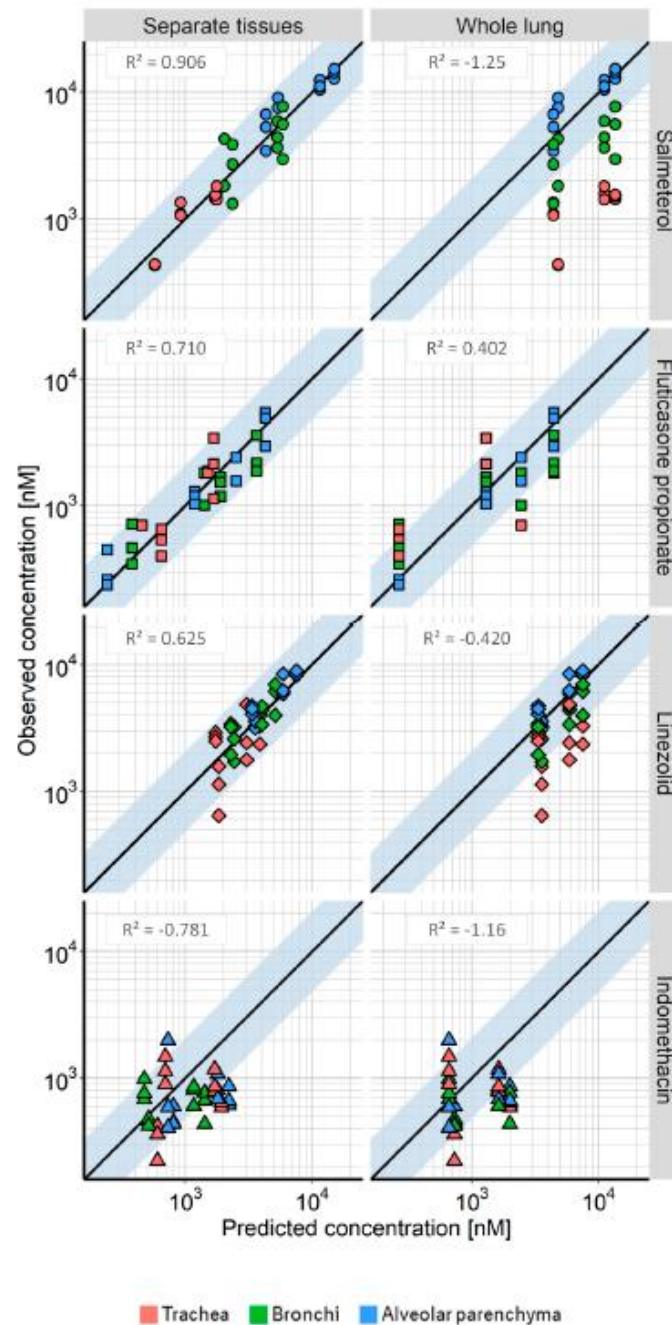


Figure 4. Goodness-of-fit plots of observed vs. predicted concentrations in the trachea (red), bronchi (green), and alveolar parenchyma (blue). Observed localized pulmonary concentrations plotted against (left) the predictions of concentrations in the separate pulmonary tissues; and (right) against predictions of total lung concentrations. Circles: salmeterol, squares: fluticasone propionate, diamonds: linezolid, triangles: indomethacin. The shaded area shows the two-fold error range.

Figure 4 shows the goodness-of-fit plots for both modelling of separate lung tissues and modelling of total lung concentrations compared to the observed concentrations in all three tissues. The model with separate compartments for trachea, bronchi, and alveolar parenchyma better described the data for all drugs, as shown by a better correlation (overall R^2 of 0.879 for combined data of separate tissues across all drugs vs. 0.267 for combined data of whole lung predictions), as well as more predictions falling within the two-fold error range. The greatest improvement in terms of correlation was achieved for SAL, resulting in a R^2 of 0.906 for the prediction of separate tissues, compared with an R^2 of -1.25 for the prediction of total lung concentrations. The “whole lung” model tended to overpredict the concentrations in trachea and bronchi, which was especially evident for SAL and LIN.

3.4. Pulmonary Absorption Half-Lives

The pulmonary absorption half-lives (Table 2) were fastest for the alveolar parenchyma, followed by bronchi and trachea. Absorption half-lives calculated for the whole lung were similar to those in the alveolar region. The allometrically scaled values for humans were approximately four times larger than the absorption half-lives calculated for rats.

Table 2. Pulmonary absorption half-lives ($t_{1/2}$)¹ derived from model parameters.

Drug	Tissue	$t_{1/2}$ (Rat)	$t_{1/2}$ (Human) ²
Salmeterol	Trachea	1.2 h	4.75 h
	Bronchi	57 min	3.77 h
	Alveolar	45 min	2.91 h
	Full lung	48.3 min	3.20 h
Fluticasone propionate	Trachea	52.4 min	3.48 h
	Bronchi	18.6 min	1.23 h
	Alveolar	5.99 min	23.8 min
	Full lung	7.28 min	28.9 min
Linezolid	Trachea	0.5 s	2.0 s
	Bronchi	0.2 s	0.8 s
	Alveolar	0.1 s	0.4 s
	Full lung	0.1 s	0.5 s
Indomethacin	Trachea	14 s	55 s
	Bronchi	2.7 s	11 s
	Alveolar	1.5 s	6.0 s
	Full lung	1.6 s	6.2 s

¹ Unidirectional flow from the lung compartments to the central compartment. ² Human half-lives were allometrically scaled from rat values.

While these trends held true for all drugs, the absolute half-lives differed substantially between drugs. Both LIN and IND showed half-lives in the range of seconds, indicating rapid redistribution from the lung. In contrast, half-lives of FP and SAL ranged from minutes to hours, even in the rat, translating up to approximately five hours for SAL in the human trachea. Out of all drugs, FP showed the highest difference in half-life estimates between the different pulmonary tissues.

3.5. Time-Dependency of Tissue-to-Plasma Ratios

The estimates for K_p for all drugs were further compared to the observed tissue-to-plasma ratios that could be extracted from the in vivo concentration measurements. Figure 5 shows the observed ratios for all drugs at the times of tissue sampling as a percentage of the tissue-to-plasma ratio at steady state (the model estimate for K_p).

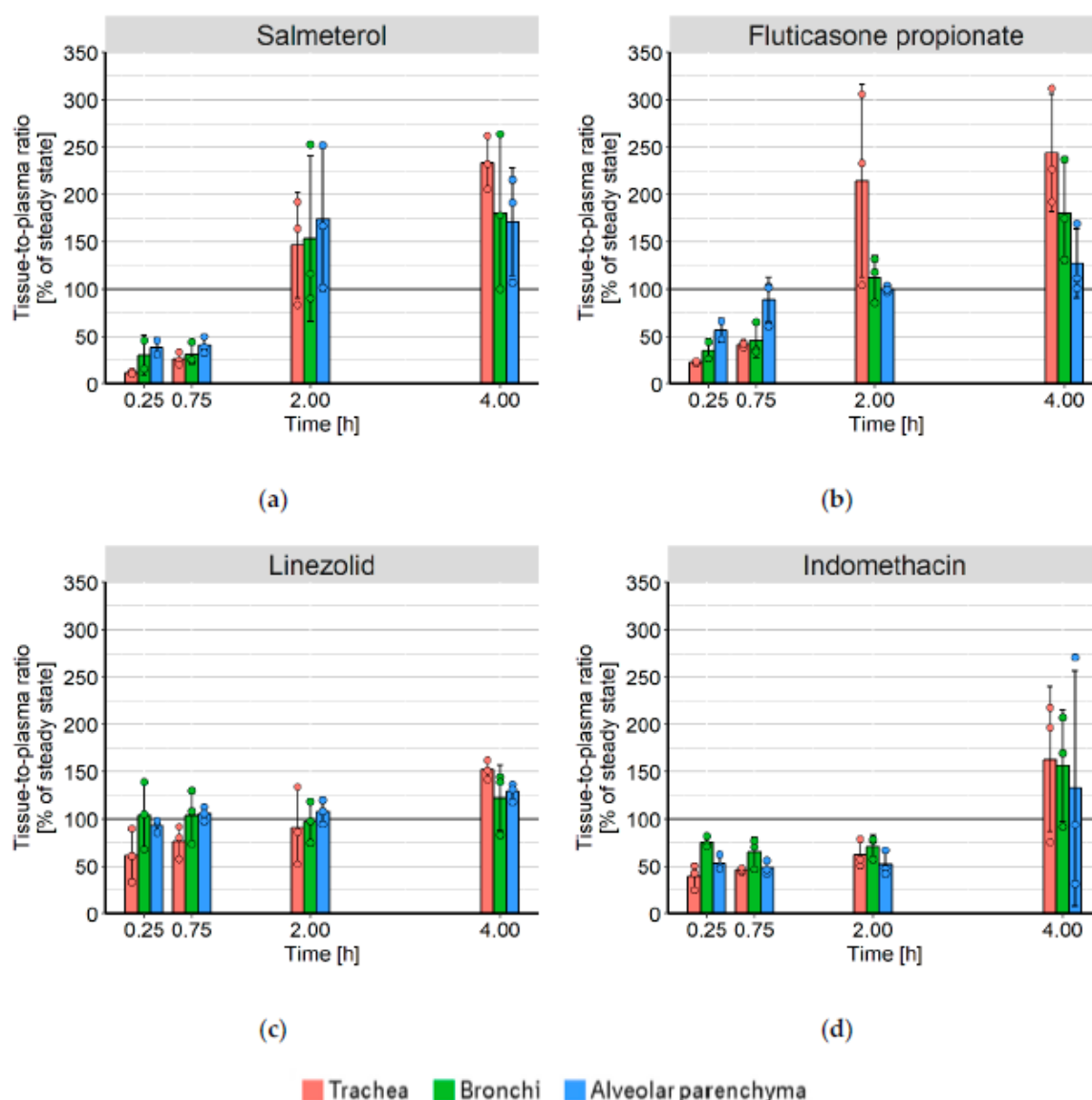


Figure 5. Observed tissue-to-plasma concentration ratios in the trachea (red), bronchi (green), and alveolar parenchyma (blue) as a percentage of steady state (the model estimate of K_p) for (a) salmeterol, (b) fluticasone propionate, (c) linezolid, and (d) indomethacin. The bars represent the mean value including the standard deviation, the filled circles represent the individual data points.

The equilibrium for LIN was achieved much faster than for SAL or FP, with only a slight delay shown in the trachea. The tissue-to-plasma ratios for LIN in the alveolar parenchyma and the bronchi were approximately stable after 15 min. The tissue-to-plasma ratios of SAL and FP were, however, not constant over time. Concentrations in the trachea did not reach steady state within the four-hour experiment, as the ratio between trachea and plasma concentrations was still rising between two and four hours. Tissue-to-plasma ratios of the alveolar parenchyma were stable after two hours but were higher than the expected ratio at steady state for SAL.

3.6. Effect of Distributional Delay on Plasma $EC_{50,Free}$ Estimates of SAL

The extended PK/PD model for SAL was used to simulate unbound plasma and bronchial concentrations and the predicted effect for a range of doses. The simulated effect and unbound plasma concentrations at 0.25 h, 0.75 h, 2 h, and 4 h were used for the determination of PD parameter estimates. Each investigated time point provided different estimates for the plasma $EC_{50,free}$. When compared

to the true value (0.0271 nM) the EC_{50} estimates determined at 0.25 h or 0.75 h overestimated the true $EC_{50,free}$ by 6.62- and 2.62-fold, respectively (Figure 6). However, PD experiments at 2 h or 4 h resulted in an underestimation (0.467- and 0.418-fold) of the $EC_{50,free}$, resulting in an approximately 16-fold divergence of estimates within the investigated timeframe. The ratio between the estimates and the true $EC_{50,free}$ directly corresponded to the ratio between unbound concentrations in plasma and bronchi.

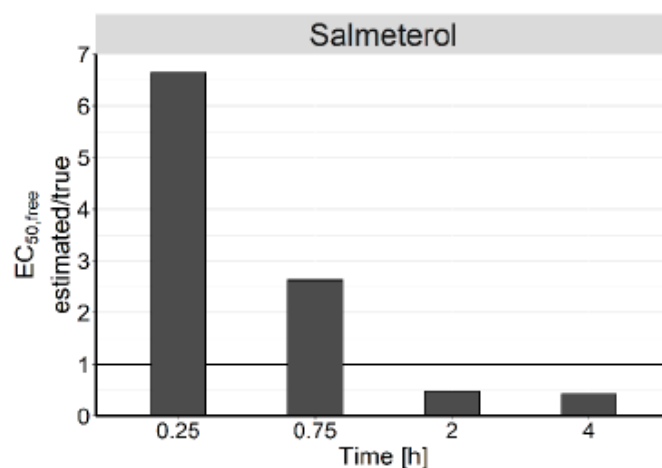


Figure 6. Plasma $EC_{50,free}$ estimates of salmeterol normalized to the true EC_{50} value, determined at four different time points. Unbound bronchial tissue concentrations were assumed to be directly correlated to the effect.

4. Discussion

The present study provides for the first time a systematic quantitative investigation of tissue retention in different pulmonary tissues for a set of four structurally diverse drugs. The retention for the trachea, bronchi, and the alveolar parenchyma of two neutral and one basic drugs was extensively investigated in vivo and was adequately described by a semi-mechanistic PK model. This model described the distribution into lung tissues considering physiological as well as drug driven differences, especially the fraction unbound in plasma, tissue-specific blood flows and K_p values. This investigation also highlights potential pitfalls derived from distributional delays to target tissues, when PK or PD predictions are based on single time point observations.

The available plasma PK data allowed the estimation of systemic PK parameters for FP, LIN, and IND. The plasma PK of SAL, FP, and LIN were best described by two-compartment models, which is in accordance with the literature [9,21,22]. While LIN PK in rats was previously only described by non-compartmental analysis [23], compartmental analyses of human PK typically do employ two compartments [24–26], which supports the use of a two-compartment PK model. IND concentrations in plasma were best captured by a one-compartment model, which is expected for acidic drugs with high plasma protein binding [27].

Preliminary PK studies for other drugs indicated that tissue sampling at three time points (after 1 h, 2 h, and 3 h) would not be sufficient to adequately quantify tracheal blood flow. Therefore, a stochastic simulation-estimation analysis was performed to select an adequate number and timing of tissue samples (Supplementary Material 1, Section 2). Based on these results, the studies to evaluate regional pulmonary disposition included four optimized time points for tissue sampling: Two of them were scheduled within the first hour (during the infusion) to capture the initial delay in tissue concentrations before the distribution equilibrium between plasma and the respective lung tissue is reached. As the blood flow is assumed the limiting parameter for this delay, these measurements were judged the most informative for the estimation of tissue blood flow. The last tissue samples were taken 2 and 4 h after start of the infusion. This 4-h time point was the latest possible time point due to the

experimental setup, which was limited by the maximal tolerated time of anesthesia. The reason for the 4-h time point was to capture the tissue-to-plasma ratio at, or at least nearing distribution equilibrium to support the estimation of K_p .

The here developed study design allowed an adequate estimation of the tissue-specific parameters (CV for most parameters <20%). Exceptions were the K_p values of IND and the bronchial blood flow, which were estimated with only slightly higher imprecision (see Table 1). In the case of IND, the suggested model was not able to accurately capture the pulmonary disposition (compare Figure 3d). This indicates that acidic drugs may provide different pulmonary PK characteristics compared to neutral and basic drugs and that the strictly perfusion-limited approach used in this investigation may not be appropriate for this drug type. However, it has to be noted that this has so far only been shown for one acidic drug. Further studies are necessary to confirm or refute similar behavior for different acids. As IND showed comparable permeability to the other tested drugs, permeability-limited kinetics were not deemed a reasonable explanation, and since binding to plasma proteins was accounted for, this was also deemed improbable as a cause. IND is known for being a substrate of active transport processes [28], so this might be a possible cause of the altered concentration–time profiles in pulmonary tissues.

The results of the *in vivo* PK studies revealed a time-dependency of tissue-to-plasma ratios. The extent of this varied for each drug-tissue combination. The semi-mechanistic PK model was able to describe this behavior based on the drug- and tissue-specific parameters. This was in accordance with the results of previous investigations [7] of regional localization of drugs in the lung, which also showed tissue-specific differences in tissue abundance over time. However, as Hamm et al. only qualitatively evaluated the relative abundance in bronchiolar and peripheral lung tissue at two time points (2 min and 30 min), a quantitative assessment of pulmonary distribution mechanisms was not possible based on their data. In this work, four time points and combination of the tissue distribution data of four drugs with varying physicochemical properties were necessary to achieve adequate estimates for both the pulmonary blood flows and tissue affinity.

The K_p values estimated in this study were vastly different between all four drugs. Out of all four drugs, SAL showed the highest tissue affinity (i.e., the highest estimated K_p values). While SAL is also quite lipophilic ($\log P$ of 2.5), this is likely due to the basic interactions with acidic phospholipids in the tissue (basic pK_a of 9.8). This mechanism has been postulated before to be the major driver of tissue affinity for moderate-to-strong bases (basic $pK_a > 7$) [18,29]. Furthermore, lysosomal trapping is known to play a role in the pulmonary tissue affinity of SAL [30,31], which is also attributable to SAL being a lipophilic base. The other drug showing moderate affinity to pulmonary tissues was FP, a neutral and highly lipophilic drug. For this type of drug, affinity is thought to be mainly determined by hydrophobic interactions with neutral lipids [32]. LIN, the other predominantly neutral drug (basic pK_a of 1.8 [33,34]), did not show any increased affinity to pulmonary tissues in comparison to plasma and the K_p estimates were in a similar range than those reported by Slatter et al. [23]. Since LIN is less lipophilic than FP, and therefore does not have pronounced interactions with lipid structures in the tissue, this was not unexpected. IND showed the lowest affinity to pulmonary tissues, with tissue concentrations being more than two-fold lower than those in plasma. This may in part be due to its high affinity to plasma proteins, keeping the equilibrium on the plasma side. In addition, even though IND is highly lipophilic ($\log P$ of 4.08 [35]), the negative charge may prevent its partitioning into lipid membranes.

In addition to the variation in tissue affinity between the drugs, there were also differences in localized distribution. While FP and IND showed no discernable differences in affinity to the three lung tissues, both SAL and LIN showed higher affinity towards the alveolar parenchyma compared to the conducting airways. This behavior of SAL and FP is in line with the results of Hamm et al. [7]. Since FP and IND are both highly lipophilic and do not show differences in binding across different pulmonary tissues, the regional differences in tissue for both SAL and LIN are likely not caused by the hydrophobic tissue interactions. Instead, as the most pronounced difference was found for SAL, it is

likely that the electrostatic interactions with acidic phospholipids or lysosomal trapping are important contributors to the observed difference in tissue exposure.

As a consequence of the observed regional differences in tissue affinity and blood flow, the semi-mechanistic PK model that included the separate tissue compartments described the local pulmonary concentrations of these drugs better than the model based on total lung concentrations (see Figure 4). The K_p estimates provided by the latter were close to those obtained for the alveolar parenchyma, which is not surprising, as this tissue is assumed to constitute about 80% of the total lung. Additionally, the total lung K_p estimates were in line with those found in the literature. The total lung K_p estimated for SAL (37.7 ± 2.7), FP (6.21 ± 0.73), LIN (0.781 ± 0.035), and IND (0.347 ± 0.086) were close to the values predicted by the Rodgers and Rowland method (32.5, 9.05, 0.706, and 0.228, respectively). The Rodgers and Rowland method is used to predict K_p values based on physicochemical drug properties (pKa, logP, blood-plasma ratio, and plasma protein binding), as well as physiological tissue composition [18,32]. In comparison with K_p values determined by the lung slice method [36], SAL showed slightly lower, (lung slice K_p between 46.5 and 64.8 [30,36]), and FP slightly higher affinity in our experiments (lung slice K_p 3.41 [36]). The overall good agreement indicates that analyses based on total lung concentrations and using K_p prediction methods like the Rodgers and Rowland method may be sufficient for predicting alveolar drug concentration–time profiles. However, if the drug's target is located in the conducting airways, total lung concentrations may not be a meaningful surrogate, especially not for basic drugs.

Differences in pulmonary blood flow also lead to variations in concentrations between the different lung tissues. While the alveolar parenchyma is supplied by the pulmonary circulation (i.e., the total cardiac output), both the bronchi and the trachea are supplied by the systemic circulation. The estimate for alveolar blood flow in rats (10.6 L/h/kg) was lower than most values for cardiac output found in the literature (mean value: 15.1 L/h/kg), but was still within the reported range (10.3–20 L/h/kg [37–41]). The combined blood flows of bronchi and trachea amounted to 0.831 L/h/kg, which is higher compared to literature values for tracheobronchial blood flow (2.1% of cardiac output [12], 0.216–0.420 L/h/kg). However, the estimate for tracheal blood flow (0.054 L/h/kg) was more than two-fold lower than the weight-proportional part of the combined blood flow of 0.116 L/h/kg. To our knowledge, this is the first time that tracheal blood flow in rats has been estimated separately from the bronchial blood flow. Boger et al. [42] implemented generation-specific blood flow in their physiologically-based PK model as a function of airway diameter, based on an equation evaluated with dog data [43]. This relationship has not yet been validated for rats. However, when this equation is applied to the cumulative blood flow of bronchi and trachea found in this investigation, the resulting blood flow for the trachea would amount to 0.066 L/h/kg, which is in agreement with the actual estimate of 0.054 L/h/kg.

The alveolar parenchyma, as the best perfused tissue in the whole body [12], would typically not be expected to show a time delay compared to plasma. However, SAL and FP both showed delayed disposition in the alveolar region. By incorporating plasma protein binding (PPB) into the model this can be adequately described. We assume that the high PPB (>98%) is causative for the observed delayed disposition: Only a small portion of the drug in plasma is actually free to permeate, effectively slowing the partitioning into the lung tissues. The different combinations of tissue affinity, blood flow, and plasma protein binding lead to partitioning rates that are both tissue- and drug-specific. In general, partitioning is slow with high tissue affinity and increases with higher blood flow and fraction unbound. This held true for the trachea, which showed the slowest partitioning rates out of all three tissues.

The fact that the partitioning rate is also drug-specific makes it difficult to estimate the local tissue exposure of drugs based on plasma PK alone. Yet, since studying tissue distribution in humans is rarely possible, plasma PK is often used as a surrogate to infer on the concentration–effect relationship [4]. Our results showed that this approach might lead to very different estimates of $EC_{50,free}$ depending on the time point of the PD experiment. Due to the dependency of partitioning rates on drug properties, the time-dependent variation in PD parameter estimates will differ for each drug. A comparison of

drug potency based on plasma concentrations at a single time point would therefore not be advisable if no information on tissue distribution is available. To overcome some of the weaknesses, a thorough preclinical investigation of the target tissue distribution of new drugs seems meaningful. This definitely helps understanding the PK/PD relationships in animal models. It will also inform translation to humans as unspecific tissue binding seems to be essentially similar over a wide range of species, as shown for brain binding [44].

If tissue distribution data is available from pre-clinical experiments, attempts can be made to extrapolate the relationship to the human situation based on human physiology or allometric principles. In this investigation, pulmonary absorption half-lives were calculated from the model parameter estimates and subsequently extrapolated to human. Even if they cannot be viewed as full pulmonary half-lives, since they do not take the redistribution from plasma to the lung tissues into account, these absorption half-lives should be qualitatively comparable with absorption rate constants used for empirical models of oral inhalation without redistribution to the lung [45–47]. LIN and IND, both drugs that were not optimized for oral inhalation, showed very short absorption half-lives in the range of seconds, indicating a fast equilibrium between pulmonary tissues and plasma. This seems to be in agreement with the assumption that at least part of an orally inhaled drug shows “i.v. bolus-like” absorption after oral inhalation [45,48]. This could be true for the part of drug that is not retained in the lung or limited by slow dissolution. In contrast, SAL and FP show prolonged absorption half-lives in all investigated lung tissues. For SAL, the prolonged duration of effect achieved after oral inhalation has been associated with the pulmonary retention caused by high tissue affinity [2,8]. The pulmonary absorption half-lives calculated for FP ranged from 32 min in the alveolar region to 3.5 h in the trachea. However, most empirical PK models describing plasma PK of FP only identify a single absorption constant. This is in line with the common assumption that FP absorption from the lung is limited by the slow dissolution rather than the absorption itself. Reported absorption rate constants for FP were in the range of dissolution half-lives (3.85 h and 3.47 h, respectively [49,50]). Nevertheless, this investigation showed that even though the limiting factor may be the dissolution, FP still shows moderate retention in the conducting airways due to tissue affinity. There are also empirical models for other drugs that identified several parallel absorption processes [45–47]. For some of the drugs with rather high tissue affinity [46,47], this might be explained by different absorption rate constants depending on the lung region.

This study presents a method towards understanding localized pulmonary retention based on tissue affinity and pulmonary blood flow. However, it has to be noted that this study also showed that for drugs that are subject to permeability-limited kinetics or active transport processes, additional investigations beyond the here applied methods would be required. While permeability-limited kinetics may be implemented using *in vitro* permeability data, there is little quantitative information on expression and especially localization of transport proteins in the lung [51,52]. As most investigated drugs are lipophilic and/or well permeable, the influence of active drug transport on tissue partitioning at steady state was judged low [53]. Even though active transport processes were demonstrated in epithelial cells (i.e., between the tissue and the lining fluids) [51], the influence of the small volume of the epithelial lining fluid would be negligible on the measured pulmonary drug concentrations. Moreover, the here described approach may not be suitable for drugs that show non-linear tissue binding. For example, the sequestration into lysosomes was shown to be saturable at high unbound concentrations (>100 nM) [36]. As the highest unbound concentrations of SAL in this study were below 15 nM, tissue binding should still be within the linear range. However, this linearity might not hold true at very high inhaled doses, in which case the here described parameters could vary for different exposure levels in the lung. In contrast, other binding mechanisms relevant for the model drugs (partitioning into membranes, interactions with acidic phospholipids) are generally not saturable by commonly achieved concentrations [54]. The PK model in this study did not account for the residual blood content of the tissue samples. Even though the samples were obtained after exsanguination and rinsed with saline, especially the peripheral lung sample may still contain relevant amounts of residual

blood (up to 28% [55]). The presence of residual blood in the alveolar parenchyma may be a reason for the comparably low estimate of alveolar blood flow. Furthermore, since lung tissue affinity is also drug-specific, the model cannot be directly adapted to drugs other than those used for the investigation. To achieve this, more work would have to be done to investigate which drug properties are relevant for differences in affinity between trachea, bronchi, and alveolar parenchyma, such as lipophilicity, charge, and affinity to plasma proteins. For a systematic analysis, more data for drugs with different physico-chemical characteristics would be needed. Moreover, an examination of the regional tissue composition with regard to lipid types and lysosome content [56–59] would be very helpful. This data could be used to evaluate if the K_p prediction models such as Rodgers and Rowland can be used to extrapolate the model to different drugs. Additionally, the here presented model could be further extended to oral inhalation. By developing the model on drug PK after intravenous administration, the distribution process between plasma and lung tissue could be investigated separately from other relevant processes. However, to make the model applicable to oral inhalation, the PK processes specific to oral inhalation, like deposition patterns, mucociliary clearance, pulmonary dissolution, and absorption from the epithelial lining fluid [4] would have to be implemented. With these processes included, this type of model could be used to assess advantages and disadvantages of pulmonary drug delivery depending on physico-chemical drug characteristics and the target location within the lung.

5. Conclusions

In summary, this manuscript introduces a semi-mechanistic model to describe regional pulmonary tissue retention based on physiological and drug-specific parameters. The model successfully captured the pulmonary disposition of the investigated neutral and basic drugs. Additional investigations are required; especially regarding acidic drugs since further PK processes in the lung seem to be relevant. The *in vivo* studies showed that structural differences between the conducting airways and the alveolar parenchyma resulted in different tissue affinity and retention times for basic drugs. Considering whole lung concentrations was in most cases not representative of the conducting airways, representing the target site for many locally-acting orally inhaled drugs. The estimated pulmonary blood flows for alveolar parenchyma and cumulative blood flow for both trachea and bronchi were in accordance with literature values. This supports the separate tissue retention estimates for trachea and bronchi, which were, to the knowledge of the authors, reported for the first time in this study.

The high tissue affinity and extensive protein binding of SAL, in combination with low blood flow resulted in marked distributional delay in the conducting airways. Further investigations on the estimation of PD parameters from a single time point revealed that, under these circumstances, plasma concentrations are no valid surrogate for pulmonary target-site concentrations. This work highlights the importance of being aware of the physiologic differences between lung tissues and their impact on local PK, as well as the use of time-resolved PK data combined with model-based approaches to gain a better understanding of local lung retention and local efficacy to guide identification of drugs for lung diseases.

Supplementary Materials: The following are available online at <http://www.mdpi.com/1999-4923/12/5/408/s1>, Supplementary material 1: Stochastic simulation-estimation (SSE) study, Bioanalysis, Figure S1: Chemical structures of the four model drugs, Table S1: Physicochemical characteristics of the model drugs, Figure S2: Structure of the model used in the SSE study, Table S2: Parameters used for the simulation of concentration–time profiles for the SSE study, Table S3: Bias (mean) and coefficient of variation (CV) of the parameter estimates from the SSE study, Figure S3: Parameter estimate distribution for the initial and optimized study designs, Table S4: Study design and sample weights, Figure S4–S8: Calibration curves and exemplary LC-MS chromatograms, Figure S9: Concentration–time profiles predicted for plasma (black) and total lung in comparison to the observed concentrations in the separate lung tissues, Supplementary Material 2: Phoenix model code.

Author Contributions: Conceptualization, A.H., C.B., S.G.W., and J.M.B.; Data curation, C.B.; Formal analysis, A.H.; Funding acquisition, S.G.W.; Investigation, A.H. and C.B.; Methodology, A.H., C.B., S.G.W., and J.M.B.; Project administration, S.G.W. and J.M.B.; Resources, S.G.W. and J.M.B.; Software, A.H. and S.G.W.; Supervision, C.B., S.G.W., and J.M.B.; Validation, A.H., S.G.W., and J.M.B.; Visualization, A.H.; Writing—original draft, A.H.;

Writing—review and editing, A.H., C.B., S.G.W., and J.M.B. All authors have read and agreed to the published version of the manuscript.

Funding: This research was funded by Boehringer Ingelheim Pharma GmbH & Co. KG.

Acknowledgments: We thank Anne Weber, Heidi Assfalg, and Nadine Klick for the excellent performance of the in vivo experiments as well as Tom Bretschneider for the bioanalytical support. We would also like to thank Achim Sauer for proofreading and valuable discussions. Additional thanks goes to Sylvia Blum who developed the novel lung preparation technique.

Conflicts of Interest: Clemens Braun and Jens Markus Borghardt are employees at Boehringer Ingelheim Pharma GmbH & Co. KG, Biberach, Germany. The PhD work of Anneke Himstedt is funded by Boehringer Ingelheim Pharma GmbH & Co. KG. Sebastian Wicha received research grants from Boehringer Ingelheim Pharma GmbH & Co. KG related to the here published work.

References

1. Kelly, H.W. Establishing a therapeutic index for the inhaled corticosteroids: Part i: Pharmacokinetic/pharmacodynamic comparison of the inhaled corticosteroids. *J. Allergy Clin. Immunol.* **1998**, *102*, S36–S51. [[CrossRef](#)]
2. Lombardi, D.; Cuenoud, B.; Krämer, S.D. Lipid membrane interactions of indacaterol and salmeterol: Do they influence their pharmacological properties? *Eur. J. Pharm. Sci.* **2009**, *38*, 533–547. [[CrossRef](#)] [[PubMed](#)]
3. Begg, M.; Edwards, C.D.; Hamblin, J.N.; Pefani, E.; Wilson, R.; Gilbert, J.; Vitulli, G.; Mallett, D.; Morrell, J.; Hingle, M.I. Translation of inhaled drug optimization strategies into clinical pharmacokinetics and pharmacodynamics using gsk2292767a, a novel inhaled phosphoinositide 3-kinase δ inhibitor. *J. Pharmacol. Exp. Ther.* **2019**, *369*, 443–453. [[CrossRef](#)] [[PubMed](#)]
4. Borghardt, J.M.; Kloft, C.; Sharma, A. Inhaled therapy in respiratory disease: The complex interplay of pulmonary kinetic processes. *Can. Respir. J.* **2018**, *2018*, 1–12. [[CrossRef](#)]
5. Mutlu, G.M.; Factor, P. Alveolar epithelial β 2-adrenergic receptors. *Am. J. Respir. Cell Mol. Biol.* **2008**, *38*, 127–134. [[CrossRef](#)]
6. Backstrom, E.; Hamm, G.; Nilsson, A.; Fihn, B.M.; Strittmatter, N.; Andren, P.; Goodwin, R.J.A.; Friden, M. Uncovering the regional localization of inhaled salmeterol retention in the lung. *Drug Deliv.* **2018**, *25*, 838–845. [[CrossRef](#)]
7. Hamm, G.R.; Bäckström, E.; Brülls, M.; Nilsson, A.; Strittmatter, N.; Andrén, P.E.; Grime, K.; Fridén, M.; Goodwin, R.J. Revealing the regional localization and differential lung retention of inhaled compounds by mass spectrometry imaging. *J. Aerosol Med. Pulm. Drug Deliv.* **2020**, *33*, 43–53. [[CrossRef](#)]
8. Hendrickx, R.; Bergström, E.L.; Janzén, D.L.L.; Fridén, M.; Eriksson, U.; Grime, K.; Ferguson, D. Translational model to predict pulmonary pharmacokinetics and efficacy in man for inhaled bronchodilators. *CPT Pharmacomet. Syst. Pharmacol.* **2018**, *7*, 147–157. [[CrossRef](#)]
9. Weber, B.; Hochhaus, G. A pharmacokinetic simulation tool for inhaled corticosteroids. *AAPS J.* **2013**, *15*, 159–171. [[CrossRef](#)]
10. Iqbal, K.; Broeker, A.; Nowak, H.; Rahmel, T.; Nussbaumer-Pröll, A.; Österreicher, Z.; Zeitlinger, M.; Wicha, S. A pharmacometric approach to define target site-specific breakpoints for bacterial killing and resistance suppression integrating microdialysis, time-kill curves and heteroresistance data: A case study with moxifloxacin. *Clin. Microbiol. Infect.* **2020**. [[CrossRef](#)]
11. Boger, E.; Evans, N.; Chappell, M.; Lundqvist, A.; Ewing, P.; Wigenborg, A.; Fridén, M. Systems pharmacology approach for prediction of pulmonary and systemic pharmacokinetics and receptor occupancy of inhaled drugs. *CPT Pharmacomet. Syst. Pharmacol.* **2016**, *5*, 201–210. [[CrossRef](#)] [[PubMed](#)]
12. Brown, R.P.; Delp, M.D.; Lindstedt, S.L.; Rhomberg, L.R.; Beliles, R.P. Physiological parameter values for physiologically based pharmacokinetic models. *Toxicol. Ind. Health* **1997**, *13*, 407–484. [[CrossRef](#)] [[PubMed](#)]
13. Anderson, P.J.; Zhou, X.; Breen, P.; Gann, L.; Logsdon, T.W.; Compadre, C.M.; Hiller, F.C. Pharmacokinetics of (r, s)-albuterol after aerosol inhalation in healthy adult volunteers. *J. Pharm. Sci.* **1998**, *87*, 841–844. [[CrossRef](#)] [[PubMed](#)]
14. Minto, C.; Li, B.; Tattam, B.; Brown, K.; Seale, J.P.; Donnelly, R. Pharmacokinetics of epimeric budesonide and fluticasone propionate after repeat dose inhalation—intersubject variability in systemic absorption from the lung. *Br. J. Clin. Pharmacol.* **2000**, *50*, 116–124. [[CrossRef](#)]

15. Rohatagi, S.; Arya, V.; Zech, K.; Nave, R.; Hochhaus, G.; Jensen, B.; Barrett, J. Population pharmacokinetics and pharmacodynamics of ciclesonide. *J. Clin. Pharmacol.* **2003**, *43*, 365–378. [[CrossRef](#)]
16. Ting, L.; Aksenov, S.; Bhansali, S.; Ramakrishna, R.; Tang, P.; Geller, D. Population pharmacokinetics of inhaled tobramycin powder in cystic fibrosis patients. *CPT Pharmacomet. Syst. Pharmacol.* **2014**, *3*, 1–7. [[CrossRef](#)]
17. Wu, K.; Goyal, N.; Stark, J.G.; Hochhaus, G. Evaluation of the administration time effect on the cumulative cortisol suppression and cumulative lymphocytes suppression for once-daily inhaled corticosteroids: A population modeling/simulation approach. *J. Clin. Pharmacol.* **2008**, *48*, 1069–1080. [[CrossRef](#)]
18. Rodgers, T.; Leahy, D.; Rowland, M. Physiologically based pharmacokinetic modeling 1: Predicting the tissue distribution of moderate-to-strong bases. *J. Pharm. Sci.* **2005**, *94*, 1259–1276. [[CrossRef](#)]
19. Johnson, M.; Butchers, P.; Coleman, R.; Nials, A.; Strong, P.; Summer, M.; Vardey, C.; Whelan, C. The pharmacology of salmeterol. *Life Sci.* **1993**, *52*, 2131–2143. [[CrossRef](#)]
20. R Core Team. *A Language and Environment for Statistical Computing*, 3.3.2; R Foundation for Statistical Computing: Vienna, Austria, 2016.
21. Bhagwat, S.; Schilling, U.; Chen, M.J.; Wei, X.; Delvadia, R.; Absar, M.; Saluja, B.; Hochhaus, G. Predicting pulmonary pharmacokinetics from in vitro properties of dry powder inhalers. *Pharm. Res.* **2017**, *34*, 2541–2556. [[CrossRef](#)]
22. Soulele, K.; Macheras, P.; Karalis, V. Pharmacokinetic analysis of inhaled salmeterol in asthma patients: Evidence from two dry powder inhalers. *Biopharm. Drug Dispos.* **2017**, *38*, 407–419. [[CrossRef](#)] [[PubMed](#)]
23. Slatter, J.G.; Adams, L.A.; Bush, E.C.; Chiba, K.; Daley-Yates, P.T.; Feenstra, K.L.; Koike, S.; Ozawa, N.; Peng, G.W.; Sams, J.P.; et al. Pharmacokinetics, toxicokinetics, distribution, metabolism and excretion of linezolid in mouse, rat and dog. *Xenobiotica* **2002**, *32*, 907–924. [[CrossRef](#)] [[PubMed](#)]
24. Beringer, P.; Nguyen, M.; Hoem, N.; Louie, S.; Gill, M.; Gurevitch, M.; Wong-Beringer, A. Absolute bioavailability and pharmacokinetics of linezolid in hospitalized patients given enteral feedings. *Antimicrob. Agents Chemother.* **2005**, *49*, 3676. [[CrossRef](#)] [[PubMed](#)]
25. Bhalodi, A.A.; Papasavas, P.K.; Tishler, D.S.; Nicolau, D.P.; Kuti, J.L. Pharmacokinetics of intravenous linezolid in moderately to morbidly obese adults. *Antimicrob. Agents Chemother.* **2013**, *57*, 1144. [[CrossRef](#)]
26. Plock, N.; Buerger, C.; Joukhadar, C.; Kljucar, S.; Kloft, C. Does linezolid inhibit its own metabolism?—population pharmacokinetics as a tool to explain the observed nonlinearity in both healthy volunteers and septic patients. *Drug Metab. Dispos.* **2007**, *35*, 1816–1823. [[CrossRef](#)]
27. Pilari, S.; Huisinga, W. Lumping of physiologically-based pharmacokinetic models and a mechanistic derivation of classical compartmental models. *J. Pharmacokinet. Pharmacodyn.* **2010**, *37*, 365–405. [[CrossRef](#)]
28. Kouzuki, H.; Suzuki, H.; Sugiyama, Y. Pharmacokinetic study of the hepatobiliary transport of indomethacin. *Pharm. Res.* **2000**, *17*, 432–438. [[CrossRef](#)]
29. Rodgers, T.; Leahy, D.; Rowland, M. Tissue distribution of basic drugs: Accounting for enantiomeric, compound and regional differences amongst β -blocking drugs in rat. *J. Pharm. Sci.* **2005**, *94*, 1237–1248. [[CrossRef](#)]
30. Bäckström, E.; Boger, E.; Lundqvist, A.; Hammarlund-Udenaes, M.; Fridén, M. Lung retention by lysosomal trapping of inhaled drugs can be predicted in vitro with lung slices. *J. Pharm. Sci.* **2016**, *105*, 3432–3439. [[CrossRef](#)]
31. Kazmi, F.; Hensley, T.; Pope, C.; Funk, R.S.; Loewen, G.J.; Buckley, D.B.; Parkinson, A. Lysosomal sequestration (trapping) of lipophilic amine (cationic amphiphilic) drugs in immortalized human hepatocytes (fa2n-4 cells). *Drug Metab. Dispos.* **2013**, *41*, 897–905. [[CrossRef](#)]
32. Rodgers, T.; Rowland, M. Physiologically based pharmacokinetic modelling 2: Predicting the tissue distribution of acids, very weak bases, neutrals and zwitterions. *J. Pharm. Sci.* **2006**, *95*, 1238–1257. [[CrossRef](#)] [[PubMed](#)]
33. Chiang, P.-C.; Hu, Y. Simultaneous determination of log_d, log_p, and p_{ka} of drugs by using a reverse phase hplc coupled with a 96-well plate auto injector. *Comb. Chem. High Throughput Screen.* **2009**, *12*, 250–257. [[CrossRef](#)] [[PubMed](#)]
34. Taylor, R.; Sunderland, B.; Luna, G.; Czarniak, P. Evaluation of the stability of linezolid in aqueous solution and commonly used intravenous fluids. *Drug Des. Dev. Ther.* **2017**, *11*, 2087. [[CrossRef](#)] [[PubMed](#)]
35. Inagi, T.; Muramatsu, T.; Nagai, H.; Terada, H. Mechanism of indomethacin partition between n-octanol and water. *Chem. Pharm. Bull.* **1981**, *29*, 2330–2337. [[CrossRef](#)]

36. Bäckström, E.; Lundqvist, A.; Boger, E.; Svanberg, P.; Ewing, P.; Hammarlund-Udenaes, M.; Fridén, M. Development of a novel lung slice methodology for profiling of inhaled compounds. *J. Pharm. Sci.* **2016**, *105*, 838–845. [[CrossRef](#)]
37. Coleman, T.G. Cardiac output by dye dilution in the conscious rat. *J. Appl. Physiol.* **1974**, *37*, 452–455. [[CrossRef](#)]
38. Delp, M.; Manning, R.; Bruckner, J.; Armstrong, R. Distribution of cardiac output during diurnal changes of activity in rats. *Am. J. Physiol.-Heart Circ. Physiol.* **1991**, *261*, H1487–H1493. [[CrossRef](#)]
39. Hachamovitch, R.; Wicker, P.; Capasso, J.M.; Anversa, P. Alterations of coronary blood flow and reserve with aging in fischer 344 rats. *Am. J. Physiol.-Heart Circ. Physiol.* **1989**, *256*, H66–H73. [[CrossRef](#)]
40. Tsuchiya, M.; Ferrone, R.A.; Walsh, G.M.; Frohlich, E.D. Regional blood flows measured in conscious rats by combined fick and microsphere methods. *Am. J. Physiol.-Heart Circ. Physiol.* **1978**, *235*, H357–H360. [[CrossRef](#)]
41. Walsh, G.M.; Tsuchiya, M.; Frohlich, E.D. Direct fick application for measurement of cardiac output in rat. *J. Appl. Physiol.* **1976**, *40*, 849–853. [[CrossRef](#)]
42. Boger, E.; Fridén, M. Physiologically based pharmacokinetic/pharmacodynamic modeling accurately predicts the better bronchodilatory effect of inhaled versus oral salbutamol dosage forms. *J. Aerosol. Med. Pulm. Drug Deliv.* **2019**, *32*, 1–12. [[CrossRef](#)] [[PubMed](#)]
43. Bernard, S.L.; Glenn, R.W.; Polissar, N.L.; Luchtel, D.L.; Lakshminarayan, S. Distribution of pulmonary and bronchial blood supply to airways measured by fluorescent microspheres. *J. Appl. Physiol.* **1996**, *80*, 430–436. [[CrossRef](#)] [[PubMed](#)]
44. Di, L.; Umland, J.P.; Chang, G.; Huang, Y.; Lin, Z.; Scott, D.O.; Troutman, M.D.; Liston, T.E. Species independence in brain tissue binding using brain homogenates. *Drug Metab. Dispos.* **2011**, *39*, 1270–1277. [[CrossRef](#)] [[PubMed](#)]
45. Bartels, C.; Looby, M.; Sechaud, R.; Kaiser, G. Determination of the pharmacokinetics of glycopyrronium in the lung using a population pharmacokinetic modelling approach. *Br. J. Clin. Pharmacol.* **2013**, *76*, 868–879. [[CrossRef](#)]
46. Borghardt, J.M.; Weber, B.; Staab, A.; Kunz, C.; Formella, S.; Kloft, C. Investigating pulmonary and systemic pharmacokinetics of inhaled olodaterol in healthy volunteers using a population pharmacokinetic approach. *Br. J. Clin. Pharmacol.* **2016**, *81*, 538–552. [[CrossRef](#)]
47. Melin, J.; Prothon, S.; Kloft, C.; Cleton, A.; Amilon, C.; Jorup, C.; Bäckman, P.; Olsson, B.; Hamrén, U.W. Pharmacokinetics of the inhaled selective glucocorticoid receptor modulator azd5423 following inhalation using different devices. *AAPS J.* **2017**, *19*, 865–874. [[CrossRef](#)]
48. Soulele, K.; Macheras, P.; Silvestro, L.; Savu, S.R.; Karalis, V. Population pharmacokinetics of fluticasone propionate/salmeterol using two different dry powder inhalers. *Eur. J. Pharm. Sci.* **2015**, *80*, 33–42. [[CrossRef](#)]
49. Krishnaswami, S.; Hochhaus, G.; Möllmann, H.; Barth, J.; Derendorf, H. Interpretation of absorption rate data for inhaled fluticasone propionate obtained in compartmental pharmacokinetic modeling. *Int. J. Clin. Pharmacol. Ther.* **2005**, *43*, 117–122. [[CrossRef](#)]
50. Rohrschneider, M.; Bhagwat, S.; Krampe, R.; Michler, V.; Breitzkreutz, J.; Hochhaus, G. Evaluation of the transwell system for characterization of dissolution behavior of inhalation drugs: Effects of membrane and surfactant. *Mol. Pharm.* **2015**, *12*, 2618–2624. [[CrossRef](#)]
51. Bosquillon, C. Drug transporters in the lung—do they play a role in the biopharmaceutics of inhaled drugs? *J. Pharm. Sci.* **2010**, *99*, 2240–2255. [[CrossRef](#)]
52. Sakamoto, A.; Matsumaru, T.; Yamamura, N.; Uchida, Y.; Tachikawa, M.; Ohtsuki, S.; Terasaki, T. Quantitative expression of human drug transporter proteins in lung tissues: Analysis of regional, gender, and interindividual differences by liquid chromatography–tandem mass spectrometry. *J. Pharm. Sci.* **2013**, *102*, 3395–3406. [[CrossRef](#)] [[PubMed](#)]
53. Horvath, G.; Mendes, E.S.; Schmid, N.; Schmid, A.; Conner, G.E.; Salathe, M.; Wanner, A. The effect of corticosteroids on the disposal of long-acting β_2 -agonists by airway smooth muscle cells. *J. Allergy Clin. Immunol.* **2007**, *120*, 1103–1109. [[CrossRef](#)] [[PubMed](#)]
54. Hallifax, D.; Houston, J.B. Saturable uptake of lipophilic amine drugs into isolated hepatocytes: Mechanisms and consequences for quantitative clearance prediction. *Drug Metab. Dispos.* **2007**, *35*, 1325–1332. [[CrossRef](#)] [[PubMed](#)]

55. Oeff, K.; König, A. Das blutvolumen einiger rattenorgane und ihre restblutmenge nach entbluten bzw. Durchspülung. Bestimmung mit p32-markierten erythrocyten. *Naunyn-Schmiedebergs Archiv für Experimentelle Pathologie und Pharmakologie* **1955**, *226*, 98–102. [PubMed]
56. Bligh, E.G.; Dyer, W.J. A rapid method of total lipid extraction and purification. *Can. J. Biochem. Physiol.* **1959**, *37*, 911–917. [CrossRef] [PubMed]
57. Folch, J.; Lees, M.; Sloane Stanley, G.H. A simple method for the isolation and purification of total lipides from animal tissues. *J. Biol. Chem.* **1957**, *226*, 497–509.
58. Koivusalo, M.; Haimi, P.; Heikinheimo, L.; Kostianen, R.; Somerharju, P. Quantitative determination of phospholipid compositions by esi-ms: Effects of acyl chain length, unsaturation, and lipid concentration on instrument response. *J. Lipid Res.* **2001**, *42*, 663–672.
59. Pulfer, M.; Murphy, R.C. Electrospray mass spectrometry of phospholipids. *Mass. Spectrom. Rev.* **2003**, *22*, 332–364. [CrossRef]



© 2020 by the authors. Licensee MDPI, Basel, Switzerland. This article is an open access article distributed under the terms and conditions of the Creative Commons Attribution (CC BY) license (<http://creativecommons.org/licenses/by/4.0/>).

3.2 Publication II: Identifying favorable drug characteristics for potential oral inhalation drugs

Understanding the suitability of established antibiotics for oral inhalation from a pharmacokinetic perspective: an integrated model-based investigation based on rifampicin, ciprofloxacin and tigecycline in vivo data

Anneke Himstedt, Clemens Braun, Sebastian G. Wicha,
Jens M. Borghardt

Journal of Antimicrobial Chemotherapy, 77(11) (2022) 2922-2932

Impact factor: 5.758 (2022)

Synopsis:

Apart from chronic lung diseases like asthma and COPD, oral inhalation is often considered an attractive route of administration for anti-infective treatment of pulmonary infections. However, few antibiotics have been approved for inhaled use, as most cases are off-label nebulization of parenteral formulations, and little is known about local concentrations after oral administration. Because established antibiotics are optimized for oral or parenteral administration, their physicochemical characteristics differ from those considered optimal for inhalation. The presumed benefits derived from experience with inhaled asthma and COPD medications may not hold true for all re-purposed antibiotics.

Here, the rat PBPK model developed for publication I (3.1) was refined to include a differentiation between ELF, interstitial, and intracellular space. The model was then applied to detailed tissue distribution data after i.v. infusion of rifampicin, ciprofloxacin, and tigecycline, respectively. This allowed evaluating concentrations in plasma, trachea, bronchi, and alveolar tissue, as well as tracheal and (bronchio-)alveolar lining fluid within the same animals. In a second step, the model was humanized and extended to allow simulations of the PK after oral inhalation. After linking the PK compartments to bacterial PK/PD models, an exemplary sensitivity analysis was conducted to identify favorable drug characteristics for the oral-inhaled switch of established antibiotics on the one hand, and the development of new inhaled antibiotics on the other hand. Simulations of antibacterial efficacy were used to investigate benefits of oral inhalation over i.v. administration for the selected drugs, as well as the impact of specific PK optimization based on the established inhaled drug salmeterol.

The model successfully described the systemic and pulmonary PK of all three drugs observed in rats. The simulations of bronchial intracellular and ELF-residing bacteria suggested low permeability, a high epithelial efflux ratio, and long post-antibiotic effect as the driving parameters for local efficacy. Typical optimization parameters for orally inhaled drugs served mainly to increase pulmonary selectivity and had less influence on pure efficacy.

Understanding the suitability of established antibiotics for oral inhalation from a pharmacokinetic perspective: an integrated model-based investigation based on rifampicin, ciprofloxacin and tigecycline *in vivo* data

Anneke Himstedt^{1,2}, Clemens Braun², Sebastian Georg Wicha^{1†} and Jens Markus Borghardt^{2*†}

¹Department of Clinical Pharmacy, Institute of Pharmacy, University of Hamburg, Hamburg, Germany; ²Research DMPK, Drug Discovery Sciences, Boehringer Ingelheim Pharma GmbH & Co. KG, Biberach, Germany

*Corresponding author. E-mail: Jens_Markus.Borghardt@boehringer-ingelheim.com
†Authors contributed equally.

Received 8 March 2022; accepted 16 June 2022

Background: Treating pulmonary infections by administering drugs via oral inhalation represents an attractive alternative to usual routes of administration. However, the local concentrations after inhalation are typically not known and the presumed benefits are derived from experiences with drugs specifically optimized for inhaled administration.

Objectives: A physiologically based pharmacokinetic/pharmacodynamic (PBPK/PD) model was developed to elucidate the pulmonary PK for ciprofloxacin, rifampicin and tigecycline and link it to bacterial PK/PD models. An exemplary sensitivity analysis was performed to potentially guide drug optimization regarding local efficacy for inhaled antibiotics.

Methods: Detailed pulmonary tissue, endothelial lining fluid and systemic *in vivo* drug concentration–time profiles were simultaneously measured for all drugs in rats after intravenous infusion. Using this data, a PBPK/PD model was developed, translated to humans and adapted for inhalation. Simulations were performed comparing potential benefits of oral inhalation for treating bronchial infections, covering intracellular pathogens and bacteria residing in the bronchial epithelial lining fluid.

Results: The PBPK/PD model was able to describe pulmonary PK in rats. Often applied optimization parameters for orally inhaled drugs (e.g. high systemic clearance and low oral bioavailability) showed little influence on efficacy and instead mainly increased pulmonary selectivity. Instead, low permeability, a high epithelial efflux ratio and a pronounced post-antibiotic effect represented the most impactful parameters to suggest a benefit of inhalation over systemic administration for locally acting antibiotics.

Conclusions: The present work might help to develop antibiotics for oral inhalation providing high pulmonary concentrations and fast onset of exposure coupled with lower systemic drug concentrations.

Introduction

Oral drug inhalation is often investigated for treatment of pulmonary infections,^{1–4} as it is expected to achieve high and fast target-site exposure with limited systemic concentrations by means of direct administration to the target site. This avoids the first-pass effect in the liver, especially for drugs with low oral bioavailability or limited lung penetration from the systemic circulation. Typically, the bronchial lining fluid or sputum is the assumed infection site, and only in severe cases the infection is also delocalized into the pulmonary tissues, resulting in direct target-site exposure after oral inhalation.^{4–6} While there are a few commercially available formulations for oral inhalation (e.g. inhaled

formulations of tobramycin and colistin for the treatment of cystic fibrosis), often inhaled administration of antibiotics is off-label use of parenteral formulations (e.g. nebulization of aztreonam or levofloxacin), for which a systematic comparison to the intravenous or oral route has not been performed.^{7,8} While tobramycin exhibits prolonged pulmonary exposure and high efficacy after oral inhalation,⁹ presumably due to its polar nature and low permeability, the same could not be shown for ciprofloxacin.¹⁰ In conclusion, not all attempts at reconstituting an established antibiotic drug for oral inhalation have been successful.

Established oral or parenterally administered antibiotics typically have distinct pharmacokinetic (PK) and pharmacodynamic (PD) characteristics from drugs specifically optimized for inhaled

Himstedt et al.

administration. For these optimized drugs, the advantages of inhalation over systemic administration were well investigated,¹¹ e.g. β -sympathomimetic drugs, such as salmeterol, generally show high potency, high systemic clearance, high affinity to lung tissue, and/or low solubility to increase the duration of local exposure and the pulmonary selectivity. Developing a molecule designed for oral inhalation is a challenging endeavour, both due to the respiratory system being a highly complex heterogeneous target and the increased variability added by specific processes associated with oral inhalation, such as the inhalation manoeuvre, drug deposition and mucociliary clearance.¹¹ While switching from oral or intravenous administration to oral inhalation during drug discovery often leads to the design of molecules exhibiting completely different PK and PD characteristics than the original drug candidates,¹¹ this extensive redesigning is not possible for already established drugs. With regards to antibiotics, there remains a lack of quantitative knowledge about the local PK and its relevance on the PD outcome. The question remains whether the same benefits shown by optimized drugs for inhalation can also be assumed for the inhalation of antibiotics, which were not specifically optimized for inhalation.

One way to measure pulmonary drug concentrations in the clinics is bronchioalveolar lavage fluid (BALF) sampling. However, this is seldom done in a time-dependent manner and has limited value for differentiation of regional concentrations, e.g. conducting airways versus alveolar region, or extracellular versus intracellular space. This can lead to uncertainty regarding the optimal dose and posology for newly inhaled antibiotics,⁴ as well as their general suitability for oral inhalation. Therefore, questions remain, which antibiotics are well suited for oral inhalation even without further optimization and what characteristics should be the focus when aiming towards optimizing antibiotics for oral inhalation based on some well-known chemical structures for commonly applied antibiotics.

To provide some guidance for these questions, the objectives of the here presented investigation were to (i) develop a semi-mechanistic physiology based (PB)PK model to elucidate the systemic and pulmonary PK of the three model drugs ciprofloxacin, rifampicin and tigecycline after intravenous administration in rats and scale this towards oral inhalation in human, and (ii) to investigate the influence of drug-specific PK/PD parameters on local and systemic efficacy after oral inhalation in human to provide insights on desirable properties for a switch from oral or intravenous administration to inhalation.

Materials and methods

Chemicals

Rifampicin was sourced from the in-house compound dispensary at Boehringer Ingelheim Pharma GmbH & Co. KG, (Biberach, Germany). Ciprofloxacin, meropenem and tigecycline were purchased from Sigma-Aldrich (St Louis, MO, USA) and TCI Deutschland GmbH (Eschborn, Germany), respectively. Deuterated internal standards were purchased for rifampicin [2H8-rifampicin, (ALSACHIM, Duisburg, Germany)], meropenem (meropenem-d6, Sigma-Aldrich) and ciprofloxacin (ciprofloxacin-d8, Sigma-Aldrich). Tetracycline (Sigma-Aldrich) was used as an internal standard for tigecycline.

Animal experiments

Twelve male Han Wistar rats, weighing 276–321 g (mean 298 g), purchased from Janvier Labs (Le Genest-Saint-Isle, France) were used for the *in vivo* studies. All animal care and experimental procedures were conducted in compliance with the German and European Animal Welfare Act (EU Directive 2010/63/EU) and were approved by the Regierungspräsidium Tübingen as the responsible local German authority (license reference number 19-013-G).

A cassette of ciprofloxacin, rifampicin, meropenem and tigecycline was infused over 1 h (5 mg/kg, infusion rate 5 mL/h/kg) to the anaesthetized animals using a standard infusion pump. At 0.25, 0.75, 1.5 and 4 h after start of the infusion ($N=3$ rats/timepoint), the rats were exsanguinated in deep anaesthesia. The lung was dissected into trachea, the left and right lung and peripheral alveolar tissue. By flushing with buffer, epithelial lining fluid (ELF) was collected from the trachea and the left lung. Bronchial tissue was prepared from the left and right lung lobes. Tissue samples were prepared as described previously.¹² Blood was sampled until the end of the respective experiment and plasma samples were prepared. All samples were stored at -20°C . More details about the experimental procedure and the sample preparation can be found in the Supplementary data (Supplementary Sections 1 and 2 and Table S1, available as Supplementary data at JAC Online).

Bioanalysis

Drug concentrations in plasma, ELF and tissue homogenates were determined by HPLC-MS/MS (Supplementary Section 3 and Tables S2 and S3). Prior to bioanalysis, plasma and tissue samples were spiked with internal standard solution and diluted with acetonitrile for protein precipitation. ELF concentrations were corrected by the ratio of urea concentrations in plasma and ELF samples to correct for the dilution during the sampling process.

PBPK model

The PBPK modelling analysis was carried out in Phoenix WinNonlinTM 8.0 (Certara, L.P., Princeton, NJ, USA). The semi-mechanistic model consisted of an empirical systemic PK model and physiologically based representations of the different lung regions (see Figure 1a). The tissue compartments for trachea, bronchi and alveolar region were further divided into interstitial space, intracellular space and ELF with permeability-based distribution kinetics. The apparent permeability in the model (P_{app}) refers to the crossing of two lipid bilayers. Since crossing from interstitial space into cells only involves one membrane, this permeation process was assumed to be twice as fast. The systemic PK parameters were estimated based on the rat plasma concentration-time data. This resulted in empirical one- or two-compartment models depending on the drug characteristics. Pulmonary tissue-specific physiological parameters such as volumes and surface areas were defined based on available physiological values from literature,^{13,14} and blood flows characterizing the perfusion of the different parts of the lung were based on previous work¹² (Table 1). The remaining drug-specific parameters (partition coefficients $K_{pU,T/B/A}$, efflux ratios $Eff_{T/A}$ and apparent permeabilities P_{app}) were estimated from the rat PK data. Drug binding was assumed to be the same in plasma and tissue interstitium, while binding to cellular components was described by K_{pu} values. To fit the model to the observed tissue concentration-time profiles, total tissue concentrations were calculated from the separate tissue compartments (e.g. the tracheal tissue concentration was calculated as a weighted average of all related tracheal compartments). As there were no measurements of bronchial ELF to inform the efflux ratio, the same value which was estimated for the trachea was used, assuming higher similarity of the epithelial constitution and transporter expression between the bronchi and the trachea than between bronchi and the alveolar region.¹⁵ The decision to estimate P_{app} instead of using measured

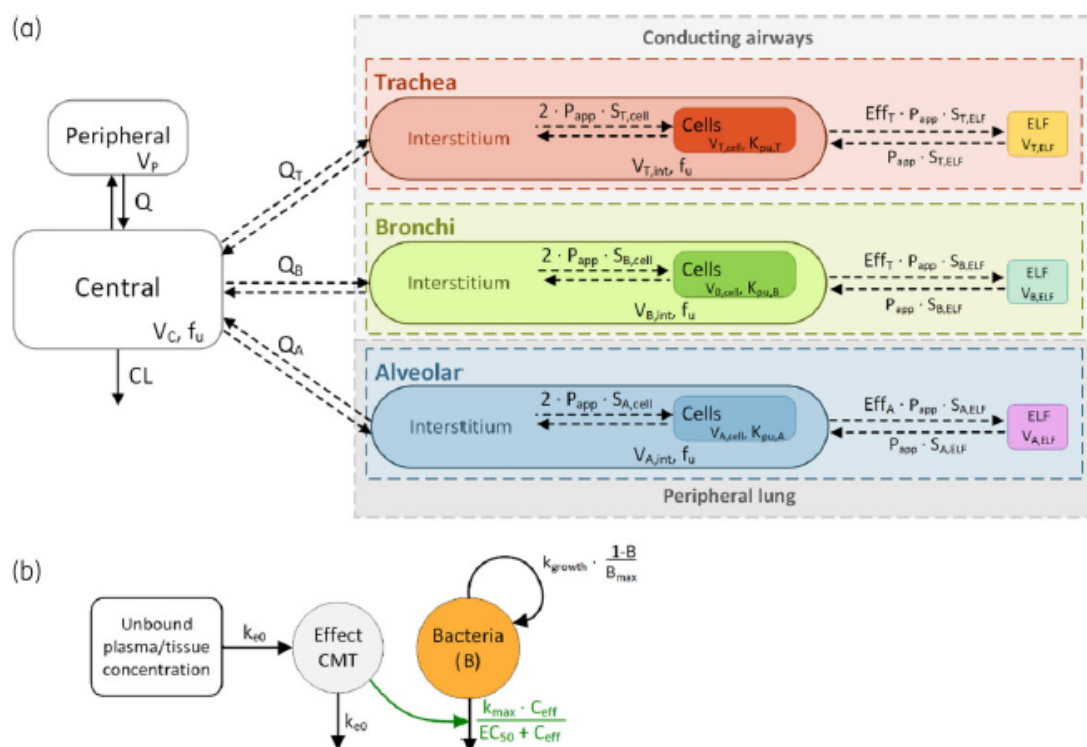


Figure 1. Structure of (a) the PK and (b) the PD model. The coloured boxes with dashed outlines (trachea, bronchi and alveolar) depict the combination of compartments corresponding to the measured total tissue concentrations. Parameters of the PK model: CL, systemic clearance; Q , intercompartmental clearance; $Q_{T/B/A}$, perfusion rates of the trachea, bronchi and alveolar region, respectively. V , volume of distribution; f_u , fraction unbound; P_{app} , apparent permeability; S , Surface areas; Eff, efflux ratio; K_{pu} , partition coefficients. Subscripts: C, central compartment (CMT); P, peripheral CMT; A, alveolar; B, bronchi; T, trachea; int, interstitial; cell, cellular; ELF, epithelial lining fluid. Parameters of the PD model: k_{eo} , first-order equilibration rate constant; k_{growth} , growth rate of the bacteria; k_{max} , maximum kill rate; C_{eff} , concentration in the effect CMT; EC_{50} , concentration achieving the half-maximal effect; B_{max} , maximal bacterial concentration. This figure appears in colour in the online version of *JAC* and in black and white in the print version of *JAC*.

permeability values was made to compensate for uncertainties in reported physiological ELF volumes and pulmonary surface areas. For tetracycline, both a constant and concentration-dependent fraction unbound in plasma (f_u) were investigated (see [Supplementary Section 4](#)). To compare the overall goodness-of-fit of the developed model across drugs, the absolute average fold error (AAFE) of model predictions was calculated as described in Equation 1:

$$AAFE = 10^{\frac{\sum |\log_{10}(\frac{Pred}{Obs})|}{N}} \quad (1)$$

with *Obs* denoting observed concentrations (plasma, tissue and ELF samples), and *Pred* being the corresponding concentrations predicted by the model. N denotes the total number of data points.

Translational approach

The final PBPK model first developed for rats was encoded in R (Version 4.0.2),¹⁶ using the *deSolve* package (Version 1.28,¹⁷), *ggplot2* (Version 3.3.3,¹⁸) was used for visualization. The model was translated to humans as described in the following and combined with an oral absorption compartment (to account for swallowed drug after oral drug inhalation). The full ordinary differential equation system can be found in the [Supplementary data](#) ([Supplementary Section 4](#)). The systemic PK for humans, absorption rates and oral bioavailability were taken from literature,^{19–24} and a non-linear

clearance was implemented for rifampicin.²² The body weight-normalized physiological volumes and surface areas, partition coefficients and efflux ratios were kept the same as the rat model.²⁵ The resulting parameter values can be found in [Table 1](#). Blood flows to the lung regions were allometrically scaled from rat with an exponent of 0.75.²⁶

For the simulation of plasma and pulmonary concentration–time profiles after oral inhalation, drug dissolution and mucociliary clearance processes were added to the model as first-order rates (see [Figure S1](#)). As all model drugs display high solubility, the dissolution rate was considered high and set, i.e. to 50 h^{-1} . The mucociliary clearance was set to 0.938 h^{-1} .²⁷ As the focus of this investigation was not on formulation characteristics, a generic plausible deposition pattern was implemented for oral inhalation.^{28,29} All drugs were assumed to deposit 50% of the emitted dose in the mouth–throat area with subsequent absorption via the gastro-intestinal tract of the swallowed fraction, and 1%, 9% and 40% in the trachea, bronchi and alveolar region, respectively.

PD model

The PBPK model was combined with a bacterial growth models ([Figure 1b](#)) linked to the unbound concentrations in the central compartment (plasma), bronchial interstitium, intracellular space and ELF. The PD model assumed saturable bacterial growth (saturation at 10^{10} cfu/mL) starting at 10^6 cfu/mL .³⁰ The maximum kill rate (k_{max}) was set to three times the growth rate of the bacteria (k_{growth} , based on *Staphylococcus aureus*)³⁰

3 Cumulative part

Himstedt *et al.*

Table 1. PK/PD parameters [coefficient of variation (% CV), if estimated] of the semi-mechanistic model

Parameter (Unit ^a)	Drug-specific parameters						
	Ciprofloxacin		Rifampicin		Tigecycline		Tigecycline Salmeterol PK
	Rat	Human	Rat	Human	Rat	Human	Human
CL (L/h)	2.95 (4.73%)	33.4	0.471 (7.09%)	–	1.49 (4.50%)	18.6	93.0
V _{max} (mg/h)	–	–	–	525	–	–	–
K _M (mg/L)	–	–	–	35.3	–	–	–
V _C (L)	0.724 (7.48%)	14.0	1.77 (14.2%)	87.2	0.581 (5.36%)	100	122
Q1 (L/h)	0.724 (11.2%)	85.1	–	–	1.45 (14.1%)	73.5	174
V _{s1} (L)	2.95 (8.20%)	40.6	–	–	1.39 (15.2%)	554	352
Q2 (L/h)	–	32.2	–	–	–	–	–
V _{p2} (L)	–	84.0	–	–	–	–	–
f _u (–)	0.700	0.700	0.200	0.200	Concentration dependent	0.200	0.018
P _{app} (10 ^{–5} cm/s)	0.845 (23.9%)	0.845 (23.9%)	5.75 (87.2%)	5.75 (87.2%)	0.190 (20.4%)	0.132 (20.4%)	3.92
K _{pu,T} ^b (–)	4.22 (14.0%)	4.22 (14.0%)	14.0 (17.1%)	14.0 (17.1%)	2.40 (8.57%)	2.73 (8.57%)	362
K _{pu,B} ^b (–)	3.69 (8.14%)	3.69 (8.14%)	32.5 (11.8%)	32.5 (11.8%)	8.64 (15.3%)	8.23 (21.5%)	1030
K _{pu,A} ^b (–)	5.70 (12.1%)	5.70 (12.1%)	51.9 (12.9%)	51.9 (12.9%)	15.8 (12.2%)	19.2 (24.2%)	2180
Eff _T (–)	1.24 (8.50%)	1.24 (8.50%)	2.56 (11.3%)	2.56 (11.3%)	6.48 (20.5%)	7.30 (20.3%)	2.30
Eff _A (–)	0.854 (15.4%)	0.854 (15.4%)	3.67 (17.9%)	3.67 (17.9%)	4.51 (20.4%)	5.25 (20.4%)	2.30
F _{oral} (–)	0.690	0.690	0.948	0.948	0.001	0.001	0.120
k _a (/h)	0.760	0.760	1.77	1.77	1.00	1.00	0.330
k _{eo} (/h)	0.139	0.139	0.173	0.173	0.347	0.347	0.347
EC ₅₀ (mg/L)	0.250	0.250	0.500	0.500	0.00250	0.00250	0.00250
k _{max} (/h)	3.60	3.60	3.60	3.60	1.32	1.32	1.32
Physiological parameters							
	Trachea		Bronchi		Alveolar		
	Rat	Human	Rat	Human	Rat	Human	
Q (L/h)	0.0540	0.136	0.777	0.195	10.6	2.67	
V _{Total} (L/kg)	0.000137	0.000137	0.000547	0.000547	0.00287	0.00287	
V _{cell} (L/kg)	0.000117	0.000117	0.000468	0.000468	0.00151	0.00151	
V _{int} (L/kg)	1.05 × 10 ^{–5}	1.05 × 10 ^{–5}	4.21 × 10 ^{–5}	4.21 × 10 ^{–5}	0.00118	0.00118	
V _{ELF} (L/kg)	0.929 × 10 ^{–5}	0.929 × 10 ^{–5}	3.71 × 10 ^{–5}	3.71 × 10 ^{–5}	0.000186	0.000186	
SA _{cell} (dm ²)	3.38	3.38	13.5	13.5	372	372	
SA _{ELF} (dm ²)	0.0184	0.0184	5.25	5.25	171	171	
Bacterial growth model							
B _{max} (cfu/mL)	10 ¹⁰						
k _{growth} (/h)	1.20						

Systemic PK parameters were taken from^{19–24}.

Physiological parameters for pulmonary tissues were taken from^{12–14}.

^aClearances and volumes of rats are given per kg body weight.

^bCellular partition coefficients. For comparison with more typical whole tissue partition coefficients, see Table S4.

for the bactericidal antibiotics ciprofloxacin and rifampicin, and to slightly larger than k_{growth} (1.32 h^{–1}) for the bacteriostatic tigecycline (see Table 1). EC₅₀ values were chosen so that high-dose treatment for *S. aureus*³¹ resulted in bacteriostasis in plasma 12 h after the first intravenous administration. Hence, the utilized parameterization represents a suboptimal scenario, but avoids that the simulated scenarios will display (mostly) maximum killing and assured a meaningful sensitivity analysis. To simulate the post-antibiotic effect (PAE), an effect compartment was introduced, with the rate k_{eo} corresponding to the reported PAE.^{32,33}

$$k_{eo} = \frac{\ln(2)}{PAE} \quad (2)$$

Dose–response intravenous versus oral inhalation

The human version of the PBPK/PD model was used to simulate dose–response profiles in plasma and bronchial compartments after intravenous infusion over 1 h and oral inhalation. The efficacy was evaluated based on the reduction of bacteria over one dosing interval

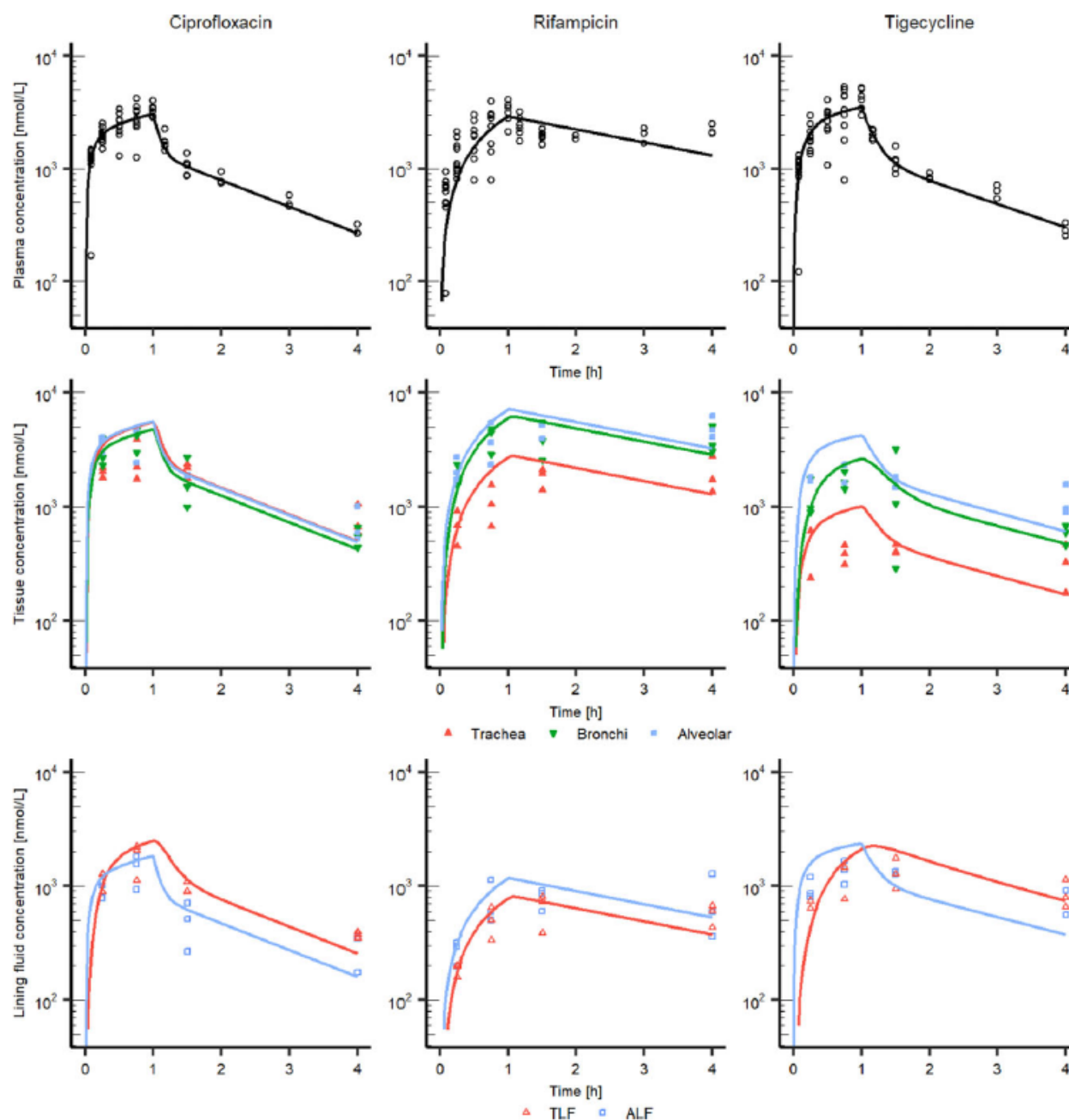


Figure 2. Observed (symbols) and predicted (lines) concentration–time profiles after intravenous administration of 5 mg/kg in rats. TLF, tracheal lining fluid; ALF, alveolar lining fluid. This figure appears in colour in the online version of *JAC* and in black and white in the print version of *JAC*.

(12 h, bi-daily dosing), both for the first dose and at steady-state. To investigate the influence of optimization for inhaled drugs, the same analysis was performed for tigecycline where the PK parameters were replaced with those of salmeterol (see Table 1). The apparent permeability of salmeterol was scaled from Caco-2 permeability measured in-house with the mean estimated shift from literature values for ciprofloxacin and rifampicin (factor 2.8). The efflux ratio was taken from the *in vitro* efflux ratio observed in the Caco-2 assay.

Sensitivity analysis

To identify parameters of interest for optimization in drug discovery regarding bacterial killing in bronchial ELF and intracellular space after oral inhalation, a sensitivity analysis was performed. To this end, each drug-specific parameter was increased and decreased 2-fold, and the resulting change in effect was evaluated. The dose resulting in bacteriostasis after single dose administration was chosen as a basis for the sensitivity.

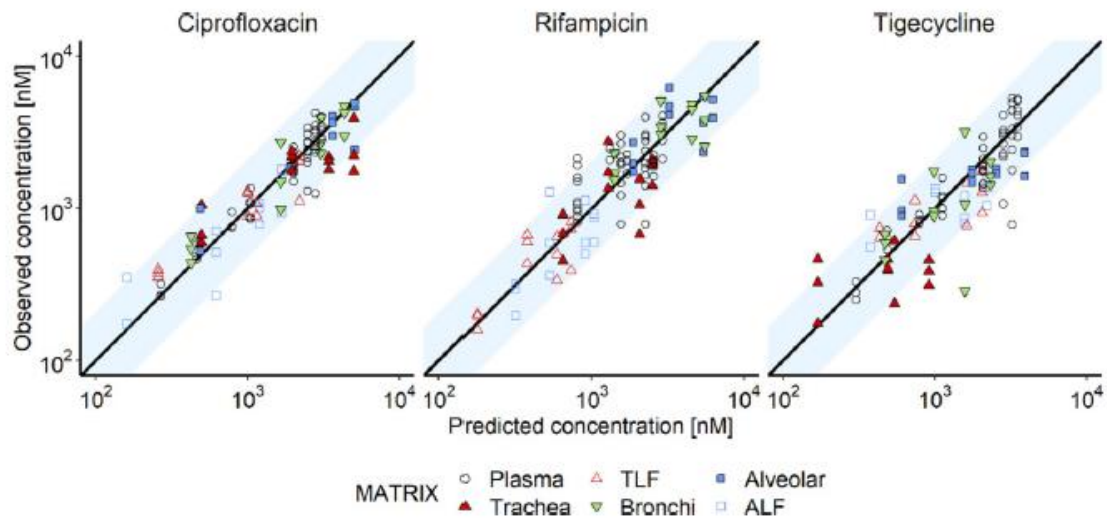


Figure 3. Goodness-of-fit evaluation of model predictions. The shaded area represents the 2-fold error range. TLF, tracheal lining fluid; ALF, alveolar lining fluid. This figure appears in colour in the online version of *JAC* and in black and white in the print version of *JAC*.

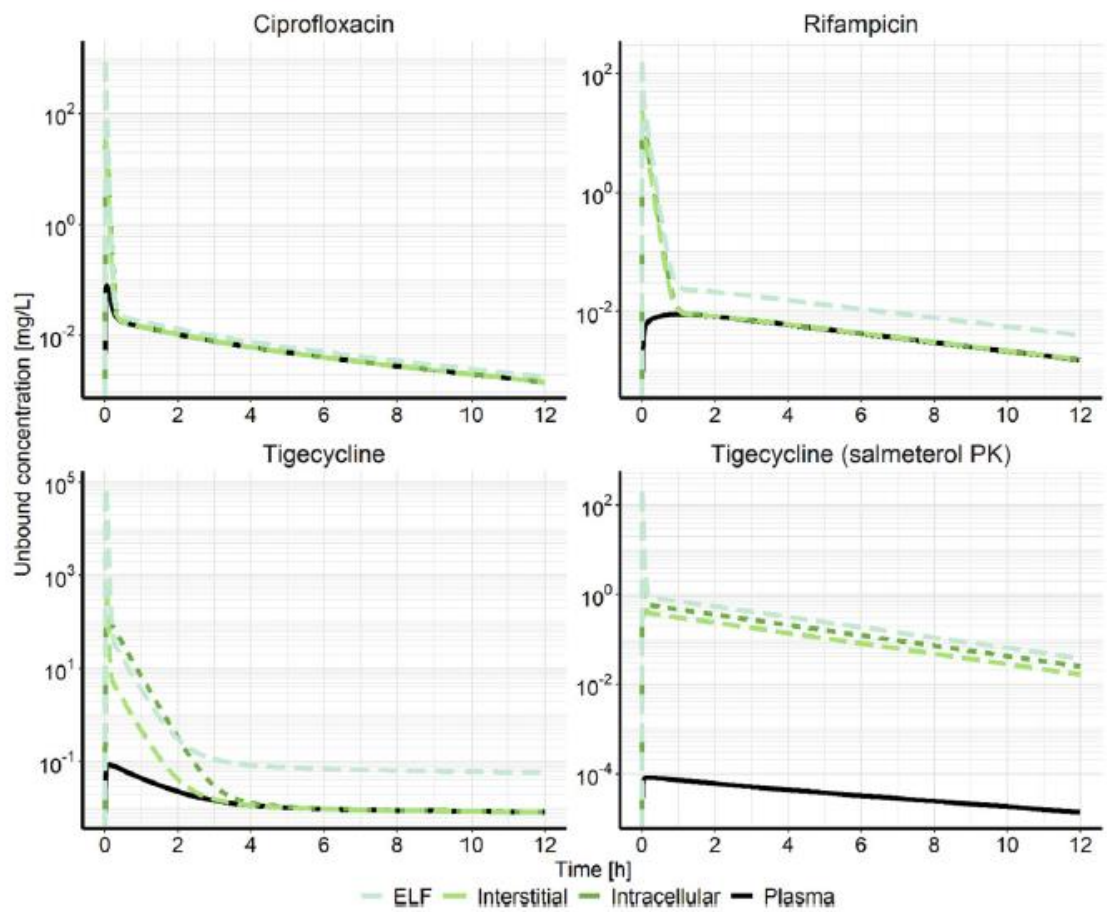


Figure 4. Simulated unbound concentration–time profiles after oral inhalation in humans. The doses were chosen based on the dose–response simulation as the respective doses resulted in bacteriostasis for intracellular infections (138, 68.2, 38.0 and 0.90 mg for ciprofloxacin, rifampicin, tigecycline and tigecycline with salmeterol PK, respectively). This figure appears in colour in the online version of *JAC* and in black and white in the print version of *JAC*.

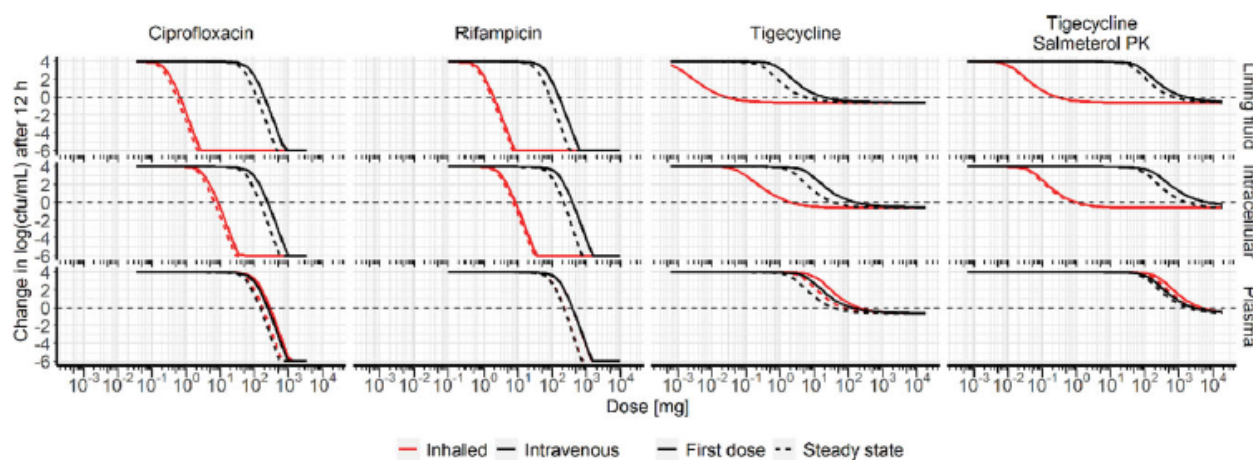


Figure 5. Simulated human dose–response profiles for the three model drugs in bronchial ELF, intracellular space and plasma. This figure appears in colour in the online version of *JAC* and in black and white in the print version of *JAC*.

Results

PK rat model

The experimental data from the infusion study showed a bi-exponential decline in plasma concentrations for ciprofloxacin, tigecycline and meropenem, which was best described by a two-compartment systemic model. In case of rifampicin, a one-compartment model was sufficient. Unfortunately, meropenem proved to be highly unstable in tissue samples and was therefore excluded from further analyses. Total tissue concentrations of the other three model drugs followed a similar shape as the plasma concentration–time profile, with concentrations in the trachea typically lower than in the bronchi or alveolar parenchyma. The observed and predicted concentration–time profiles can be found in Figure 2.

The semi-mechanistic PBPK model was able to adequately describe plasma, total tissue and ELF concentrations for all three compounds simultaneously, with an AAFE of 1.35, and 90.4% of observed values within 2-fold of the prediction (see Figure 3). However, the model overestimated tracheal and alveolar concentrations of tigecycline during the first hour (see Figure 2, middle right).

The implementation of concentration-dependent protein binding for tigecycline did improve the description of observed data (Akaike information criterion of 1935 versus 1976, compare also Figures S2–S4). However, the estimated parameters (permeability, partition coefficients and efflux ratios) were in a similar range. The concentration-dependent binding of tigecycline has only been measured in a limited concentration range (0.1–100 mg/L),^{34,35} and the here used model may not be adequate for the initially exceedingly high local concentrations after oral inhalation. A constant fraction unbound was therefore assumed for the following translational and sensitivity analyses. The estimated model parameters are found in Table 1.

Comparison of intravenous versus inhaled dose–response curves

The humanized PBPK model was used to simulate unbound concentrations in plasma and bronchial tissues (interstitial,

intracellular and ELF). The corresponding concentration–time profiles after oral inhalation can be found in Figure 4. The simulated dose–response profiles after oral inhalation and intravenous administration showed a left-shift to lower effective doses for bronchial infections by inhalation compared with intravenous administration, more pronounced for the ELF than for intracellular pathogens (compare Figure 5). Systemic efficacy was comparable for ciprofloxacin and rifampicin or slightly worse for tigecycline after inhalation.

Using the conceptual PBPK/PD model, the inhaled doses resulting in bacteriostasis in bronchial ELF and intracellular space at steady-state were 0.50 and 6.9 mg for ciprofloxacin, 1.6 and 7.0 mg for rifampicin, and 0.025 and 1.9 mg for tigecycline, respectively. The corresponding intravenous doses required for bacteriostasis at steady-state were 108 and 138 mg for ciprofloxacin, 68.2 and 273 mg for rifampicin, and 5.0 and 38 mg for tigecycline. Inhaled doses were factor 216, 200 and 53 lower in the ELF for ciprofloxacin, tigecycline and rifampicin, respectively. In the bronchial cells, the required inhaled doses were 20 times lower for both ciprofloxacin and tigecycline, and 39 times lower for rifampicin.

PK parameters optimized for pulmonary targeting via oral inhalation resulted in the largest shift between intravenous and inhaled administration. Changing the PK of tigecycline to that of salmeterol indicated that inhalation required 3000-fold and 2000-fold lower doses for ELF and intracellular infections, respectively, with bacteriostatic inhaled doses of 0.20 and 0.90 mg for the ELF and intracellular space.

Sensitivity analysis

The sensitivity analysis indicated the potency (EC_{50}) as the most influential parameter for ciprofloxacin, rifampicin and tigecycline with substituted salmeterol PK for both ELF and intracellular space (see Figure 6). While the potency was also an influential parameter for tigecycline, the PAE, as represented by k_{e0} , had the most impact on bacterial killing after 12 h. Other influential parameters were the estimated permeability (P_{app}) and the efflux ratio (Eff_T). However, these two were only relevant for targets in

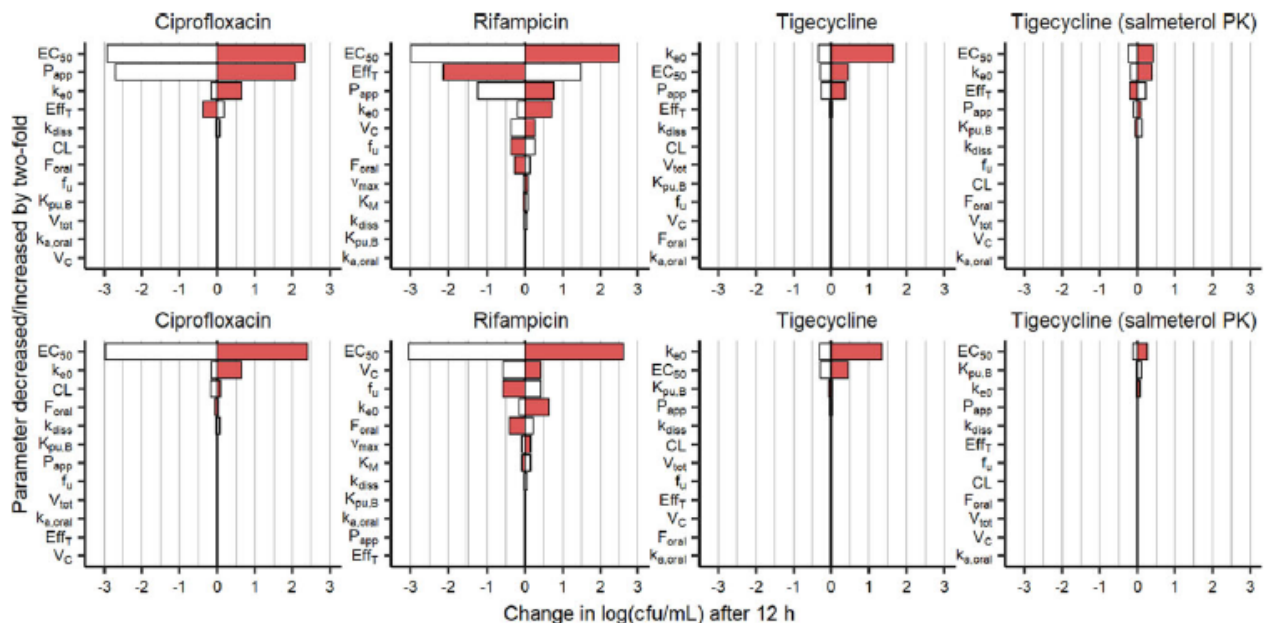


Figure 6. Results of the sensitivity analysis regarding the change in \log_{10} (cfu/mL) over one dosing interval at steady-state after inhaled administration. Upper row, bronchial lining fluid; bottom row, intracellular. Filled bars represent the shift in cfu/mL caused by an increase of the parameter in question; open bars represent a decrease of the parameter. This figure appears in colour in the online version of *JAC* and in black and white in the print version of *JAC*.

the ELF. The other parameters, even typical optimization parameters for orally inhaled drugs, such as CL and the oral bioavailability appeared to have negligible influence. Starting out with optimized PK parameters (salmeterol PK) for tigecycline reduced the influence of k_{e0} substantially.

Discussion

Repurposing already established orally or intravenously administered antibiotics for oral inhalation is a complex endeavour, which has seldom been systematically evaluated. This work provides insights on favourable PK/PD characteristics for an oral/intravenous-to-inhaled switch for antibiotics targeting bronchial infections, based on detailed pulmonary tissue, endothelial lining fluid and systemic *in vivo* drug concentration–time profiles in rats and a quantitative model-based approach.

The semi-mechanistic PBPk model adequately described granular pulmonary distribution across three established antibiotics after intravenous administration in rats mainly based on physiological information. Drug-specific parameters were either estimated across tissues (permeability) or separately for the trachea, bronchi and alveolar region (partition coefficients and epithelial efflux ratios). Observed ELF/unbound plasma concentration ratios for ciprofloxacin were in a similar range, if slightly lower than reported before.³⁶ The investigated model drugs are all established antibiotics with varying PK/PD properties. However, none of them was optimized for oral inhalation. The aim of this work was to identify favourable drug properties to support a switch to oral inhalation from more common routes of administration. Perhaps unsurprisingly, as the dose selected for the sensitivity analyses was close to the ED_{50} for ciprofloxacin

and rifampicin, the potency was identified as the most influential parameter for overall efficacy. This was less pronounced for tigecycline, as the selected dose was closer to the maximally effective dose. High potency decreases the dose needed to achieve the desired effect, facilitating formulation in inhalation devices which are often limited regarding the dose. Other characteristics, such as low permeability and a high efflux ratio in the bronchial epithelium, were more important for efficacy in the lining fluid. Both parameters influence drug clearance from the site of action, i.e. the ELF and therefore increase the local residence time and increase the time over the minimal inhibitory concentration. The PAE, implemented via the first-order rate k_{e0} seemed to have a high impact, especially for tigecycline. Combined with the high initial pulmonary concentrations after oral inhalation, the slow clearance from the effect compartment (k_{e0} , i.e. a long PAE) results in prolonged high efficacy. However, if k_{e0} takes on higher values—corresponding to a shorter PAE—this advantage disappears (compare the dose-response profiles for ciprofloxacin with a 10-fold increased k_{e0} , Figure S5). This might explain the lower efficacy after inhalation and the conflicting results with real-life evidence from attempts to develop an inhaled ciprofloxacin product,^{37,38} which failed due to limited advantages over oral administration.

Exchanging the tigecycline PK model with that of salmeterol nicely showed the impact of PK characteristics designed for inhalation (compare Figure 4), showing high long-lasting unbound drug concentrations in all bronchial compartments over the whole dosing interval, combined with lower free plasma concentrations. While it did not substantially improve local efficacy, the combination of high systemic clearance, high affinity to pulmonary tissues and low oral bioavailability resulted in increased

pulmonary selectivity compared with the other scenarios (see Figure 5). This may not be necessary for the here investigated drugs, as the systemic safety is not the limiting factor. However, it may be an important consideration for antibiotics with a narrow safety margin. In addition, the sensitivity analysis showed that PK optimization drastically reduced the influence of k_{e0} , indicating that good pulmonary PK may be more meaningful for inhaled administration of drugs without prolonged PAE.

A few limitations of this investigation have to be acknowledged. The PBPK model showed a trend towards consistent overprediction of tracheal concentrations at early timepoints and underprediction at later timepoints. One could speculate that the well-stirred hypothesis typically applied in PBPK modelling does not hold true for the trachea, which contains cartilage rings. It might be that the unique tissue composition of the trachea leads to slow diffusivity, altering the distribution characteristics of drugs. The sensitivity analysis for tigecycline was performed without accounting for the non-linear plasma protein binding, and a fixed unbound fraction was assumed, as the simpler model was deemed sufficient for the sensitivity analysis (see Supplementary Section 5 and Figure S6). Also, the permeability of rifampicin could not be reliably estimated (% CV of 87.2%). This was most likely because the permeability is not the limiting step in this case, as rifampicin is classified as a well permeable drug.³⁹ In addition, some of the assumptions of the here presented models might not hold true for all inhaled antibiotics. If substantial binding to ELF components would be expected, the parameters describing the epithelial efflux may be overestimated as the ELF concentrations would represent bound and unbound drug. This was for example demonstrated for tobramycin and colistin, for which binding to mucins has been reported.^{40,41} In this case, supplementing the analysis with *in vitro* binding assays would be recommended, e.g. as demonstrated by Bäckström *et al.*⁴²

Finally, this work is a hypothetical scenario with several assumptions. The chosen bacterial model is simplistic and the derived doses in this work should not be interpreted as absolute values, but could only be compared relatively between oral inhalation and intravenous administration. A more mechanistic implementation of bacterial dynamics and PAE may refine our findings. The physiological volumes and surface areas implemented in the model are subject to uncertainty, and the simulated intracellular concentrations are not supported by direct measurements of interstitial or intracellular concentrations. To account for this, the apparent permeability (P_{app}) was estimated instead of fixed to measured values. In addition, the influence of formulation-related parameters, such as dissolution rate and deposition pattern, was not investigated further. This was done intentionally, as the aim was to identify favourable drug properties for optimization or alternatively to guide the drug candidate selection for an inhalation optimization programme, rather than the pharmaceutical development of suitable formulations and devices. These questions could be better addressed by an investigation of plasma and ELF PK (e.g. via exhaled breath condensate)^{43,44} after oral inhalation in humans or complementary by dedicated deposition studies, e.g. with insoluble particles.⁴⁵ The focus of this investigation was put on bronchial infections, i.e. infections of the conducting airways and the analyses will have to be adapted for infections of the peripheral lung. For example, if

the target would be in the alveolar region, fast clearance from the site of action can be anticipated based on the high surface area and the rich perfusion.⁴⁶ In that case, strategies like a prolonged PAE, or even extremely low permeability and slow dissolution may be reasonable. Lastly, the sensitivity analyses did not consider pulmonary selectivity, and only a single dose level was investigated per scenario. To achieve maximum efficacy, it might be required to optimize more than a single parameter to also maintain the drug for a long time in the lung. These aspects may be an interesting starting point for follow-up analyses. Another interesting addition would be the analogous evaluation of antibiotics, which are commercially available as orally inhaled formulations, such as tobramycin, to understand what molecular properties made it suitable for the respective indications. Based on our results, the low permeability of tobramycin could be one of the reasons, as once deposited in the conducting airways, tobramycin would remain for a long time in the airway lining and is only slowly absorbed to the tissues.

In conclusion, the here described pulmonary PBPK/PD model was able to describe the time-dependent pulmonary PK for three model drugs in rats after intravenous administration. According to the humanized model, oral inhalation required lower doses than intravenous administration to achieve bacteriostasis in both bronchial lining fluid and cells, and showed pulmonary selectivity for all three model drugs, which was still valid at steady-state. The subsequent sensitivity analysis suggested that often applied optimization parameters for drugs for oral inhalation (e.g. high systemic clearance and low bioavailability) showed little influence on pure efficacy, i.e. allowing for lower doses to be used, and instead mainly increased pulmonary selectivity. In contrast, low permeability, a high epithelial efflux ratio and a pronounced PAE were indicated as the most impactful parameters for inhaled antibiotics and therefore might be an indication for the suitability of a switch from oral or intravenous administration to oral inhalation both for established antibiotics and during drug discovery.

Acknowledgements

We thank Anne Weber, Heidi Assfalg and Nadine Klick for the excellent performance of the *in vivo* experiments as well as Tom Bretschneider, Alexandra Vogel, Anna Lachenmaier and Steffen Schrade for the bioanalytical support. We would also like to thank Achim Sauer for proofreading and valuable discussions. Additional thanks go to Sylvia Blum who developed the novel lung preparation technique, and Nicolas Pairet and his team for the determination of urea concentrations.

Funding

This work was supported by Boehringer Ingelheim Pharma GmbH & Co. KG as part of the PhD work of A.H. at the University of Hamburg.

Transparency declarations

At the time of submission, A.H., C.B. and J.M.B. are employees at Boehringer Ingelheim Pharma GmbH & Co. KG, Biberach, Germany. The PhD work of A.H. is funded by Boehringer Ingelheim Pharma GmbH & Co. KG as part of a research grant to the University of Hamburg. S.G.W.

Himstedt et al.

received research grants from Boehringer Ingelheim Pharma GmbH & Co. KG related to the here published work.

Supplementary data

Supplementary Sections 1 to 8, including Figures S1 to S6 and Tables S1 to S4 are available as Supplementary data at JAC Online.

References

- 1 Contreras LG, Sung J, Ibrahim M et al. Pharmacokinetics of Inhaled Rifampicin Porous Particles for Tuberculosis Treatment: Insight into Rifampicin Absorption from the Lungs of Guinea Pigs. *Mol Pharm* 2015; **12**: 2642–50.
- 2 Weers J, Metzheiser B, Taylor G et al. A gamma scintigraphy study to investigate lung deposition and clearance of inhaled amikacin-loaded liposomes in healthy male volunteers. *J Aerosol Med Pulm Deliv* 2009; **22**: 131–8.
- 3 Stass H, Nagelschmitz J, Willmann S et al. Inhalation of a dry powder ciprofloxacin formulation in healthy subjects: a phase I study. *Clin Drug Investig* 2013; **33**: 419–27.
- 4 Boisson M, Mimoz O, Hadzic M et al. Pharmacokinetics of intravenous and nebulized gentamicin in critically ill patients. *J Antimicrob Chemother* 2018; **73**: 2830–7.
- 5 Geller DE, Rosenfeld M, Waltz DA et al. Efficiency of pulmonary administration of tobramycin solution for inhalation in cystic fibrosis using an improved drug delivery system. *Chest* 2003; **123**: 28–36.
- 6 Geller DE, Pitlick WH, Nardella PA et al. Pharmacokinetics and bioavailability of aerosolized tobramycin in cystic fibrosis. *Chest* 2002; **122**: 219–26.
- 7 McKinzie CJ, Chen L, Ehlert K et al. Off-label use of intravenous antimicrobials for inhalation in patients with cystic fibrosis. *Pediatr Pulmonol* 2019; **54**: S27–45.
- 8 Cystic Fibrosis Canada. Canadian consensus statement on aerosolized antibiotic use in cystic fibrosis. <https://www.cysticfibrosis.ca/our-programs/healthcare/guidelines-and-standards-of-care>.
- 9 Bilal H, Tait JR, Lang Y et al. Simulated intravenous versus inhaled tobramycin with or without intravenous ceftazidime evaluated against hypermutable *Pseudomonas aeruginosa* via a dynamic biofilm model and mechanism-based modeling. *Antimicrob Agents Chemother* 2022; **66**: e02203-21.
- 10 Alhajj N, O'Reilly NJ, Cathcart H. Developing ciprofloxacin dry powder for inhalation: A story of challenges and rational design in the treatment of cystic fibrosis lung infection. *Int J Pharm* 2021; **613**: 121388.
- 11 Pasqua E, Hamblin N, Edwards C et al. Developing inhaled drugs for respiratory diseases: a medicinal chemistry perspective. *Drug Discov Today* 2021; **27**: 134–50.
- 12 Himstedt A, Braun C, Wicha SG et al. Towards a quantitative mechanistic understanding of localized pulmonary tissue retention—A combined *in vivo/in silico* approach based on four model drugs. *Pharmaceutics* 2020; **12**: 408.
- 13 Yu JY, Rosania GR. Cell-based multiscale computational modeling of small molecule absorption and retention in the lungs. *Pharm Res* 2010; **27**: 457–67.
- 14 Fröhlich E, Mercuri A, Wu S et al. Measurements of deposition, lung surface area and lung fluid for simulation of inhaled compounds. *Front Pharmacol* 2016; **7**: 181.
- 15 van der Deen M, de Vries EG, Timens W et al. ATP-binding cassette (ABC) transporters in normal and pathological lung. *Respir Res* 2005; **6**: 59.
- 16 Core Team R. *R: A language and environment for statistical computing*. R Foundation for Statistical Computing, 2016.
- 17 Soetaert KE, Petzoldt T, Setzer RW. Solving differential equations in R: package deSolve. *J Stat Softw* 2010; **33**: 1–25.
- 18 Wickham H. *ggplot2, Elegant Graphics for Data Analysis*. Springer New York, 2016.
- 19 Wart SAV, Owen JS, Ludwig EA et al. Population pharmacokinetics of tigecycline in patients with complicated intra-abdominal or skin and skin structure infections. *Antimicrob Agents Chemother* 2006; **50**: 3701–7.
- 20 Korth-Bradley JM, Baird-Bellaire SJ, Patat AA et al. Pharmacokinetics and Safety of a Single Intravenous Dose of the Antibiotic Tigecycline in Patients With Cirrhosis. *J Clin Pharmacol* 2011; **51**: 93–101.
- 21 Dudley MN, Ericson J, Zinner SH. Effect of dose on serum pharmacokinetics of intravenous ciprofloxacin with identification and characterization of extravascular compartments using noncompartmental and compartmental pharmacokinetic models. *Antimicrob Agents Chemother* 1987; **31**: 1782–6.
- 22 Svensson R, Simonsson U. Application of the multistate tuberculosis pharmacometric model in patients with rifampicin-treated pulmonary tuberculosis. *CPT Pharmacometrics Syst Pharmacol* 2016; **5**: 264–73.
- 23 Soulele K, Macheras P, Silvestro L et al. Population pharmacokinetics of fluticasone propionate/salmeterol using two different dry powder inhalers. *Eur J Pharm Sci* 2015; **80**: 33–42.
- 24 Soulele K, Macheras P, Karalis V. Pharmacokinetic analysis of inhaled salmeterol in asthma patients: Evidence from two dry powder inhalers. *Biopharm Drug Dispos* 2017; **38**: 407–19.
- 25 Rodgers T, Leahy D, Rowland M. Physiologically based pharmacokinetic modeling 1: predicting the tissue distribution of moderate-to-strong bases. *J Pharm Sci* 2005; **94**: 1259–76.
- 26 Kleiber M. Body size and metabolic rate. *Physiol Rev* 1947; **27**: 511–41.
- 27 Weber B, Hochhaus G. A pharmacokinetic simulation tool for inhaled corticosteroids. *AAPS J* 2013; **15**: 159–71.
- 28 Hofmann W. Modelling inhaled particle deposition in the human lung—A review. *J Aerosol Sci* 2011; **42**: 693–724.
- 29 Martin AR, Finlay WH. Model calculations of regional deposition and disposition for single doses of inhaled liposomal and dry powder ciprofloxacin. *J Aerosol Med Pulm Drug Deliv* 2018; **31**: 49–60.
- 30 Iqbal K, Broeker A, Nowak H et al. A pharmacometric approach to define target site-specific breakpoints for bacterial killing and resistance suppression integrating microdialysis, time-kill curves and heteroresistance data: A case study with moxifloxacin. *Clin Microbiol Infect* 2020; **26**: 1255.e1–e8.
- 31 EUCAST. Clinical breakpoints and dosing of antibiotics. https://www.eucast.org/clinical_breakpoints/.
- 32 Noviello S, Ianniello F, Leone S et al. In vitro activity of tigecycline: MICs, MBCs, Time-Kill Curves and Post-Antibiotic Effect. *J Chemother* 2013; **20**: 577–80.
- 33 Stubbings W, Bostock J, Ingham E et al. Mechanisms of the post-antibiotic effects induced by rifampicin and gentamicin in *Escherichia coli*. *J Antimicrob Chemother* 2006; **58**: 444–8.
- 34 Mukker JK, Singh RP, Derendorf H. Determination of atypical nonlinear plasma-protein-binding behavior of tigecycline using an *in vitro* microdialysis technique. *J Pharm Sci* 2014; **103**: 1013–9.
- 35 Muralidharan G, Micalizzi M, Speth J et al. Pharmacokinetics of tigecycline after single and multiple doses in healthy Subjects. *Antimicrob Agents Chemother* 2005; **49**: 220–9.
- 36 Gontijo AVL, Brillault J, Grégoire N et al. Biopharmaceutical characterization of nebulized antimicrobial agents in rats: 1. Ciprofloxacin, moxifloxacin, and grepafloxacin. *Antimicrob Agents Chemother* 2014; **58**: 3942–9.

- 37** Brillault J, Tewes F, Couet W et al. In vitro biopharmaceutical evaluation of ciprofloxacin/metal cation complexes for pulmonary administration. *Eur J Pharm Sci* 2017; **97**: 92–8.
- 38** Tran T-T, Vidailiac C, Yu H et al. A new therapeutic avenue for bronchiectasis: Dry powder inhaler of ciprofloxacin nanoplex exhibits superior ex vivo mucus permeability and antibacterial efficacy to its native ciprofloxacin counterpart. *Int J Pharm* 2018; **547**: 368–76.
- 39** Biganzoli E, Cavenaghi LA, Rossi R et al. Use of a Caco-2 cell culture model for the characterization of intestinal absorption of antibiotics. *Farmaco* 1999; **54**: 594–9.
- 40** Huang JX, Blaskovich MAT, Pelington R et al. Mucin binding reduces colistin antimicrobial activity. *Antimicrob Agents Chemother* 2015; **59**: 5925–31.
- 41** Hunt BE, Weber A, Berger A et al. Macromolecular mechanisms of sputum inhibition of tobramycin activity. *Antimicrob Agents Chemother* 1995; **39**: 34–9.
- 42** Bäckström E, Engren T, Fihn B-M et al. Possible extraction of drugs from lung tissue during broncho-alveolar lavage suggest uncertainty in the procedure's utility for quantitative assessment of airway drug exposure. *J Pharm Sci* 2022; **111**: 852–8.
- 43** Khoubnasabjafari M, Fathi-Azarbayjani A, Rahimpour E et al. Concentration profile of tobramycin in exhaled breath condensate after inhalation of a single dose: A pilot study. *J Drug Deliv Sci Tec* 2021; **62**: 102394.
- 44** Kruizinga MD, Birkhoff WAJ, van Esdonk MJ et al. Pharmacokinetics of intravenous and inhaled salbutamol and tobramycin: An exploratory study to investigate the potential of exhaled breath condensate as a matrix for pharmacokinetic analysis. *Brit J Clin Pharmacol* 2020; **86**: 175–81.
- 45** Smith JRH, Bailey MR, Etherington G et al. Effect of particle size on slow particle clearance from the bronchial tree. *Exp Lung Res* 2008; **34**: 287–312.
- 46** Borghardt JM, Kloft C, Sharma A. Inhaled therapy in respiratory disease: The complex interplay of pulmonary kinetic processes. *Can Respir J* 2018; **2018**: 1–11.

3.3 Publication III: Evaluation of model-based approaches to infer pulmonary exposure

Inferring pulmonary exposure based on clinical PK data: accuracy and precision of model-based deconvolution methods

Anneke Himstedt, Jens M. Borghardt, Sebastian G. Wicha

Journal of Pharmacokinetics and Pharmacodynamics, 49(2) (2022) 135-149

Impact factor: 2.745 (2022)

Synopsis:

Even if the pre-clinical PK characteristics of orally inhaled drug candidates is well-understood, translation of pulmonary PK/PD to humans and clinical measurements of local concentrations remain challenging. In addition, oral inhalation comes with higher variability in the PK, both between individuals and between occasions. Pharmacometric approaches may allow to infer pulmonary exposure based on plasma PK data after i.v. and inhaled administration, even when pulmonary concentration measurements are not available. In the literature, different model structures have been applied for varying drug profiles to describe drug absorption from the lung. A set of five published empirical absorption models with varying degrees of complexity was investigated regarding the feasibility of inferring pulmonary exposure and retention metrics from plasma PK using a simulation-estimation analysis.

As a first step, structural identifiability was evaluated without added variability to assess the probability of choosing an unsuited absorption model and the potential error in inferred PK metrics. Here, the five models were additionally tested on data generated with the semi-mechanistic model developed for salmeterol in publication I (3.1), as this model was trained on actual time-resolved pulmonary concentration data. Secondly, the analysis was repeated in a population PK setting for selected models with variability as seen in the original data. Different methodologies of parameter estimation – sequential and simultaneous estimation of systemic and absorption PK parameters – were compared. In the majority of cases, the adequate absorption model could be correctly identified and the error in pulmonary exposure and retention metrics was less than two-fold, provided that the systemic PK was characterized well. This investigation also suggested that prior knowledge about the relevancy of pulmonary PK processes is key to the interpretation of PK data from orally inhaled drugs. Without information on the effective lung dose and the relevance of MCC or pulmonary metabolism, the simple

3.3 Publication III: Evaluation of model-based approaches to infer pulmonary exposure

first-order absorption model was indistinguishable from one with an additional non-absorptive loss process. Importantly, the resulting pulmonary metrics were vastly different, depending on whether the simpler or more complex model structure was used. The method of parameter estimation steps did not affect the results to a meaningful degree for the dataset investigated.



Inferring pulmonary exposure based on clinical PK data: accuracy and precision of model-based deconvolution methods

Anneke Himstedt^{1,2} · Jens Markus Borghardt² · Sebastian Georg Wicha¹ Received: 25 January 2021 / Accepted: 1 September 2021 / Published online: 28 September 2021
© The Author(s) 2021

Abstract

Determining and understanding the target-site exposure in clinical studies remains challenging. This is especially true for oral drug inhalation for local treatment, where the target-site is identical to the site of drug absorption, i.e., the lungs. Modeling and simulation based on clinical pharmacokinetic (PK) data may be a valid approach to infer the pulmonary fate of orally inhaled drugs, even without local measurements. In this work, a simulation-estimation study was systematically applied to investigate five published model structures for pulmonary drug absorption. First, these models were compared for structural identifiability and how choosing an inadequate model impacts the inference on pulmonary exposure. Second, in the context of the population approach both sequential and simultaneous parameter estimation methods after intravenous administration and oral inhalation were evaluated with typically applied models. With an adequate model structure and a well-characterized systemic PK after intravenous dosing, the error in inferring pulmonary exposure and retention times was less than twofold in the majority of evaluations. Whether a sequential or simultaneous parameter estimation was applied did not affect the inferred pulmonary PK to a relevant degree. One scenario in the population PK analysis demonstrated biased pulmonary exposure metrics caused by inadequate estimation of systemic PK parameters. Overall, it was demonstrated that empirical modeling of intravenous and inhalation PK datasets provided robust estimates regarding accuracy and bias for the pulmonary exposure and pulmonary retention, even in presence of the high variability after drug inhalation.

Keywords Pharmacokinetics · Pulmonary · Target-site exposure · Modeling and simulation · Inhalation

Introduction

One key assumption of pharmacokinetic/pharmacodynamic (PK/PD) analyses is that the local drug concentration at the target site, i.e. the target organ, is driving the efficacy. While determining the local tissue PK might be possible in preclinical experiments [1], adequate determination of the local concentration–time profile in clinical studies is challenging. While there are methods to determine tissue concentrations in humans (e.g. microdialysis [2] or imaging techniques [3]), data based on these methods is rarely

available due to the related complexity [2, 4]. Furthermore, more invasive methods may be difficult to justify in routine clinical studies. Therefore, plasma concentration–time profiles are often considered as a surrogate in PK/PD analyses assuming to provide an adequate representation also for the tissue concentrations [5].

For inhaled drugs, high local tissue concentrations and consequently high pulmonary efficacy can be achieved even before drug absorption into the systemic circulation. This also means that directly considering the plasma concentration as a surrogate for pulmonary tissue concentration and pulmonary efficacy might be of limited value. Instead, it is essential to make best use of the plasma PK data to indirectly infer the local pulmonary PK, which can be considered a better surrogate for pulmonary efficacy. In theory, deconvoluting the plasma PK profiles by numerical deconvolution methods (e.g., point-area deconvolution) allows to infer on pulmonary PK [6, 7]. However, these traditional deconvolution methods often assume linear

✉ Sebastian Georg Wicha
sebastian.wicha@uni-hamburg.de

¹ Department of Clinical Pharmacy, Institute of Pharmacy, University of Hamburg, Bundesstrasse 45, 20146 Hamburg, Germany

² Research DMPK, Drug Discovery Sciences, Boehringer Ingelheim Pharma GmbH & Co. KG, Biberach, Germany

systemic disposition kinetics and / or a single linear (pulmonary) absorption process, which might often not hold true [8]. Instead, model-based deconvolutions can account for these complexities and (pulmonary) absorption models of varying complexity were applied to infer on pulmonary exposure and residence time after oral drug inhalation, which are relevant for the extent and duration of efficacy, respectively [9–11]. These two PK characteristics can subsequently facilitate the comparison between different drugs or inform whether an inhaled drug qualifies for twice daily or even once daily dosing. To perform a (model-based) deconvolution, it is essential to have both data after drug inhalation and after intravenous (i.v.) dosing [12]. However, even having both datasets available, different model structures as well as different approaches combining i.v. and inhalation data in a model building process were published [9, 10, 12–16]. So far, however, a systematic comparison of all available models and whether sequential or simultaneous parameter estimation is best for inhalation PK models is missing. Potentially even more important, it was also never quantitatively evaluated if un-biased and precise inference of the extent of pulmonary exposure and retention time can be achieved based on realistic clinical datasets.

This modeling and simulation study aims at evaluating the overall suitability of PK modeling for inferring the extent and duration of pulmonary exposure based on plasma PK data and, if suitable, identify the best modeling strategy for this purpose. The focus lays on (1) to evaluate the impact of the choice of a pulmonary absorption model on inferring pulmonary exposure, and (2) to compare whether sequential or simultaneous parameter estimation based on i.v. and inhalation PK is meaningful, and (3) to quantify bias and imprecision of the different methods when inferring on extent and duration of pulmonary exposure. To this end, different model structures and modelling strategies were compared based on previously applied clinical studies for inhaled drug programs. Ultimately, this analysis gives insights into what modelling based on clinical data can provide and what the limitations might be.

Methods

Investigated pulmonary absorption models

Models with structurally different pulmonary absorption components were built and parameterized based on the respective publications [9, 12, 14–16], and are shown in Fig. 1. All parameter values used in this study can be found in the supporting information (Supplementary Material S2.2, Table S2). Concomitant absorption of swallowed

drug via the gastro-intestinal tract was not accounted for to reduce unnecessary complexity, as this absorption process can be prevented by ingesting active charcoal parallel to drug inhalation in clinical studies [17, 18].

Evaluation of the structural identifiability of pulmonary absorption models

A simulation-estimation analysis with models I (a single absorption process), II (two parallel absorption processes), IIIa (three parallel absorption processes), Transit, and NaL (single absorption process with parallel non-absorptive loss) was performed in R (Version 3.2.2) utilizing the package “deSolve” (Version 1.28) [19, 20]. All of these structural models were used to simulate plasma and lung concentration–time profiles over 48 h, resulting in five datasets (one for each model in Fig. 1, except for Model IIIb). To avoid distortion in the identifiability analysis, these profiles were simulated without residual error, which however was included in the second analysis to evaluate the performance of pulmonary absorption models in a clinical trial setting (see below). A lung volume of 0.84 L [21] was assumed to convert unabsorbed amounts to pulmonary concentrations. The models applied in this step will be referred to as the “Simulation Model”. A very rich sampling scheme with concentration data simulated every 0.01 h was selected to rule out the impact of sparse sampling designs and thereby to focus on the structural identifiability between the different models. Afterwards, each of the five models was applied for parameter estimation (“estimation model”) based on the simulated plasma concentration data resulting from each of the Simulation Models. Thus, in total 25 estimation analyses were performed. Since the focus of this part of the work laid on the comparison of pulmonary absorption models, the systemic disposition parameters of the Estimation Models were fixed to the published values and only the pulmonary PK parameters were estimated. If identifiability of the absorption parameters was given based on a non-singular Fisher information matrix and non-infinite standard errors, full plasma and inferred lung concentration–time profiles were generated with the newly estimated parameter values. Both these predictions were compared to the before simulated plasma and lung concentration–time profiles. For each Estimation Model, ten retries were performed to avoid convergence to local minima (Supplementary Material S2.2). Only when plasma equivalence was given (see “evaluation criteria” below), the model-based simulations were further compared with regard to the pulmonary exposure. A schematic representation of this workflow can be found in Fig. 2.

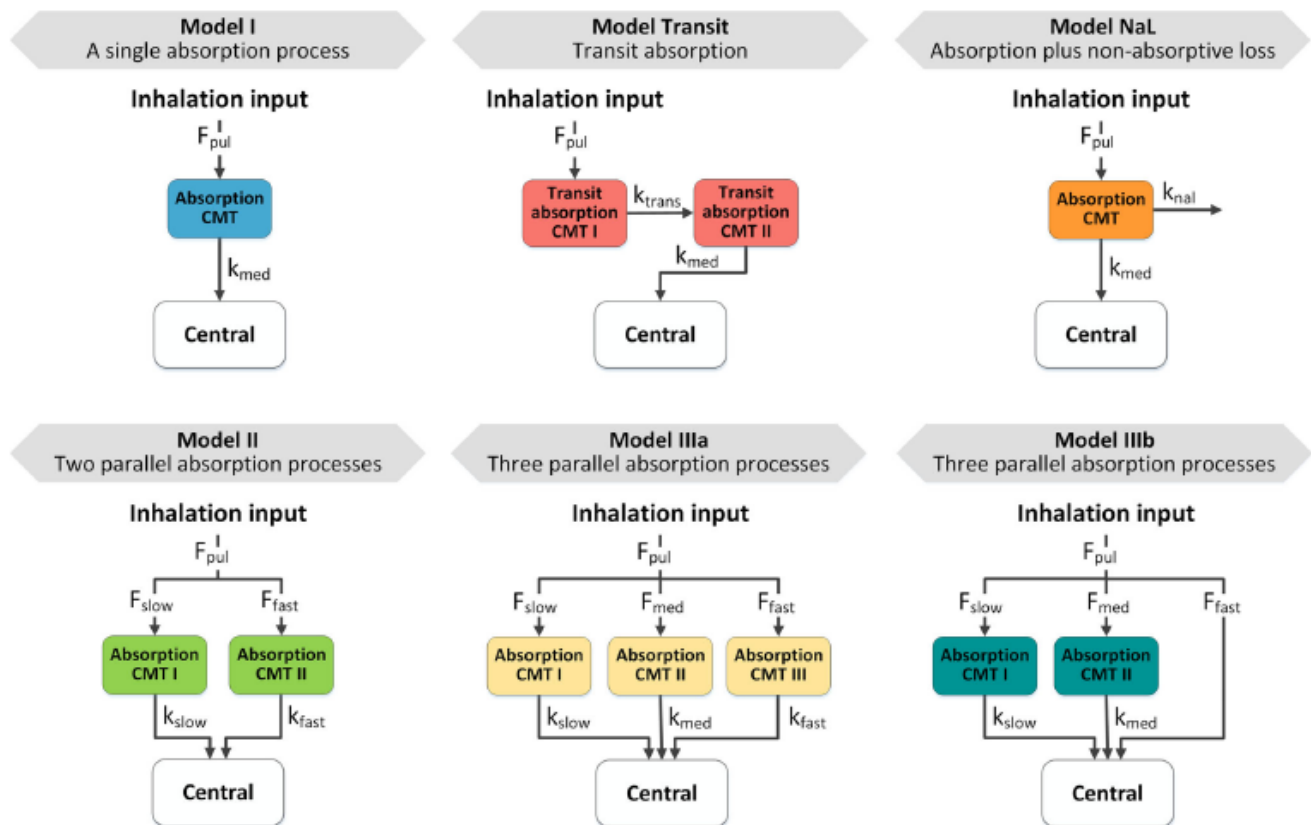


Fig. 1 Structural models for pulmonary absorption. Structure and parameterization were based on published models [6, 7, 9–12]. CMT compartment, F_{pul} pulmonary bioavailability or designated lung dose,

$F_{slow/med/fast}$ fraction of the lung dose slowly/intermediately/fast absorbed, $k_{slow/med/fast}$ slow/intermediate/fast absorption rate constants, k_{trans} transit rate constant, k_{nal} non-absorptive loss rate constant

Link between empiric and mechanistic PK modeling

All empirical models described here consider the pulmonary drug absorption one-directionally, i.e. no back flow from the systemic disposition to the lung is accounted for. To evaluate the potential bias caused by this simplification, all models were additionally fitted to data generated using a semi-mechanistic PK model for salmeterol [1] (Supplementary Material S2.3). This semi-mechanistic model was previously developed with both plasma and lung concentration data and accounted for back-flow from the systemic disposition to the lung. Thus, five additional simulation-estimation analysis were performed, finally resulting in 30 different combinations of the Simulation and Estimation Models.

Performance of pulmonary absorption models in a clinical trial setting

Models I-III cannot be differentiated based on prior mechanistic understanding of the pulmonary PK. Therefore, these models are often discriminated solely based on

their description of the available (plasma and urine) PK data [9, 15]. To explore the performance of these models to infer extent and duration of pulmonary exposure based on real-life clinical datasets, population PK analyses were carried out in NONMEM® Version 7.4.3 (ICON development solutions, Ellicott City, USA). Here, the chosen Simulation Models ('Model II' and 'IIIa') were reproduced in NONMEM® with the model structure, parameter values for population as well as all variability estimates, number of subjects, and sampling schemes taken directly from the respective publications (Supplementary Material S2.2, Table S2) [9, 15, 22]. As these models were built on some of the richest datasets for PK after both i.v. administration and inhalation published to date, these examples were taken as best-case examples to investigate how meaningful and accurate model-based deconvolution methods can be. Slight adjustments were made to the stochastic part of the original models, i.e., only up to four inter-individual and/or inter-occasional variabilities were included. This was done to prevent selecting a model structure over another model structure only due to a different number of included variability parameters. The residual variability was assumed to be proportional, oral absorption processes for 'Model II', and the inter-

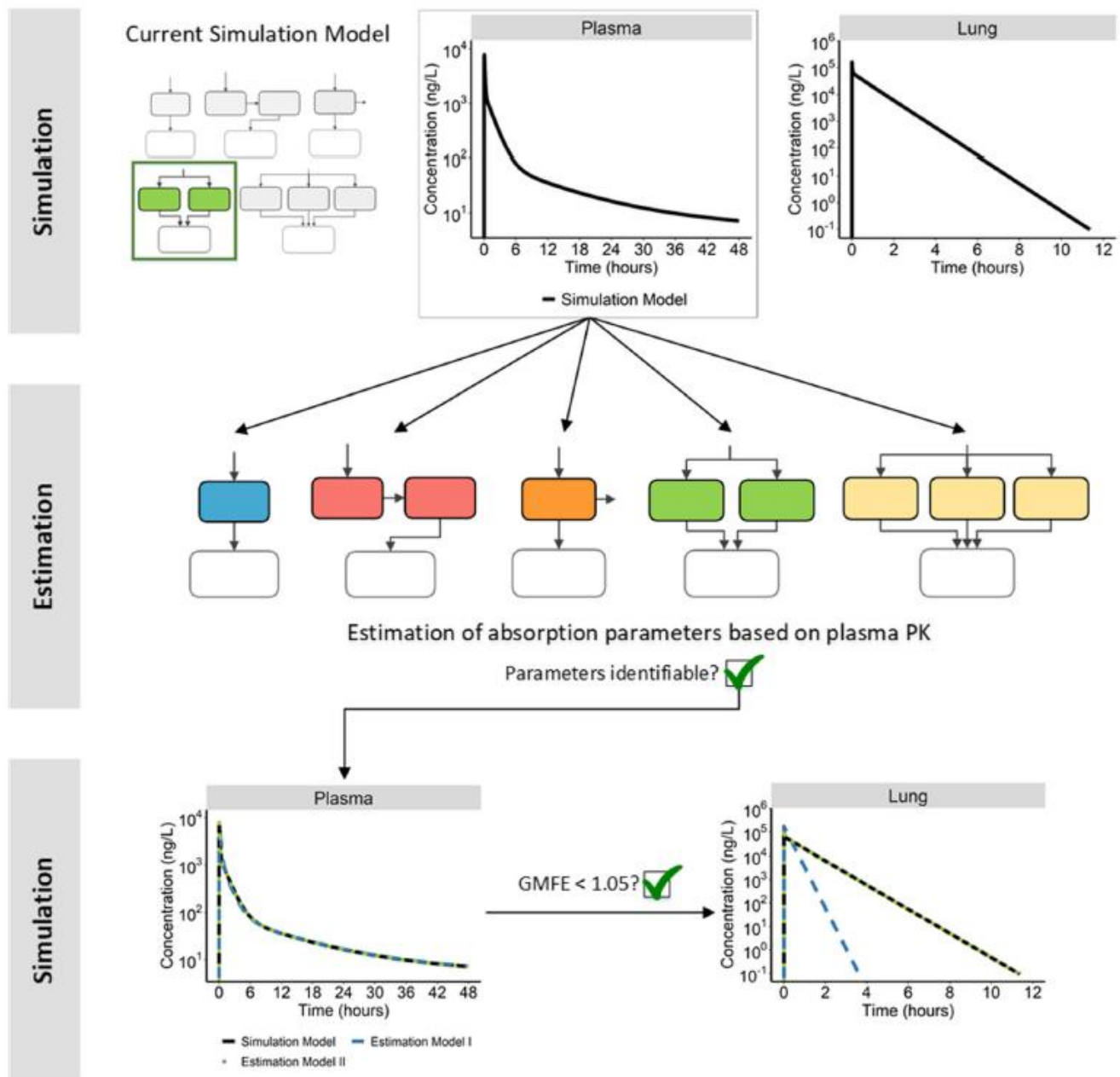


Fig. 2 Schematic of structural identifiability evaluation workflow. *PK* pharmacokinetics, *GMFE* geometric mean fold error of the plasma PK profile simulated with the estimation models

individual variability on the first proportionality factor (PF1) identified for ‘Model IIIa’ were not included. A summary of the dataset characteristics as provided in the respective publications, including the modifications to the stochastic models made in this study, can be found in Table 1.

The Simulation Models were used to generate PK datasets after i.v. administration and oral inhalation, this time including residual, inter-individual, and inter-occasion variability. Analogous to the first analysis, related models (parallel absorption models that were proven to be

structurally identifiable, see Table 1) were fitted to the simulated plasma concentration–time datasets. The Estimation Models were chosen to evaluate the influence of capturing the right number of absorption processes on the extent and duration of exposure (AUC_{0-inf} for both plasma and lung and $t_{C24h,lung}$). These PK metrics were calculated based on the population parameters. Furthermore, the influence of the systemic model on the same metrics was investigated in the analysis with ‘Model II’ as the Simulation model.

Table 1 Data summary for the two simulation models used in the population PK approach

	Population analysis I	Population analysis II
Simulation model	II (AZD5423)	IIIa (Olodaterol)
Number of subjects	13 (13)	88 (48)
Inhalation (intravenous)		
Inhalation and intravenous PK in the same subjects?	Yes	No
Urine data	No	Yes
Type of trial	Single dose (cross-over intravenous and inhalation)	Single dose (intravenous) Single and multiple dose (inhalation)
Systemic PK model	Four compartment model	Four compartment model
Inter-individual variability	F_{pul} , CL , $V1$, $Q2$	CL , $V1$, $Q2$
Inter-occasion variability	–	F_{pul}
Estimation models	II, I	IIIa, II, IIIb
	Three or four compartment systemic model	

CL systemic clearance, $V1$ central volume of distribution, $Q2$ intercompartmental clearance to the second systemic compartment

As the i.v. and inhalation study arms for ‘Model II’ (AZD5423) were conducted in the same individuals, the generated PK data from this model was used to compare different modeling approaches: These were.

- (i) sequential modeling of i.v. and inhalation data, with either fixed systemic population PK parameters as well as their variance (PPP, theta and omega values estimated in a first step based on i.v. data),
- (ii) fixed individual systemic PK parameters (IPP, fixed empiric Bayesian estimates), and
- (iii) simultaneous estimation of both systemic and pulmonary PK parameters based on the combined dataset of i.v. and inhalation data (ALL) [23].

Estimation of parameters based on PK datasets generated with ‘Model IIIa’ was done sequentially, using the PPP approach. Here, the individual PK parameters (i.e., the Empirical Bayes Estimates) of the four compartmental systemic model in the inhalation trial could vary within the pre-estimated inter-individual variability. To evaluate the probability of choosing the “right” model, model fits to the same dataset were compared with regard to the Akaike Information Criterion (AIC, [24]).

For all population analyses, the parameter estimation was performed using first-order conditional estimation (FOCE) with interaction. If the estimation step failed, up to two retries with varying initials were performed. The simulation-estimation process was repeated 500 times for each analysis.

Non-compartmental analysis of simulated datasets

In addition, or instead of analyzing clinical PK data with population approaches, non-compartmental analyses (NCA) [25] are often applied and can be used to infer absorption kinetics. Therefore, model-based predictions were compared to results from the NCA. To infer the pulmonary AUC_{0-inf} , the equation for AUC calculation in plasma (Eq. 1) was adjusted to the lung, inserting F_{pul} as the bioavailability (F) and the pulmonary absorption rate k_a as the elimination rate from the lung:

$$AUC_{0-inf} = \frac{Dose \cdot F}{CL} \quad (1)$$

$$AUC_{0-inf lung} = \frac{Dose_{inhaled} \cdot F_{pul}}{k_a \cdot V_{lung}} \quad (2)$$

V_{Lung} was set to 0.840 L based on literature values for lung weight [21]. A more detailed description of the NCA can be found in the supplementary material (Supplementary Material, S4). The above-mentioned metrics were calculated separately for each individual. Mean values were used for comparison to model-predicted population values.

Evaluation criteria

Evaluation of the structural identifiability of pulmonary absorption models

Pulmonary absorption models were deemed equivalent with regard to the systemic exposure if the newly predicted

plasma concentration–time profiles deviated from the originally simulated PK profiles by less than five percent, based on the geometric mean fold error (GMFE) comparing both profiles [26]. The GMFE was considered the best metric for this comparison, as it simultaneously compares the full plasma concentration–time profiles and equally weights under- and overpredicted concentrations:

$$GMFE = 10^{\frac{\sum \left| \log_{10} \left(\frac{Pred_i}{Obs_i} \right) \right|}{N}} \quad (3)$$

with Obs_i denoting the i th plasma concentration simulated by the original Simulation Model, and $Pred_i$ being the i th plasma concentration predicted by the Estimation Model. N denotes the total number of simulated data points.

Two different pulmonary exposure metrics were considered to determine the overall pulmonary exposure (area under the lung concentration–time curve, $AUC_{0-inf, lung}$) and the retention in the lungs (time to reach the before simulated pulmonary concentration after 24 h, $t_{C24h, lung}$). The $t_{C24h, lung}$ was considered to evaluate the duration of exposure instead of the more common terminal (pulmonary) elimination half-life, due to the fact that the terminal pulmonary half-life would be mainly dependent on the slowest absorption rate, whereas $t_{C24h, lung}$ is a compromise by all (up to three) parallel pulmonary absorption processes. Furthermore, we are not aware of any inhaled drugs, for which the dosing interval is longer than 24 h so that we consider $t_{C24h, lung}$ the better surrogate for this analysis than the terminal half-life. Adequate inference of lung exposure was considered for both metrics if the reevaluated value was within 80–125% of the originally simulated values, analogous to commonly applied bioequivalence criteria [27].

Performance of pulmonary absorption models in a clinical trial setting

For the population PK analyses, the acceptance criterion was 80–125% for $AUC_{0-inf, plasma}$. As the pulmonary PK metrics were inferred rather than measured, the related predictions of the pulmonary exposure were considered acceptable if predictions were within twofold of the true value for both the extent and duration of pulmonary exposure.

The accuracy of the exposure metrics was further evaluated based on the respective distribution (median, 2.5th and 97.5th percentiles of the predicted metrics). Furthermore, the relative bias of the mean (%Bias) was evaluated as follows, inserting the newly predicted and originally simulated exposure metrics as $Pred$ and Obs , respectively, and the total number of predicted values as N :

$$\%Bias = \frac{1}{N} \cdot \sum \frac{(Pred - Obs)}{Obs} \cdot 100 \quad (4)$$

Results

Evaluation of the structural identifiability of pulmonary absorption models

The results of the evaluation of structural identifiability can be grouped into four different scenarios regarding the predefined criteria (deviation of plasma profiles by less than 5%, and pulmonary $AUC_{0-inf, lung}$ and $t_{C24h, lung}$ within 80–125% of the simulated values), as shown in Table 2. Scenario (1) both plasma and lung exposure were described adequately; Scenario (2) plasma exposure was described adequately, but pulmonary exposure was not; Scenario (3) plasma concentration–time profiles were not captured well; and Scenario (4) the parameters were not identifiable (model not structurally identifiable). Only scenario 2 would result in inferring wrong pulmonary exposure without the possibility to discriminate the models based on plasma concentration data. One example for scenario 2 is the simulation with ‘Model NaL’ and re-estimation with ‘Model I’, as shown in Fig. 3. In this case, choosing the ‘wrong’ pulmonary absorption model would result in a 49.0-fold error in pulmonary AUC. Even though this might be expected, the analyses still underlined that these models can theoretically well describe clinical plasma PK data but would result in completely different pulmonary PK profiles (compare Fig. 3).

Examples for Scenarios 1 and 3 can be found in the supplementary material (Supplementary Material S3, Fig. S3). Plasma PK was described well in most simulation-estimation evaluations, except for simulations with ‘Model IIIa’. As expected, non-identifiable parameters were generally encountered when trying to fit more complex models (with more parameters) to data generated with simpler models, e.g. estimation with ‘Model II’ and ‘IIIa’ on simulated data of models ‘I’, ‘Transit’, and ‘NaL’. ‘Model NaL’ was unidentifiable if used for re-estimation, due to the correlation between F_{Pul} and k_{NaL} .

Link between empiric and mechanistic PK modeling

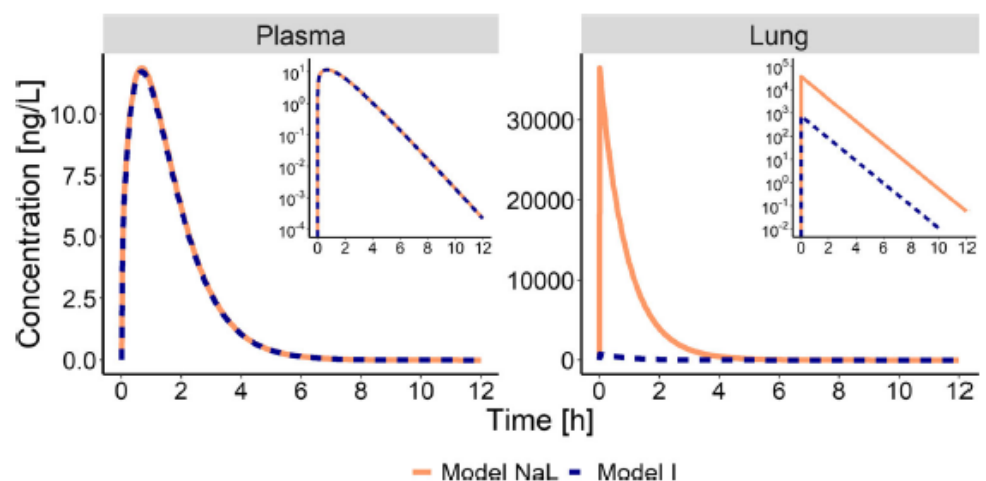
Of all models, only ‘Model II’ allowed adequately inferring on pulmonary exposure that was simulated with the semi-mechanistic model. The omission of redistribution of drug from plasma to the lung did not impact on inferred pulmonary exposure, showing a deviation from the simulation

Table 2 Description of systemic and pulmonary exposure

		<i>Estimation Model</i>				
		I	Transit	NaL	II	IIIa
<i>Simulation Model</i>	I	1	1	4	1	4
	Transit	2	1	4	4	4
	NaL	2	2	4	4	4
	II	2	2	4	1	4
	IIIa	3	3	3/4	1	1
	Semi-mechanistic	2	2	4	1	4

Rows: simulation model, columns: estimation model. 1: Adequate description of plasma and lung exposure; 2: adequate description of plasma, inadequate description of pulmonary exposure; 3: inadequate description of plasma PK (lung PK not investigated); 4: non-identifiable parameters. The color coding denotes the severity of error in inferring on pulmonary PK by choosing the Estimation Model over the true model: green: No relevant error, yellow: theoretically relevant error, but distinction based on plasma PK data possible; red: relevant error, no distinction possible based on plasma PK data (Color figure online)

Fig. 3 Simulated plasma (left) and lung (right) concentration–time profiles. Solid lines: ‘Model NaL.’ used for simulation. Dashed lines: Predictions based on ‘Model I’ used for re-estimation



of < 1% for both extent and duration of pulmonary exposure (Supplementary Material S2.3, Fig. S2).

Performance of pulmonary absorption models in a clinical trial setting

Simulation with ‘Model II’

Most of the Estimation Models used in the population simulation-estimation study involving ‘Model II’, with the exception of estimation with ‘Model I’ using the PPP method, were able to describe both plasma and pulmonary $AUC_{0-\infty}$ adequately, with over 90% of the runs within 80–125% of the true value. However, when comparing the retention in the lung, as determined by $t_{C24h,lung}$, both Estimation Models including ‘Model I’ for pulmonary absorption deviated substantially from the true value with a

bias of -60% to -50% (see Table 3). Applying the correct model resulted in all but one of the evaluations (using the PPP method) within twofold of the true $AUC_{0-\infty,lung}$. For the $t_{C24h,lung}$, 100% were within twofold. In all cases, the true model (four compartment systemic model and/or ‘Model II’) performed best with regard to the AIC. When using the PPP method, the estimates returned by the true model were slightly less precise in comparison to the other model structures with a median and 2.5th and 97.5th percentiles of 101% (62.8%, 147%) of the true value for $AUC_{0-\infty,lung}$ (see Table 3). Figure 4 shows an exemplary distribution of these exposure metrics.

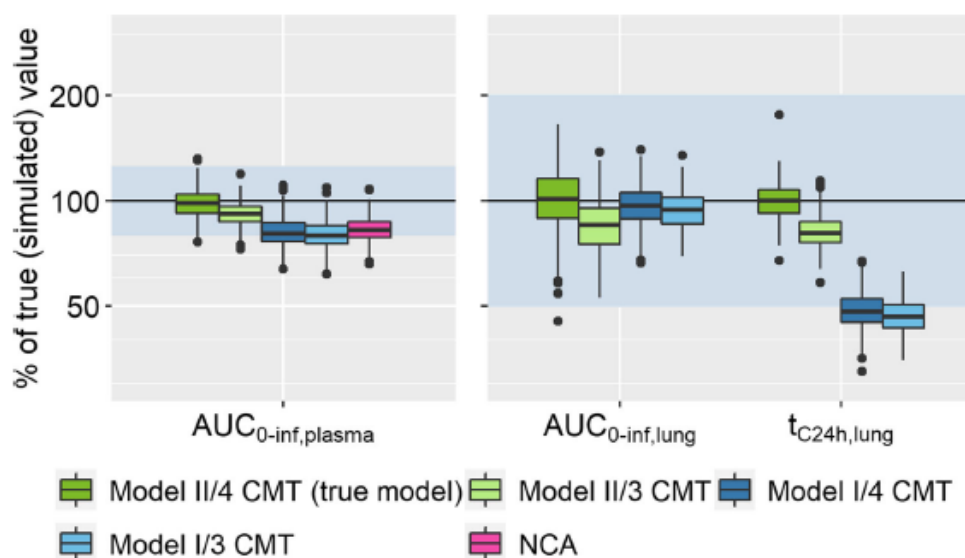
Choosing a three compartmental systemic disposition model instead of four compartments resulted in only slightly worse predictions in this analysis. However, the combination of a three-compartment systemic model with ‘Model II’ for pulmonary absorption converged in only

Table 3 Median [2.5th and 97.5th percentile], and width of the 95% interval of PK metrics inferred for oral drug inhalation

Absorption model	Systemic model	AUC _{0-inf,plasma}			AUC _{0-inf,lung} (extent of pulmonary exposure)			t _{C24h,lung} (duration of pulmonary exposure)		
		PPP	IPP	ALL	PPP	IPP	ALL	PPP	IPP	ALL
Model II	4 CMT	98.5%	99.5%	98.6%	101%	102%	103%	24.0 h	23.9 h	23.8 h
		[83.1%, 118%],	[85.7%, 116%],	[84.7%, 116%],	[62.8%, 147%],	[74.1%, 134%],	[76.5%, 135%],	[19.2 h, 29.4 h],	[19.0 h, 29.0 h],	[19.1 h, 28.8 h],
		34.9%	30.3%	31.3%	84.2%	59.9%	58.1%	10.2 h	10.0 h	9.69 h
Model II	3 CMT	91.9%	97.3%	96.6%	85.1%	82.4%	79.3%	19.6 h	19.9 h	18.9 h
		[76.6%, 107%],	[83.3%, 113%],	[82.5%, 111%],	[60.3%, 118%],	[55.5%, 117%],	[59.3%, 107%],	[16.0 h, 24.1 h],	[15.7 h, 25.9 h],	[16.0 h, 22.4 h],
		30.4%	29.3%	28.5%	57.7%	61.5%	47.7%	8.07 h	10.2 h	6.41 h
Model I	4 CMT	80.7%	94.4%	93.6%	96.5%	96.0%	90.6%	11.7 h	9.88 h	9.46 h
		[68.3%, 97.1%],	[81.0%, 111%],	[80.4%, 110%],	[74.0%, 128%],	[74.1%, 119%],	[68.4%, 118%],	[9.20 h, 14.7 h],	[7.50 h, 12.5 h],	[7.15 h, 12.3 h],
		28.8%	30.0%	29.6%	54.0%	42.5%	49.2%	5.50 h	5.00 h	5.19 h
Model I	3 CMT	79.2%	91.2%	90.1%	94.1%	91.4%	91.0%	11.3 h	9.52 h	9.62 h
		[67.2%, 94.6%],	[78.4%, 107%],	[77.2%, 105%],	[75.1%, 118%],	[72.0%, 115%],	[74.2%, 114%],	[9.10 h, 13.9 h],	[7.50 h, 12.1 h],	[7.62 h, 12.1 h],
		27.4%	28.6%	27.8%	42.9%	43.0%	40.2%	4.80 h	4.60 h	4.48 h

Values for AUCs are given as percentage of the true value, t_{C24h,lung} is given as absolute values. Simulation Model: 'Model II/4CMT'. CMT: compartments. PPP: fixed systemic population parameters; IPP fixed individual parameters; ALL: simultaneous fit of all parameters

Fig. 4 Exposure metrics estimated on data simulated with 'Model II/4cmt using the PPP method. 3 CMT and 4 CMT denote the number of systemic PK compartments; 'Model I' or 'II' describes the pulmonary absorption model, with one or two parallel absorption processes, respectively. The shaded area represents the accepted range (80–125% for plasma, twofold deviation for lung metrics). Number of successful estimations: 424 (II/4 CMT), 361 (II/3 CMT), 464 (I/4 CMT), and 471 (I/3 CMT)



50–70% of runs vs. convergence of > 85% in the other scenarios. In terms of stability, the PPP method performed best, while the ALL method was slightly more unstable than the IPP approach.

Regarding the modeling approaches, PPP, IPP, and ALL performed comparable with regard to predicted systemic but also inferred extent and duration of pulmonary exposure (see Table 3). One notable exception was the combination of the PPP approach with 'Model I' as the Estimation Model. In this case, AUC_{0-inf,plasma} after

inhalation was less often predicted well (only 55% and 45% of successful runs within 80% to 125% of the true value, for a three and four compartmental systemic PK model, respectively). However, the prediction of t_{C24h,lung} was marginally better than with the other two approaches (28.7% and 40.5% of predictions within twofold of the true value, compared to 3–5% with the other methods). A comparison of the precision and the parameter estimates acquired using the three methods for the true model can be found in the supplementary material (Supplementary

Material S6, Table S5). Model predictions were also compared to the results from the NCA. While the $AUC_{0-inf,plasma}$ was described adequately for most evaluations, calculation of the MAT resulted in negative values for some subjects, preventing the calculation of $AUC_{0-inf,lung}$. Melin et al. [15] also encountered this in the original publication.

Simulation with ‘Model IIIa’

The simulation/re-estimation analysis with ‘Model IIIa’ as the Simulation Model resulted in a systematic overestimation of lung exposure, regardless which model was used for estimation (Fig. 5). $AUC_{0-inf,plasma}$ was mostly estimated well. In this case too, the true model (‘Model IIIa’) was superior with regard to the AIC. All model predictions tended towards overestimation (bias of 23.4%, 26.4%, and 27.8% for ‘Model IIIa’, ‘IIIb’, and ‘II’, respectively). ‘Model IIIa’ gave overall more precise but slightly biased estimates, 105% (87.4%, 253%) of the original value (median, 2.5th and 97.5th percentiles) for $AUC_{0-inf,plasma}$, 153% (89.0%, 299%) for $AUC_{0-inf,lung}$, and 38.1 h (22.4 h, 65.0 h) for $t_{C24h,lung}$. 74.8%, 97.9%, and 100% of the evaluations were within twofold, threefold, and fivefold of the true $AUC_{0-inf,lung}$. For the $t_{C24h,lung}$ 82.4%, 99.2%, 100% were within twofold, threefold, and fivefold, respectively. In comparison, the estimates by the other two models were less precise. The respective median values with 2.5th to 97.5th percentiles for all Estimation Models can be found in Table 4.

To further investigate potential reasons for the overestimation and imprecision of lung exposure, the estimates of the systemic PK parameters were further investigated. The parameter estimates characterizing the distribution to the deep tissue compartment (Q2 and V2) showed high variability, with V2 ranging from 10 to 2000% of the true value

used for data simulation. Further investigations revealed a correlation between V2 and the pulmonary absorption rates. As a follow-up, $AUC_{0-inf,lung}$ and $t_{C24h,lung}$ were compared between runs with accurate parameters (Q2 and V2 within 80–125% of the true values) and those with inaccurate parameters. The resulting distributions can be seen in Fig. 6. The runs with Q2 and V2 estimates close to their true values showed no overestimation of pulmonary exposure; all predictions were within twofold and over 75% of runs within 80–125% for both pulmonary exposure metrics. Precision of the predictions also improved greatly (median and 2.5th and 97.5th percentiles: 105% (81.5%, 120%) of the true value for $AUC_{0-inf,lung}$; 24.7 h (18.7 h, 29.6 h) for $t_{C24h,lung}$, ‘Model IIIa’). While the difference between the models was marginal, ‘Model IIIa’ resulted in the best predictions (Table 4). Given the published clinical designs for the i.v. study, the systemic disposition parameters could only be adequately estimated in 11.6% of the simulation estimation studies. The majority of runs with inaccurate systemic PK parameters presented a substantial overestimation of both $AUC_{0-inf,lung}$ and $t_{C24h,lung}$ with approximately 30% showing a deviation of greater than twofold from the original.

Discussion

It is challenging to evaluate the local pharmacokinetics after drug administration, especially when the target organ is identical to the site of administration. However, for many locally administered drugs it is assumed that local drug concentrations provide efficacy [28]. In these cases, a good understanding of the local PK is desirable. PK modeling based on plasma PK data might be one of the easiest approaches to infer pulmonary exposure after drug inhalation. In contrast to experimental determination of

Fig. 5 Exposure metrics estimated on data simulated with ‘Model IIIa’. The shaded area represents the accepted range (80–125% for plasma, twofold deviation for lung metrics). Number of successful estimations: 473 (IIIa), 472 (IIIb), and 474 (II)

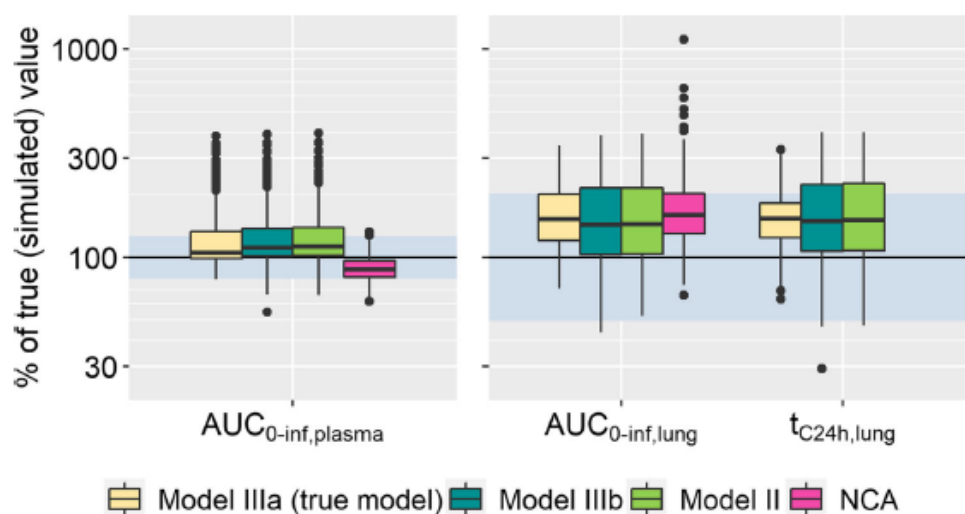


Table 4 Median [2.5th and 97.5th percentile], width of the 95% interval, and relative bias of the mean (%Bias) for the population analysis based on datasets simulated with ‘Model IIIa’

	Absorption model	AUC _{0-inf,lung} (extent of pulmonary exposure)			t _{C24h,lung} (duration of pulmonary exposure)		
		Total	Inadequate systemic PK	Adequate systemic PK	Total	Inadequate systemic PK	Adequate systemic PK
Median [2.5th, 97.5th percentiles], width of the 95% interval	Model IIIa	153% [89.0%, 299%], 210%	162% [100%, 299%], 199%	105% [81.5%, 120%], 38.5%	38.1 h [20.0 h, 64.5 h], 44.5 h	38.1 h [22.4 h, 65.0 h], 42.6 h	24.7 h [18.7 h, 29.6 h], 10.9 h
	Model IIIb	144% [69.3%, 337%], 268%	153% [68.1%, 340%], 271%	90.2% [71.1%, 107%], 35.9%	41.4 h [15.1 h, 84.8 h], 69.6 h	38.4 h [14.9 h, 85.2 h], 70.2 h	21.8 h [16.6 h, 26.8 h], 10.3 h
	Model II	145% [70.1%, 341%], 271%	155% [69.2%, 345%], 276%	91.2% [71.6%, 108%], 36.4%	41.8 h [15.6 h, 85.5 h], 69.8 h	38.8 h [15.3 h, 86.3 h], 70.9 h	22.1 h [16.8 h, 27.1 h], 10.3 h
	NCA	160% [92.8%, 339%], 246%	176% [110%, 338%], 228%	158% [89.0%, 336%], 247%	–	–	–
%Bias (mean)	Model IIIa	67.0%	76.7%	2.88%	58.6%	67.1%	2.86%
	Model IIIb	66.2%	77.9%	– 11.0%	72.7%	86.6%	– 7.89%
	Model II	67.7%	79.5%	– 10.2%	74.2%	85.1%	– 8.99%
	NCA	126%	124%	139%	–	–	–

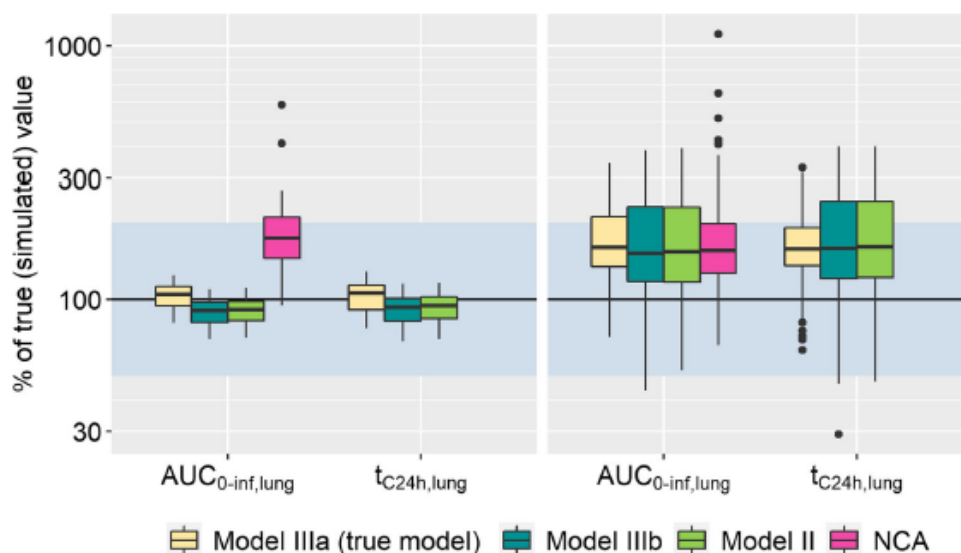


Fig. 6 Exposure metrics estimated on data simulated with ‘Model IIIa’ separated by the adequacy of systemic PK parameters (deep compartment). Left panel: adequate systemic PK; right panel: inadequate systemic PK. Adequate systemic PK: Parameters Q2 and V2 within 80–125% of the true values and the corresponding NCA

predictions. The shaded area represents the accepted range (80–125% for plasma, twofold deviation for lung metrics). Number of estimations with adequate systemic PK: 58 (each of the models). Number of estimations with inadequate systemic PK: 415, 414, and 416 for IIIa, IIIb, and II, respectively

pulmonary exposure, modeling does not require additional invasive exposure measurements or imaging data. Therefore, the aim of this work was to evaluate the possibilities and limitations of using empirical PK models for pulmonary absorption to infer both the extent and duration of pulmonary PK. This investigation showed that empirical PK modeling can be a valuable tool to infer pulmonary PK. Finally, based on the results a strategy for PK (modeling) analyses was developed, including (1) the right choice of pulmonary absorption models, and (2) a quantitative evaluation of bias and precision of inferring the extent and duration of pulmonary exposure based on realistic clinical datasets.

As a first step of performing a modeling analysis to infer the pulmonary PK, suitable model structures should be selected based on *prior* knowledge about relevant pulmonary PK processes. The reason is that most of the here investigated absorption models were discussed to have a physiological interpretation, ranging from non-absorptive loss via mucociliary clearance or pulmonary metabolism [16] to parallel absorption processes in different lung regions [9]. The only investigated model without an obvious underlying physiological reasoning is the ‘Model Transit’, as drug absorption can start everywhere in the lung simultaneously (e.g., conducting airways and alveolar space). Therefore, and as this empiric transit absorption model is rarely applied to characterize pulmonary absorption, this model structure will not be further discussed.

Pre-selection of plausible models can be done for example based on *in vitro* experiments (e.g. dissolution measurements [29] and/or metabolic stability in lung slices [30]), or preclinical *in vivo* studies. Without this data, this modeling analysis showed that no inference on pulmonary PK is possible (i.e., different models describing the plasma PK adequately resulted in approximately 50-fold differences with regard to pulmonary exposure). If prior knowledge suggests that pulmonary metabolism is present or that mucociliary clearance is relevant due to slow dissolution, a model-based approach with implementation of these processes is necessary to achieve adequate predictions of pulmonary exposure (e.g., ‘Model NaL’). It has to be noted that, even when selecting the right model for a drug with non-absorptive loss, the parameter estimation process resulted in unidentifiable parameters. Sakagami et al. suggested that this instability can be circumvented by fixing the lung dose [31]. However, this requires detailed information about the lung dose, which is subject to great variability, both between subjects and between occasions [9, 32, 33]. It is therefore debatable, if empirical PK analysis based on plasma data will provide valuable insights into pulmonary PK for this scenario.

If the relevance of pulmonary metabolism and mucociliary clearance is negligible, it is possible to explore

pulmonary PK by implementation of parallel absorption processes (‘Model I’–‘III’). The structural identifiability evaluation showed, that in one case (simulation with ‘Model II’ and re-estimation with ‘Model I’), the pulmonary absorption models could not be distinguished based on plasma PK data, according to the predefined criteria, yet yielded different outcomes for pulmonary exposure. While both model candidates provided adequate predictions of systemic PK and the extent of pulmonary exposure, the duration of lung retention metric $t_{C24h, lung}$ was significantly underestimated with the less complex ‘Model I’. This might have consequences for selecting dosing schemes when the dosing intervals are pre-selected based on PK rather than PD readouts.

While the first part of our study was based on full PK profiles without any simulated variability to evaluate the structural identifiability and inter-changeability of the models, clinical data is typically analyzed with a population (PK) approach to quantify different variability components (inter-individual, intra-individual, inter-occasion, etc.). Both inhalation and *i.v.* data are required to perform deconvolutions. Unfortunately, *i.v.* data is rarely available in the same individuals as inhalation data. Therefore, an understanding of the implications is required, and a strategy has to be developed, how to best perform such a population approach. To this end, it is helpful to have an overview about the opportunities and limitations of the available options. The PPP method is the most widely applicable method and can always be applied if *i.v.* and inhalation data are present. Both IPP and ALL were found to be reasonable methods if *i.v.* and inhalation PK have been measured in the same subjects. However, in light of the marginal differences regarding parameter estimates (Supplementary Material, Table S5) and estimated PK metrics in this investigation, it is debatable if the added effort of conducting *i.v.* and inhalation trials in the same subjects is justified. A decision tree showing the requirements for each approach is shown in Fig. 7.

In general, modelling provided fairly accurate predictions for extent and duration of pulmonary exposure (most predictions within twofold of the true value), given that the correct model structure can be identified. Misspecification of the absorption model could result in failure to capture the duration of exposure, as could be seen in the analysis based on ‘Model II’. Analogous to the structural identifiability analysis, re-evaluation of pulmonary exposure metrics based on simulated clinical datasets with only one absorption process adequately predicted the pulmonary AUC, but substantially underestimated the retention (only 3% to 40% within twofold of the true value, i.e. $t_{C24h, lung} < 12$ h). Based on these PK estimates alone, bi-daily dosing might be chosen instead of the ‘true’ once-daily administration, showing that PD readouts should

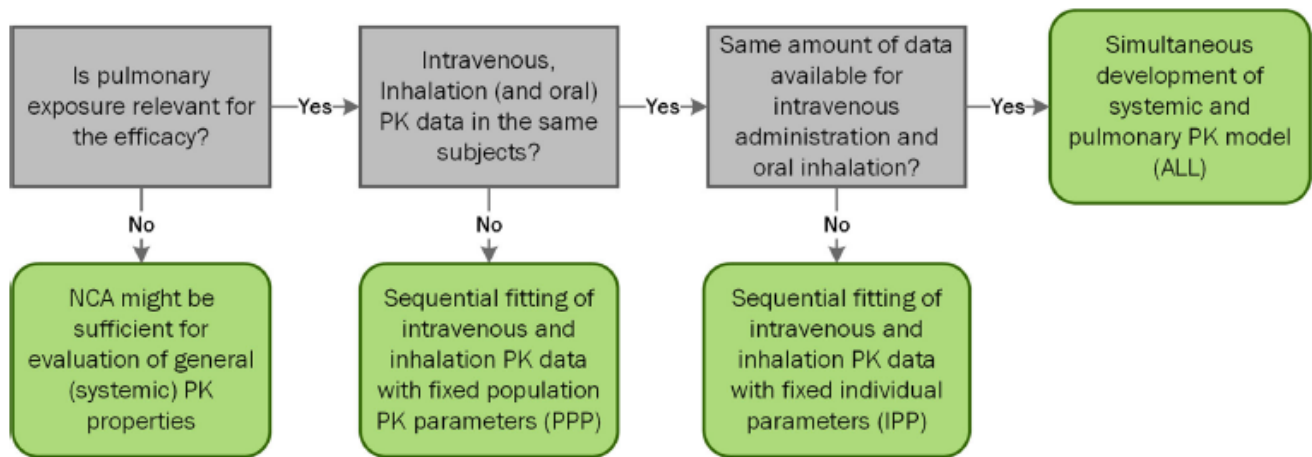


Fig. 7 Suggested decision tree for choosing a modeling approach

always be considered, when possible for the respective mechanism of action, to make these decisions. However, the true model would always have been chosen based on statistical model-selection criteria. Therefore, when carefully performing such a modeling analysis, a proper discrimination between these models seems possible. Finally, based on the here presented findings, a post-hoc analysis similar to the presented approach based on the finally selected model structure, the estimated PK parameters, and the investigated data set should be considered to assess the robustness of the model-based inference on pulmonary PK. If the results prove to be reliable and do not contradict other available information, the predictions should provide a reasonable basis to support dosing and posology decisions.

It should be kept in mind that even with the ‘correct’ pulmonary absorption model and an adequate modeling strategy there are still some critical aspects to consider. For example, the population PK analysis based on ‘Model IIIa’ demonstrated a bias in both pulmonary exposure metrics caused by inaccurate estimation of systemic PK parameters. Here, a high correlation was found between the volume of distribution of the systemic deep tissue compartment V_2 and the slow pulmonary absorption rate. Probably, the slow absorption rate constant (k_{slow}) was compensating for underestimation of the systemic terminal half-life based on i.v. data. Lower estimates for V_2 led to a shorter terminal elimination half-life, and in the inhalation trials with longer sampling times (up to 8 days after the last dose), the terminal half-life of ~ 30 h was therefore attributed to the slow absorption from the lung. Even in the original publication, the absence of flip-flop kinetics could only be demonstrated by the inclusion of urine data [9]. This potential bias in both extent and duration of pulmonary exposure further underlines the importance of high

quality i.v. PK data and could have possibly been avoided by extending the sampling times after i.v. administration. However, this may not always be feasible, as orally inhaled drugs potentially produce (dose-limiting) side effects precluding the use of higher doses to be able to observe the ‘true’ terminal phase in the PK profile [34, 35]. The identification of flip-flop kinetics for an inhaled drug with a high volume of distribution may indicate that the terminal phase after i.v. administration is not adequately captured by the PK data. This is even more likely if the long pulmonary retention is hypothesized to be the result of high tissue affinity to the lung, as this should be relevant after both i.v. administration and inhalation. In these cases, the slowest absorption constant should not be smaller than the elimination constant. Interestingly, for ‘Model IIIa’, only $\sim 10\%$ of the simulation-estimation analyses allowed adequately estimating the systemic disposition parameters. This also means that in $\sim 90\%$ of the analyses there would have been a relevant risk of overestimating the extent and duration of pulmonary exposure. However, even in these cases, given the correct model structure, most predictions ($> 70\%$) were still within twofold and less than 3% outside threefold of the true value.

Last but not least, the population PK modeling approaches were also compared to the commonly applied NCA, inferring on pulmonary retention based on the NCA-based pulmonary absorption rate. These analyses, performed in parallel to the population PK analyses, yielded ambivalent results for both scenarios. While the NCA performed on the dataset simulated with ‘Model IIIa’ resulted in plausible, yet biased values, the simulation with ‘Model II’ could not be analyzed with an NCA, as for some individuals the MRT after inhalation was shorter than after i.v. administration. Even for individuals with a positive MAT, the mean predicted $AUC_{0-\text{inf},\text{lung}}$ was over tenfold higher than

the true value (a more detailed investigation of this can be found in the online Supplementary Material). Therefore, based on our analysis, an NCA-based deconvolution of the data cannot be recommended to infer pulmonary exposure.

Few limitations of the present study are acknowledged: One limitation of all the here investigated model structures is that re-distribution from plasma to lung tissue is not accounted for, potentially leading to underestimation of lung concentrations at later time points. However, the comparison of the investigated models with a semi-mechanistic model for salmeterol that does include backflow to the lung showed only minimal deviations in the predicted lung tissue. This suggests that the impact on inferred lung exposure was negligible in this investigation. It should be considered that salmeterol displays high systemic clearance after drug absorption from the lung. For drugs with slower elimination from the systemic perfusion, also the relevance of re-distribution to the lungs would increase.

Another limitation is that investigated models cannot discriminate between dissolution and absorption. This may not be a problem for some of the investigated drugs (e.g. olodaterol for ‘Model IIIa’), which are dissolving very quickly (or are already administered as a solution). However, the absorption of fluticasone propionate (‘Model I’) has been postulated to be limited by its dissolution rate, possibly even masking parallel absorption of dissolved drug with differing rates limiting the applicability of the presented approach. Furthermore, as pulmonary concentrations of inhaled drugs can differ regionally due to local physiology and deposition patterns, considering the averaged drug concentrations of the whole lung might not provide entirely accurate depictions of actual target site concentration [1, 36]. In some cases, even making the best use of the plasma PK data, plasma concentrations may not be a good surrogate, e.g. due to accumulation in lung tissue (active transport, lysosomal trapping). Here, additional information about the relevant processes may help the interpretation of results.

A limitation of sequentially fitting i.v. and inhalation data from different individuals (PPP approach) is the assumption that the systemic PK of subjects is comparable in the i.v. and the inhalation PK studies. This might not always hold true. For example, it might be important to consider if the i.v. study was performed in healthy volunteers, and inhalation trials included in the dataset were conducted in patients with potentially altered physiology. In general, sequentially fitting the i.v. and inhalation data (PPP and IPP) might result in underestimation of the parameter uncertainty for the pulmonary absorption parameters [23]. The influence of sequential fitting methods on parameter uncertainty was previously investigated in more detail by Zhang et al. [37, 38]. Notably, the PK analyses in this work were performed with only one set of

simulation parameters per pulmonary absorption model, directly based on the original publications to ensure that the tested scenarios and study designs are realistic. A repetition with different simulation parameters may result in different conclusions. For example, the lower the difference between the parallel absorption rate constants, the harder it might be to differentiate between different pulmonary absorption processes.

Moreover, the analyses did not account for concentrations below the lower limit of quantification, which can have great impact on reasonable study designs and result in distortion of parameter estimates [39] but was beyond the scope of the present study. The impact of data below the limit of quantification was investigated and described in the original publications of the here chosen examples. Neither Borghardt et al. [9] nor Melin et al. [15] reported a significant effect of accounting for missing data in the modeling process. Due to the previous investigations and conclusions for the model drugs, we decided to not include these characteristics in our evaluations. However, it cannot be precluded that unaccounted-for missing data may lead to false conclusions in other cases, especially as inhaled doses are typically low in the μg range and this can result in high fractions of data being below the limit of quantification.

The analysis based on clinical datasets included only proportional residual variability, which might influence parameter estimation, as this may not adequately represent the measurement errors at lower concentrations. Investigating the impact of identifying the correct residual variability model on inferring pulmonary exposure may be an interesting follow-up study.

Even though the here evaluated models are based on physiological reasoning, all of them represent empirical modeling approaches. Until today, the link between these empiric model structures and mechanistic PK models is not systematically established. Adequate implementation of all the relevant pulmonary PK processes after inhalation would require more mechanistic PK models (compare mechanistic PK models e.g. by Boger et al. [40] or Hartung and Borghardt [41]). However, while these more mechanistic PK models would allow simulation of time-resolved PK profiles in different areas of the lung, these mechanistic PK models can typically not be estimated based on available clinical data. In the future, more integrative PK modeling approaches relying on plasma PK data, preclinical in vitro, and preclinical in vivo experiments can be expected to allow even better inference on pulmonary exposure and retention times, when mucociliary clearance and slow dissolution kinetics are of relevance. In any case, checking the plausibility of parameter estimates based on prior knowledge is always advisable.

Conclusion

This work illustrated the value of PK modeling to infer the extent and duration of pulmonary exposure from systemic concentration–time profiles. When the aim is to learn about the pulmonary fate of orally inhaled drugs, our analysis indicated that PK modeling is superior to NCA. It was demonstrated that when selecting the right structural systemic and pulmonary absorption model, which was not always trivial even based on rich clinical datasets, the error in the majority of predictions of extent and duration of pulmonary exposure was less than twofold. Sequential versus simultaneous estimation of systemic and pulmonary PK parameters both provided good results and only showed marginal differences in the prediction of pulmonary PK. It was also demonstrated that inferring the extent of pulmonary exposure was more robust in comparison to inferring the pulmonary retention if the wrong structural absorption model was used. However, even with very rich clinical datasets, still a moderate risk remains that the pulmonary retention is not adequately inferred. Therefore, while modelling was proven to be a useful tool to learn about the pulmonary fate of inhaled drugs, care should be taken when basing decisions about doses and especially dosing posology solely on inference from plasma PK. Given the uncertainties, a post-hoc simulation-estimation analysis to evaluate the robustness of model predictions would be recommended, and if possible, model-based predictions of the pulmonary PK should always be used in conjunction with available PD data.

Supplementary Information The online version contains supplementary material available at <https://doi.org/10.1007/s10928-021-09780-x>.

Acknowledgements This research was funded by Boehringer Ingelheim Pharma GmbH & Co. KG. We thank Astrid Bröker (University of Hamburg) and Dzenefa Alihodzic (University Medical Center Hamburg-Eppendorf) for previous work on the automation of simulation-estimation workflows.

Open Access This article is licensed under a Creative Commons Attribution 4.0 International License, which permits use, sharing, adaptation, distribution and reproduction in any medium or format, as long as you give appropriate credit to the original author(s) and the source, provide a link to the Creative Commons licence, and indicate if changes were made. The images or other third party material in this article are included in the article's Creative Commons licence, unless indicated otherwise in a credit line to the material. If material is not included in the article's Creative Commons licence and your intended use is not permitted by statutory regulation or exceeds the permitted use, you will need to obtain permission directly from the copyright holder. To view a copy of this licence, visit <http://creativecommons.org/licenses/by/4.0/>.

Funding Open Access funding enabled and organized by Projekt DEAL.

References

- Himstedt A, Braun C, Wicha SG, Borghardt JM (2020) Towards a quantitative mechanistic understanding of localized pulmonary tissue retention—a combined in vivo/in silico approach based on four model drugs. *Pharmaceutics* 12(5):408
- Dhanani J, Roberts JA, Chew M, Lipman J, Boots RJ, Paterson DL, Fraser JF (2010) Antimicrobial chemotherapy and lung microdialysis: a review. *Int J Antimicrob Agents* 36(6):491–500
- Guo Y, Chu X, Parrott NJ, Brouwer KL, Hsu V, Nagar S, Matsson P, Sharma P, Snoeys J, Sugiyama Y (2018) Advancing predictions of tissue and intracellular drug concentrations using in vitro, imaging and physiologically based pharmacokinetic modeling approaches. *Clin Pharmacol Ther* 104(5):865–889
- Dolovich MB, Bailey DL (2012) Positron emission tomography (PET) for assessing aerosol deposition of orally inhaled drug products. *J Aerosol Med Pulm Drug Deliv* 25(S1):S52–S71
- Morgan P, Van Der Graaf PH, Arrowsmith J, Feltner DE, Drummond KS, Wegner CD, Street SD (2012) Can the flow of medicines be improved? Fundamental pharmacokinetic and pharmacological principles toward improving Phase II survival. *Drug Discov Today* 17(9–10):419–424
- Vaughan D, Dennis M (1978) Mathematical basis of point-area deconvolution method for determining in vivo input functions. *J Pharm Sci* 67(5):663–665
- Yu Z, Schwartz JB, Sugita ET, Foehl HC (1996) Five modified numerical deconvolution methods for biopharmaceutics and pharmacokinetics studies. *Biopharm Drug Dispos* 17(6):521–540
- Gomeni R, Bressolle-Gomeni F (2020) Deconvolution analysis by non-linear regression using a convolution-based model: comparison of nonparametric and parametric approaches. *AAPS J*. <https://doi.org/10.1208/s12248-019-0389-8>
- Borghardt JM, Weber B, Staab A, Kunz C, Formella S, Kloft C (2016) Investigating pulmonary and systemic pharmacokinetics of inhaled olodaterol in healthy volunteers using a population pharmacokinetic approach. *Br J Clin Pharmacol* 81(3):538–552. <https://doi.org/10.1111/bcp.12780>
- Bartels C, Looby M, Sechaud R, Kaiser G (2013) Determination of the pharmacokinetics of glycopyrronium in the lung using a population pharmacokinetic modelling approach. *Br J Clin Pharmacol* 76(6):868–879. <https://doi.org/10.1111/bcp.12118>
- Dershwitz M, Walsh John L, Morishige Richard J, Connors Patricia M, Rubsamen Reid M, Shafer Steven L, Rosow Carl E (2000) Pharmacokinetics and pharmacodynamics of inhaled versus intravenous morphine in healthy volunteers. *Anesthesiology* 93(3):619–628. <https://doi.org/10.1097/0000542-20009000-00009>
- Krishnaswami S, Hochhaus G, Möllmann H, Barth J, Derendorf H (2005) Interpretation of absorption rate data for inhaled fluticasone propionate obtained in compartmental pharmacokinetic modeling. *Int J Clin Pharmacol Ther* 43(3):117–122. <https://doi.org/10.5414/CP43117>
- Borghardt JM, Weber B, Staab A, Kloft C (2015) Pharmacometric models for characterizing the pharmacokinetics of orally inhaled drugs. *AAPS J* 17(4):853–870. <https://doi.org/10.1208/s12248-015-9760-6>
- Diderichsen PM, Cox E, Martin SW, Cleton A, Ribbing J (2013) Characterizing systemic exposure of inhaled drugs: application to the long-acting beta2-agonist PF-00610355. *Clin Pharmacokinet* 52(6):443–452. <https://doi.org/10.1007/s40262-013-0048-7>
- Melin J, Prothon S, Kloft C, Cleton A, Amilon C, Jonup C, Bäckman P, Olsson B, Hamrén UW (2017) Pharmacokinetics of the inhaled selective glucocorticoid receptor modulator AZD5423 following inhalation using different devices. *AAPS J* 19(3):865–874. <https://doi.org/10.1208/s12248-016-0042-8>

16. Sakagami M (2004) Insulin disposition in the lung following oral inhalation in humans: a meta-analysis of its pharmacokinetics. *Clin Pharmacokinet* 43(8):539–552. <https://doi.org/10.2165/00003088-200443080-00004>
17. Borgström L, Nilsson M (1990) A method for determination of the absolute pulmonary bioavailability of inhaled drugs: terbutaline. *Pharm Res* 7(10):1068–1070
18. Ward JK, Dow J, Dallow N, Eynott P, Miller S, Ventresca GP (2000) Enantiomeric disposition of inhaled, intravenous and oral racemic-salbutamol in man—no evidence of enantioselective lung metabolism. *Br J Clin Pharmacol* 49(1):15–22
19. R Core Team (2016) R: a language and environment for statistical computing, 3.3.2. R Foundation for Statistical Computing, Vienna
20. Soetaert KE, Petzoldt T, Setzer RW (2010) Solving differential equations in R: package deSolve. *J Stat Softw* 33:1–25
21. Molina DK, DiMaio VJM (2012) Normal organ weights in men: part II—the brain, lungs, liver, spleen, and kidneys. *Am J Forensic Med Pathol* 33(4):368–372
22. A Study in Healthy Subjects to Investigate Pharmacokinetics of AZD5423 When Administered in Different Ways (2012) U.S. National Library of Medicine. <https://ClinicalTrials.gov/show/NCT01635985> Accessed 9 Nov 2020
23. Lacroix BD, Friberg LE, Karlsson MO (2012) Evaluation of IPPSE, an alternative method for sequential population PKPD analysis. *J Pharmacokinet Pharmacodyn* 39(2):177–193
24. Akaike H (1998) A new look at the statistical model identification. In: Parzen E, Tanabe K, Kitagawa G (eds) Selected papers of Hirotugu Akaike. Springer, New York, pp 215–222. https://doi.org/10.1007/978-1-4612-1694-0_16
25. Gabrielsson J, Weiner D (2012) Non-compartmental analysis. *Methods Mol Biol* 929:377–389. https://doi.org/10.1007/978-1-62703-050-2_16
26. Lombardo F, Waters NJ, Argikar UA, Dennehy MK, Zhan J, Gunduz M, Harriman SP, Berellini G, Rajlic IL, Obach RS (2013) Comprehensive assessment of human pharmacokinetic prediction based on in vivo animal pharmacokinetic data, part 1: volume of distribution at steady state. *J Clin Pharmacol* 53(2):167–177. <https://doi.org/10.1177/0091270012440281>
27. Guidance FDA (2001) Statistical approaches to establishing bioequivalence. Center for drug evaluation and research. United States Food and Drug Administration, Silver Spring
28. Tayab ZR, Hochhaus G (2005) Pharmacokinetic/pharmacodynamic evaluation of inhalation drugs: application to targeted pulmonary delivery systems. *Expert Opin Drug Deliv* 2(3):519–532. <https://doi.org/10.1517/17425247.2.3.519>
29. Rohrschneider M, Bhagwat S, Krampe R, Michler V, Breikreutz J, Hochhaus G (2015) Evaluation of the transwell system for characterization of dissolution behavior of inhalation drugs: effects of membrane and surfactant. *Mol Pharm* 12(8):2618–2624
30. Yilmaz Y, Williams G, Walles M, Manevski N, Krähenbühl S, Camenisch G (2019) Comparison of rat and human pulmonary metabolism using precision-cut lung slices (PCLS). *Drug Metab Lett* 13(1):53–63
31. Raut A, Dhapare S, Venitz J, Sakagami M (2020) Pharmacokinetic profile analyses for inhaled drugs in humans using the lung delivery and disposition model. *Biopharm Drug Dispos* 41(1–2):32–43
32. Borgström L, Olsson B, Thorsson L (2006) Degree of throat deposition can explain the variability in lung deposition of inhaled drugs. *J Aerosol Med* 19(4):473–483
33. Brand P, Friemel I, Meyer T, Schulz H, Heyder J, Häußinger K (2000) Total deposition of therapeutic particles during spontaneous and controlled inhalations. *J Pharm Sci* 89(6):724–731
34. Harding S (1990) The human pharmacology of fluticasone propionate. *Respir Med* 84:25–29
35. Rohatagi S, Appajosyula S, Derendorf H, Szeffler S, Nave R, Zech K, Banerji D (2004) Risk-benefit value of inhaled glucocorticoids: a pharmacokinetic/pharmacodynamic perspective. *J Clin Pharmacol* 44(1):37–47
36. Backstrom E, Hamm G, Nilsson A, Fihn BM, Strittmatter N, Andren P, Goodwin RJA, Friden M (2018) Uncovering the regional localization of inhaled salmeterol retention in the lung. *Drug Deliv* 25(1):838–845. <https://doi.org/10.1080/10717544.2018.1455762>
37. Zhang L, Beal SL, Sheiner LB (2003) Simultaneous vs. sequential analysis for population PK/PD data I: best-case performance. *J pharmacokinet Pharmacodyn* 30(6):387–404
38. Zhang L, Beal SL, Sheiner LB (2003) Simultaneous vs. sequential analysis for population PK/PD data II: robustness of methods. *J Pharmacokinet Pharmacodyn* 30(6):405–416
39. Duval V, Karlsson MO (2002) Impact of omission or replacement of data below the limit of quantification on parameter estimates in a two-compartment model. *Pharm Res* 19(12):1835–1840
40. Boger E, Evans N, Chappell M, Lundqvist A, Ewing P, Wiggenborg A, Fridén M (2016) Systems pharmacology approach for prediction of pulmonary and systemic pharmacokinetics and receptor occupancy of inhaled drugs. *CPT: Pharmacomet Syst Pharmacol* 5(4):201–210. <https://doi.org/10.1002/psp4.12074>
41. Hartung N, Borghardt JM (2020) A mechanistic framework for a priori pharmacokinetic predictions of orally inhaled drugs. *PLoS Comput Biol* 16(12):e1008466. <https://doi.org/10.1371/journal.pcbi.1008466>

Publisher's Note Springer Nature remains neutral with regard to jurisdictional claims in published maps and institutional affiliations.

4 Discussion

The results of the presented publications represent the application of pharmacometric approaches to elucidate local pulmonary PK with a focus on pulmonary absorption and distribution processes. The developed rat lung PBPK model was evaluated with unprecedented granularity of lung sub-structure PK data, including trachea, bronchi, and alveolar tissue, as well as tracheal and (bronchio-)alveolar lining fluid measured within the same animals. This adds a new facet to be able to quantitatively compare the differences in distribution characteristics between these structures, as well as help separate its impact from competing PK processes. In addition to introducing a novel method to assess localized time-resolved pulmonary PK, the results of publications I and II showed that the distribution characteristics and therefore also the concentration-time profiles may change substantially between different lung structures. The meta-analysis across published pulmonary absorption models offered further insights into the suitability of plasma PK profiles to infer on pulmonary exposure metrics and efficacious concentrations for locally acting drugs.

In the following overarching discussion, the impact of understanding pulmonary PK processes, but especially pulmonary absorption and distribution, the role of pharmacometric approaches for orally inhaled drugs – and therefore also the impact of this work – will be discussed from early drug discovery and non-clinical development to clinical development (Sections 4.1- 4.3).

4.1 Drug discovery and research

As mentioned in the introduction, the discovery and development of orally inhaled drugs is quite distinct from those for typical oral or parenteral dosage forms, as well as cost- and time-intensive. While not a small part of this is due to the development of suitable formulations and inhalation devices, care has to be taken already beforehand in the choice of drug candidates. Depending on the target-site and type of target, different strategies for the optimization of PK properties may be necessary for a favorable outcome. Whether the goal is to limit systemic exposure or to reduce the dose needed to get the desired effect, many challenges of inhaled delivery need to be addressed in the research environment. Low required concentrations overall may be achieved by selecting drugs with excellent potency; and keeping plasma concentrations low is supported by low oral bioavailability and high systemic clearance to increase pulmonary selectivity.³ Another optimization point is lung retention, which can be achieved by slow

dissolution or low permeability providing basically a slow-release effect, and high tissue affinity. This results in extending the duration of effect, as effective pulmonary concentrations are elevated for a prolonged amount of time due to slow liberation from a solid particle formulation, slow diffusion out of pulmonary tissues, or continuous release of bound drug from the tissue components, respectively. Affinity to pulmonary tissues can be investigated early in the discovery process and has the added benefit of avoiding the MCC, which impacts slowly dissolving drugs.

Especially for lung retention, understanding the distribution between pulmonary tissues and plasma (both from the systemic side and the pulmonary side) is crucial. A more mechanistic understanding may help to create a basis for the translation from preclinical experiments to human if distribution behavior can be translated better and therefore increase confidence in drug candidates with the goal of lung retention. When aiming to quantitatively understand distribution characteristics and tissue affinity, PK models need to lean more into the direction of PBPK, with at least one compartment representing the lung. Due to their reliance on physiology and physicochemical properties, these mechanistic models are uniquely fit to infer the local pulmonary PK/PD from plasma concentrations, as well as provide a basis for translation between species.⁵ However, PBPK models still need to be developed based on real-life data on physiological or physicochemical characteristics and evaluated and refined by measured PK data in the compartments or tissues of interest.

4.1.1 Published investigations of pulmonary distribution in drug discovery

A first step towards a more mechanistic implementation based on local concentrations was made by Hendrickx et al., who built a semi-physiological PK/PD model for long-acting beta agonists (LABAs) consisting of five compartments.⁶ The lung was represented by a shallow and a deep tissue compartment. Exchange between these compartments and plasma was described using physiological volumes and measured f_u in plasma and homogenized lung tissue. The rest of the parameters were estimated based on plasma and total lung concentration-time profiles after i.v. and i.t. administration in rats. Scaling the model from rats to dogs based on physiological differences in lung volume successfully predicted both plasma and lung exposure. Translation to humans showed agreement between predicted and observed bronchodilatory effect for several drugs. These results, as well as our results from publication

II (comparison of translated PK with measured tigecycline PK, section 0), show promise for the translatability of PBPK models when it comes to pulmonary absorption and distribution.

The parameters representing tissue distribution $f_{u,tissue}$ or K_p values can be obtained during the compound optimization phase. As shown by Hendrickx et al. and this work, the use of i.v. PK data as the basis for modeling allows for the characterization of distribution separately from deposition, dissolution, and absorption processes. While this approach is arguably closest to reality, this data may not always be readily producible. A less animal-intensive *ex vivo* method to assess tissue binding in the shape of $V_{u,lung}$, which is closely related to pulmonary $K_{p,u}$ was proposed by Bäckström et al., using lung slices, providing the advantage of intact cell structures with the possibility of lysosomal binding.^{54,61} Without any experimental data, the pulmonary K_p for any given drug has to be predicted *in silico* based on tissue composition and physicochemical drug properties.^{48,49}

Historically, these values are only based on whole lung concentration data and in some cases BALF measurements, which is predominantly representative of terminal bronchioles and alveolar tissue (as shown in section 3.1). This does not support conclusions about spatial distribution, which is especially important for drugs targeting the upper bronchial tract. While there have been attempts at elucidating the differences in exposure between central and peripheral lung structures before, these approaches yielded more qualitative than quantitative results. E.g., Bäckström et al. used spatial imaging techniques to compare the regionalized localization of salmeterol after i.v. and inhaled administration in rats and calculated lung targeting factors (i.e., the difference in PK associated pulmonary selectivity) for the airway epithelium, sub-epithelium, and the alveolar region.^{19,62} However, if that same factor translates to humans remains to be seen.

There have been modeling approaches assessing differences between the conducting airways and the alveolar region regarding the implementation of drug permeation based on surface areas and proposed differences in effective permeabilities. However, the method of scaling permeability is inconsistent across publications. For their partial differential equation inhalation model, Boger et al. assumed ten-fold higher permeability in the alveolar region due to the significantly thinner epithelial layer (compare also Figure 1).⁶³ For the PBPK model comparing i.v. and inhaled administration of salbutamol, a 30-fold higher permeability in the conducting airways was assumed based on experiments with the paracellular marker mannitol.⁵ In our work described in Section 0, no significant improvement of the model was found when

estimating different permeabilities for airways and alveolar region. This may have been due to the use of more lipophilic drugs for which transcellular permeation is expected to be the main route. In any case, it seems that appropriate scaling methods between lung structures need to be investigated further, and heavily depend on the drug in question. Other investigations focused on the implementation of airway generations in PBPK models, scaling physiological parameters by generation.^{5,63}

These studies, while implementing regional distribution and serving their intended purpose, did not take regional differences in unspecific tissue binding into account, and predictions were only compared to total lung and BALF concentrations. To our knowledge, the here presented work is the first to make use of detailed *in vivo* tissue distribution data to estimate K_p values for different lung structures. Depending on the region, different magnitudes of lung retention were achieved, showing that not only deposition patterns and dissolution drive the differences between conducting airways and alveolar region. A more detailed description of the implementation of also other pulmonary processes in some of these models can be found in the book chapter published within the framework of this dissertation.⁶⁴

4.1.2 Physicochemical optimization parameters for orally inhaled drugs

As one of the main drivers of tissue retention, strategies to increase tissue affinity (K_p values) have been discussed before.^{19,33} Basicity is one of the factors that can lead to prolonged retention in the lung, which is suggested to be partially induced by the trapping of ionized drug within the more acidic lysosomes.³³ This is in agreement with the results of publication I (Section 3.1), where it was shown that the basic salmeterol showed the highest tissue affinity and longest retention in the lung in comparison to the neutral and acidic drugs tested. However, this effect was more pronounced in the alveolar region and less noticeable in the conducting airways. In a similar vein, Gaohua et al. suggested that a lower pH of the ELF caused by some diseases (in their case, tuberculosis) may lead to higher ELF:plasma ratios for basic compounds after oral administration.⁶⁵

If increasing basicity is not an option, high lipophilicity has also been shown to improve lung retention, as lipophilic drugs tend to distribute faster into tissues.⁶⁶ Another factor here is the potentially slower dissolution, which can prolong the duration of pulmonary exposure as well. This effect can be seen nicely for drugs like fluticasone propionate (see e.g., publication I, Section 3.1). While these strategies work well for targets in the conducting airways, increasing

exposure in the alveolar region may need different tactics. Low permeability or slow dissociation rates from the target may be beneficial here, as this prevents rapid clearance from the lungs via the pulmonary circulation.^{3,67} With these difficulties of achieving lasting exposure and pulmonary selectivity in the highly perfused alveolar region, less drugs have been developed for oral inhalation, due to the lack of advantages over other, easier to develop forms of administration.

In the special case of anti-infective drugs, many of the required characteristics overlap with those of classical inhaled drugs. However, the distribution of drugs into the relevant (bacterial) compartments may be more complicated as the targets are not endogenous, e.g., penetration of granulomas in tuberculosis.⁶⁸ The sensitivity analysis in publication II (Section 0) nicely shows the effect of improved potency for increased efficacy (and keeping systemic concentrations and the probability for off-target systemic side effects low) but also showed that this effect is reduced when optimized PK is achieved.

Awareness of the specific requirements for orally inhaled drugs is key to help identify promising candidates early on, reducing the need for time- and labor-intensive (*in vivo*) PK and PD studies, as unsuitable compounds can be filtered beforehand.

4.2 Non-clinical development

Though not the focus of this work, the here presented results may help to also inform activities in preclinical development. Understanding pulmonary distribution may help to distinguish its effects from formulation and device-specific processes like dissolution rates and deposition patterns, affected by particle size distribution and device-specifics like the emitted dose. This in turn may help to identify needs for the formulation development. Especially for drugs exhibiting slow dissolution, being able to identify the presence of flip-flop kinetics is necessary to accurately infer on effective lung concentrations. A good understanding of localized PK can then inform e.g., toxicity studies regarding potential side effects not only systemically but also at the administration site (due to potentially higher pulmonary concentrations after drug inhalation).

4.3 Clinical development

4.3.1 Published investigations of pulmonary PK in humans

4.3.1.1 Empirical PK models

As outlined in publication III (Section 3.3), many different model types have been applied to describe PK after oral inhalation based on observed plasma concentration data after both i.v. and inhaled administration. Even though more mechanistic models are necessary for detailed and granular information about local exposure, these empirical models are still used to infer on pulmonary exposure and residence time. In many cases, the estimated absorption half-lives are used as an interpretation of the PK/PD relationship. For example, the slow absorption half-lives found in the developed models for olodaterol and glycopyrronium bromide were discussed as an indication for prolonged lung retention and an explanation for the duration of effect.^{23,69} According to our results presented in publications I and III (Sections 3.1 and 3.3), this backtranslation from plasma concentrations to pulmonary PK may be reasonable for highly water-soluble drugs. However, these results also showed that for less soluble drugs such as AZD5423⁷⁰ or fluticasone propionate, for which non-absorptive loss via MCC is more relevant, this simplification might not hold true (see the comparison between Model I and NaL in publication III). Therefore, the model for fluticasone propionate included an unspecific non-absorptive loss process, and a separate, more mechanistic model was developed for AZD5423 to investigate pulmonary exposure in more detail.⁷⁰

4.3.1.2 PBPK models

AZD5423 was shown to have a shorter absorption half-life of 0.69-0.78 h, as estimated with the empirical model.⁷¹ The applied PBPK model indicated a longer residence time in the tracheobronchial region than in the alveolar region with incomplete absorption due to MCC, which explained the discrepancy between the estimated pulmonary bioavailability and the nominal lung dose.⁷⁰ Here, the use of PBPK, combined with knowledge about the pharmacological mechanisms involved, helped the understanding of local PK/PD relationships which could not be done with an empirical absorption model. According to the authors, there is reasonable doubt regarding the usefulness of plasma concentrations as a surrogate for local exposure, i.e., for showing bioequivalence of different formulations for similar drugs. However, this analysis was also solely based on plasma PK data and simulated lung concentrations, and it would be interesting to see how these mechanistic model predictions hold up against observed lung concentrations.

One notable systems pharmacology approach including a certain amount of spatial pulmonary resolution that was evaluated against observed local concentrations is the model developed by Gaohua et al. for drugs administered for the treatment of tuberculosis.⁶⁵ They differentiated not only between upper and lower airways, but also between the different lung lobes. Simulated concentrations in humans included blood/plasma, lung mass, and ELF concentrations. These predictions were compared with available observed concentrations from biopsies, containing alveolar macrophages or bronchial tissue, and BALF measurements. As the aim was to describe the pulmonary PK of anti-tuberculosis drugs which are typically given orally, the model was based on oral administration and did not include pulmonary administration. However, like done in this work, the conclusions drawn regarding the distribution characteristics may also inform potential new models for oral inhalation for the investigated drugs. The distribution to and from pulmonary tissue compartments was implemented via regional blood flows and whole-lung K_p values calculated by the Rodgers and Rowland method.^{48,49}

To allow for easier access to PBPK approaches, additional commercial PBPK software focusing on – or at least including – oral inhalation has emerged over the years. Examples of this are Mimetikos Preludium and GastroPlus.^{52,72} In addition, there are some custom-built model systems including drug distribution on a cellular level based on the work by Yu and Rosania,⁷³ which are, however, not publicly available.^{74,75} These models show similar structures overall, with some differences as to the inclusion of lymphatic system, or the complexity of implemented processes. For a more detailed discussion of these, please refer to the book chapter published in line with this work.⁶⁴ Notably, even though all these models include spatial granularity when it comes to different regions of the lung, there is a lack of (published) investigations comparing the model predictions to observed local concentrations.

All these models have in common that there is the reliance on single measured or calculated K_p values for the whole lung. Even though the difference in blood flow and tissue volumes is accounted for, potential variations in extent of tissue binding between the pulmonary compartments are not implemented. This may not have a relevant impact on the prediction of systemic PK of orally or parenterally administered drugs, it can, however, be expected to affect the predictions of local PK, especially after pulmonary administration (compare the results of publications I and II). Assuming conservation of tissue affinity between species, the results presented in this thesis show a new methodology to investigate and implement these differences with more granularity than can be acquired in clinical trials.

4.4 Learnings from PK models for oral inhalation

As of today, PK models are mostly used for retrospective analysis of PK or PK/PD relationships to help with the interpretation of PK data and even backtranslation from plasma to pulmonary concentrations. As seen for the models compared in publication III (Section 3.3), it is important to understand which PK processes affect the PK of the drug in question to be able to infer pulmonary exposure (compare, for instance, the impact of non-absorptive loss implementation for calculated pulmonary exposure). Other times, the established model can be used to transfer learnings to other drugs in the same class. This was the case for the work done by Gaz et al., who used their PBPK/PD model to predict bronchodilation for several drugs based on local PK in the conducting airways.⁷⁶ Conclusions drawn from these more generic models can more easily be used to inform drug discovery and development programs of new drugs for oral inhalation.^{6,75} While the translation of deposition and dissolution characteristics from preclinical species to humans is challenging, these processes are mostly affected by the inhalation device and formulation development. Learnings from clinical data can then be imposed onto other drugs, while accounting for drug-specific differences in absorptive clearance from the lungs, including tissue distribution, and the systemic PK. Well-trained models are able to predict differences in deposition patterns based on the device and particle-size distributions.^{15,77,78} Being able to perform *a priori* predictions of drug performance after oral inhalation can also be helpful to assess the suitability of an (i.v.- or) oral-to-inhaled switch for already established drugs, as was done in publication II (Section 3.2).

In addition, there are also aspects to be learned from models designed for specific drugs. Thorough analysis of extensive clinical data as seen in the clinical investigations used for the basis of publication III (Section 3.3) can provide much needed information on expected variability in the PK, which is typically higher for oral inhalation than for other routes of administration.^{69,71} The availability of PK data after both i.v. administration and oral inhalation in humans, sometimes even in the same subjects, allows quantifying interindividual and inter-occasion variability not only for systemic PK parameters, but also for the processes associated with oral inhalation. As not every clinical development program includes i.v. PK studies, relying on previous knowledge about expected variability can support the planning of the inhalation studies. The lack of i.v. PK data also underlines the importance of being able to bridge from preclinical PK studies, as it may be the only way to sufficiently analyze local PK.

4.5 Challenges and outlook

One process not included in the developed semi-mechanistic PBPK models as of now is active transport in the lungs, i.e., currently it is assumed that unbound concentrations in equilibrium are the same in plasma and tissues. Even though there is some evidence of transporter expression within the epithelium, tissue, and endothelium,^{65,79} there is still a lack of quantitative information, making the implementation difficult. With increasing information about transporter expression (or even activity) within the separate pulmonary tissues becoming accessible over time, the model may be refined to include active transport processes, potentially offering explanations for some of the slight mispredictions of pulmonary tissue concentrations.

Furthermore, the predictivity of the models described in publications I and II was not yet evaluated based on PK data obtained after pulmonary administration. As mentioned before, there are strong limitations when investigating the pulmonary PK after inhalation in rodents. In addition to the described physiological reasons and experimental limitations, the interpretation of tissue concentrations of poorly soluble drugs would be challenging. The necessary discrimination between dissolved and undissolved drug is challenging with the current methodology. Human data may be more conclusive, as the uncertainty in deposition patterns after inhaled administration is lower compared to preclinical species.¹⁹ In the same vein, it would be interesting to expand the here developed humanized pulmonary distribution model with more mechanistic models for the inhalation specific processes (deposition, MCC, and dissolution models).

Another important topic is the physiological changes caused by diseases typically treated via oral inhalation. For example, the constrictions of the conducting airways caused by Asthma and COPD are known to alter deposition patterns in comparison to the ones seen in healthy volunteers. Inflammation of the lungs, a frequent problem encountered in cystic fibrosis and patients developing ventilation associated pneumonia, may induce alveolo-capillary barrier leakage, therefore increasing the systemic concentrations of inhaled antibiotics. Additionally, disease-related changes in ELF pH (e.g., acidification seen in tuberculosis) was suggested to alter ELF:plasma ratios.⁶⁵ However, to extrapolate from healthy volunteers to these special populations requires the collection of detailed *prior* knowledge how the anatomy and physiology changes under these circumstances, including quantitative information as to how the relevant PK processes affect the drug in question. This amount of data is rarely available and lack of it has to be compensated with assumptions in modeling.⁶⁴ Also here, hopefully

more data will emerge to better inform mechanistic PBPK models for oral inhalation in the future.

5 Bibliography

1. Crompton G. A brief history of inhaled asthma therapy over the last fifty years. *Prim Care Respir J* 2006; **15**: 326–31.
2. Sanders M. Inhalation therapy: an historical review. *Prim Care Respir J* 2007; **16**: 71–81.
3. Pasqua E, Hamblin N, Edwards C, Baker-Glenn C, Hurley C. Developing inhaled drugs for respiratory diseases: a medicinal chemistry perspective. *Drug Discov Today* 2021; **27**: 134–50.
4. Patton JS, Byron PR. Inhaling medicines: delivering drugs to the body through the lungs. *Nat Rev Drug Discov* 2007; **6**: 67–74.
5. Boger E, Fridén M. Physiologically Based Pharmacokinetic/Pharmacodynamic Modeling Accurately Predicts the Better Bronchodilatory Effect of Inhaled Versus Oral Salbutamol Dosage Forms. *J Aerosol Med Pulm D* 2019; **32**: 1–12.
6. Hendrickx R, Bergström EL, Janzén DLI, *et al.* Translational model to predict pulmonary pharmacokinetics and efficacy in man for inhaled bronchodilators. *Cpt Pharmacometrics Syst Pharmacol* 2018; **7**: 147–57.
7. Shao J, Talton J, Wang Y, Winner L, Hochhaus G. Quantitative Assessment of Pulmonary Targeting of Inhaled Corticosteroids Using Ex Vivo Receptor Binding Studies. *AAPS J* 2020; **22**: 39.
8. Bäckström E, Erngren T, Fihn B-M, *et al.* Possible Extraction of Drugs from Lung Tissue During Broncho-alveolar Lavage Suggest Uncertainty in the Procedure's Utility for Quantitative Assessment of Airway Drug Exposure. *J Pharm Sci* 2022; **111**: 852–8.
9. Brown RP, Delp MD, Lindstedt SL, Rhomberg LR, Beliles RP. Physiological parameter values for physiologically based pharmacokinetic models. *Toxicol Ind Health* 1997; **13**: 407–84.
10. Bernard SL, Glenny RW, Polissar NL, Luchtel DL, Lakshminarayan S. Distribution of pulmonary and bronchial blood supply to airways measured by fluorescent microspheres. *J Appl Physiol* 1996; **80**: 430–6.
11. Dunnill MS, Massarella GR, Anderson JA. A comparison of the quantitative anatomy of the bronchi in normal subjects, in status asthmaticus, in chronic bronchitis, and in emphysema. *Thorax* 1969; **24**: 176–9.
12. Parent RA. *Treatise on Pulmonary Toxicology: Comparative biology of the normal lung.* CRC press; 1992.
13. Yeh HC, Schum GM, Duggan MT. Anatomic Models of the tracheobronchial and pulmonary regions of the rat. *Anatomical Rec* 1979; **195**: 483–92.

14. Enlo-Scott Z, Swedrowska M, Forbes B. Epithelial permeability and drug absorption in the lungs. In: *Inhaled Medicines*. Academic Press, 2021; 267–99.
15. Borghardt JM, Kloft C, Sharma A. Inhaled Therapy in Respiratory Disease: The Complex Interplay of Pulmonary Kinetic Processes. *Can Respir J* 2018; **2018**: 1–11.
16. Lehnert BE, Valdez YE, Tietjen GL. Alveolar Macrophage-Particle Relationships during Lung Clearance. *Am J Respir Cell Mol Biol* 1989; **1**: 145–54.
17. Lehnert BE. Pulmonary and thoracic macrophage subpopulations and clearance of particles from the lung. *Environmental Health Perspectives* 1992; **97**: 17–46.
18. Geiser M, Casaulta M, Kupferschmid B, Schulz H, Semmler-Behnke M, Kreyling W. The Role of Macrophages in the Clearance of Inhaled Ultrafine Titanium Dioxide Particles. *Am J Resp Cell Mol* 2008; **38**: 371–6.
19. Hamm GR, Bäckström E, Brülls M, *et al.* Revealing the Regional Localization and Differential Lung Retention of Inhaled Compounds by Mass Spectrometry Imaging. *J Aerosol Med Pulm D* 2019; **33**: 43–53.
20. Hukkanen J, Pelkonen O, Hakkola J, Raunio H. Expression and regulation of xenobiotic-metabolizing cytochrome P450 (CYP) enzymes in human lung. *Crit Rev Toxicol* 2002; **32**: 391–411.
21. Shimada T, Yamazaki H, Mimura M, *et al.* Characterization of microsomal cytochrome P450 enzymes involved in the oxidation of xenobiotic chemicals in human fetal livers and adult lungs. *Drug Metabolism and Disposition* 1996; **24**: 515–22.
22. Campbell J, Landingham CV, Crowell S, *et al.* A preliminary regional PBPK model of lung metabolism for improving species dependent descriptions of 1,3-butadiene and its metabolites. *Chemico-Biological Interactions* 2015; **238**: 102–10.
23. Bartels C, Looby M, Sechaud R, Kaiser G. Determination of the pharmacokinetics of glycopyrronium in the lung using a population pharmacokinetic modelling approach. *Brit J Clin Pharmacol* 2013; **76**: 868–79.
24. Global Initiative for Asthma. Global Strategy for Asthma Management and Prevention, 2022. Available at: <https://ginasthma.org>. Accessed October 12, 2022.
25. Global Initiative for Chronic Obstructive Pulmonary Disease. Global Strategy for the Diagnosis, Management, and Prevention of Chronic Obstructive Pulmonary Disease (2021 Report). Available at: <https://goldcopd.org>. Accessed October 12, 2022.
26. Szychowiak P, Desgrouas M, Ehrmann S. Inhaled antibiotics in critical care: State of the art and future perspectives. *Infect Dis Now* 2022; **52**: 327–33.
27. McKinzie CJ, Chen L, Ehlert K, *et al.* Off-label use of intravenous antimicrobials for inhalation in patients with cystic fibrosis. *Pediatr Pulm* 2019; **54**: S27–45.

28. Boisson M, Mimoz O, Hadzic M, *et al.* Pharmacokinetics of intravenous and nebulized gentamicin in critically ill patients. *J Antimicrob Chemoth* 2018; **73**: 2830–7.
29. Ritchie TJ, Luscombe CN, Macdonald SJF. Analysis of the Calculated Physicochemical Properties of Respiratory Drugs: Can We Design for Inhaled Drugs Yet? *J Chem Inf Model* 2009; **49**: 1025–32.
30. Amidon GL, Lennernäs H, Shah VP, Crison JR. A theoretical basis for a biopharmaceutical drug classification: the correlation of in vitro drug product dissolution and in vivo bioavailability. *Pharmaceutical Research* 1995; **12**: 413–20.
31. Rohatagi S, Appajosyula S, Derendorf H, *et al.* Risk-benefit value of inhaled glucocorticoids: a pharmacokinetic/pharmacodynamic perspective. *The Journal of Clinical Pharmacology* 2004; **44**: 37–47.
32. Harding S. The human pharmacology of fluticasone propionate. *Respiratory Medicine* 1990; **84**: 25–9.
33. Bonn B, Perry M. The API. In: *Inhaled Medicines*. Academic Press, 2021; 13–34.
34. Guillon A, Secher T, Dailey LA, *et al.* Insights on animal models to investigate inhalation therapy: Relevance for biotherapeutics. *Int J Pharmaceut* 2018; **536**: 116–26.
35. Markert M, Klumpp A, Trautmann T, Guth B. A novel propellant-free inhalation drug delivery system for cardiovascular drug safety evaluation in conscious dogs. *J Pharmacol Toxicol* 2004; **50**: 109–19.
36. Fischer A, Stegemann J, Scheuch G, Siekmeier R. Novel devices for individualized controlled inhalation can optimize aerosol therapy in efficacy, patient care and power of clinical trials. *Eur J Méd Res* 2009; **14**: 71.
37. Rizk ML, Zou L, Savic RM, Dooley KE. Importance of Drug Pharmacokinetics at the Site of Action. *Clin Transl Sci* 2017; **10**: 133–42.
38. Lee JY, Garnett CE, Gobburu JVS, *et al.* Impact of Pharmacometric Analyses on New Drug Approval and Labelling Decisions. *Clin Pharmacokinet* 2011; **50**: 627–35.
39. Manolis E, Rohou S, Hemmings R, Salmonson T, Karlsson M, Milligan P. The Role of Modeling and Simulation in Development and Registration of Medicinal Products: Output From the EFPIA/EMA Modeling and Simulation Workshop. *Cpt Pharmacometrics Syst Pharmacol* 2013; **2**: 1–4.
40. Marshall S, Madabushi R, Manolis E, *et al.* Model-Informed Drug Discovery and Development: Current Industry Good Practice and Regulatory Expectations and Future Perspectives. *Cpt Pharmacometrics Syst Pharmacol* 2019; **8**: 87–96.
41. Gill KL, Gardner I, Li L, Jamei M. A Bottom-Up Whole-Body Physiologically Based Pharmacokinetic Model to Mechanistically Predict Tissue Distribution and the Rate of Subcutaneous Absorption of Therapeutic Proteins. *AAPS J* 2016; **18**: 156–70.

42. Jamei M. Recent Advances in Development and Application of Physiologically-Based Pharmacokinetic (PBPK) Models: a Transition from Academic Curiosity to Regulatory Acceptance. *Curr Pharmacol Reports* 2016; **2**: 161–9.
43. Luzon E, Blake K, Cole S, Nordmark A, Versantvoort C, Berglund EG. Physiologically based pharmacokinetic modeling in regulatory decision-making at the European Medicines Agency. *Clin Pharmacol Amp Ther* 2017; **102**: 98–105.
44. DeHaan WH, Finlay WH. In Vitro Monodisperse Aerosol Deposition in a Mouth and Throat with Six Different Inhalation Devices. *J Aerosol Med* 2001; **14**: 361–7.
45. Delvadia RR, Longest PW, Byron PR. In Vitro Tests for Aerosol Deposition. I: Scaling a Physical Model of the Upper Airways to Predict Drug Deposition Variation in Normal Humans. *J Aerosol Med Pulm Drug Deliv* 2012; **25**: 32–40.
46. Bäckström E, Fridén M. Drug distribution in lung tissue. In: *Inhaled Medicines*. Academic Press, 2021; 301–18.
47. Barré J, Chamouard JM, Houin G, Tillement JP. Equilibrium dialysis, ultrafiltration, and ultracentrifugation compared for determining the plasma-protein-binding characteristics of valproic acid. *Clin Chem* 1985; **31**: 60–4.
48. Rodgers T, Rowland M. Physiologically based pharmacokinetic modelling 2: predicting the tissue distribution of acids, very weak bases, neutrals and zwitterions. *J Pharm Sci* 2006; **95**: 1238–57.
49. Rodgers T, Leahy D, Rowland M. Physiologically based pharmacokinetic modeling 1: predicting the tissue distribution of moderate-to-strong bases. *J Pharm Sci* 2005; **94**: 1259–76.
50. Poulin P, Theil FP. Prediction of pharmacokinetics prior to in vivo studies. 1. Mechanism-based prediction of volume of distribution. *J Pharm Sci* 2002; **91**: 129–56.
51. Lukacova V, Lave T, Fraczkiwicz G, Bolger M, Woltosz W. General approach to calculation of tissue: plasma partition coefficients for physiologically based pharmacokinetic (PBPK) modeling. In: , 2008.
52. SimulationPlus(R). GastroPlus(R): Additional Dosage Routes.
53. Kuepfer L, Niederalt C, Wendl T, *et al*. Applied Concepts in PBPK Modeling: How to Build a PBPK/PD Model. *Cpt Pharmacometrics Syst Pharmacol* 2016; **5**: 516–31.
54. Bäckström E, Lundqvist A, Boger E, *et al*. Development of a Novel Lung Slice Methodology for Profiling of Inhaled Compounds. *Journal of Pharmaceutical Sciences* 2016; **105**: 838–45.
55. Rodgers T, Leahy D, Rowland M. Tissue distribution of basic drugs: Accounting for enantiomeric, compound and regional differences amongst β -blocking drugs in rat. *J Pharm Sci* 2005; **94**: 1237–48.

56. Sun H, Chow EC, Liu S, Du Y, Pang KS. The Caco-2 cell monolayer: usefulness and limitations. *Expert Opin Drug Metab Toxicol* 2008; **4**: 395–411.
57. Mathias NR, Timoszyk J, Stetsko PI, Megill JR, Smith RL, Wall DA. Permeability Characteristics of Calu-3 Human Bronchial Epithelial Cells: In Vitro - In Vivo Correlation to Predict Lung Absorption in Rats. *J Drug Target* 2002; **10**: 31–40.
58. Himstedt A, Braun C, Wicha SG, Borghardt JM. Towards a Quantitative Mechanistic Understanding of Localized Pulmonary Tissue Retention—A Combined In Vivo/In Silico Approach Based on Four Model Drugs. *Pharm* 2020; **12**: 408.
59. Himstedt A, Braun C, Wicha SG, Borghardt JM. Understanding the suitability of established antibiotics for oral inhalation from a pharmacokinetic perspective: an integrated model-based investigation based on rifampicin, ciprofloxacin and tigecycline in vivo data. *J Antimicrob Chemoth* 2022; **77**: 2922–32.
60. Himstedt A, Borghardt JM, Wicha SG. Inferring pulmonary exposure based on clinical PK data: accuracy and precision of model-based deconvolution methods. *J Pharmacokinet Phar* 2022; **49**: 135–49.
61. Bäckström E, Boger E, Lundqvist A, Hammarlund-Udenaes M, Fridén M. Lung Retention by Lysosomal Trapping of Inhaled Drugs Can Be Predicted In Vitro With Lung Slices. *J Pharm Sci* 2016; **105**: 3432–9.
62. Backstrom E, Hamm G, Nilsson A, *et al.* Uncovering the regional localization of inhaled salmeterol retention in the lung. *Drug Deliv* 2018; **25**: 838–45.
63. Boger E, Wigström O. A Partial Differential Equation Approach to Inhalation Physiologically Based Pharmacokinetic Modeling. *Cpt Pharmacometrics Syst Pharmacol* 2018; **7**: 638–46.
64. Himstedt A, Bäckman P, Borghardt JM. Physiologically-based pharmacokinetic modeling after drug inhalation. In: *Inhaled Medicines*. Academic Press, 2021; 319–58.
65. Gaohua L, Wedagedera J, Small BG, *et al.* Development of a Multicompartment Permeability-Limited Lung PBPK Model and Its Application in Predicting Pulmonary Pharmacokinetics of Antituberculosis Drugs. *CPT Pharmacometrics Syst Pharmacol* 2015; **4**: 605–13.
66. Eriksson J, Sjogren E, Thorn H, Rubin K, Backman P, Lennernas H. Pulmonary absorption - estimation of effective pulmonary permeability and tissue retention of ten drugs using an ex vivo rat model and computational analysis. *Eur J Pharm Biopharm* 2018; **124**: 1–12.
67. Pelaia G, Vatrella A, Busceti MT, *et al.* Pharmacologic rationale underlying the therapeutic effects of tiotropium/olodaterol in COPD. *Ther Clin Risk Manag* 2015; **11**: 1563–72.

68. Pasqua E, Hamblin N, Edwards C, Baker-Glenn C, Hurley C. Developing inhaled drugs for respiratory diseases: a medicinal chemistry perspective. *Drug Discov Today* 2021; **27**: 134–50.
69. Borghardt JM, Weber B, Staab A, Kunz C, Formella S, Kloft C. Investigating pulmonary and systemic pharmacokinetics of inhaled olodaterol in healthy volunteers using a population pharmacokinetic approach. *Brit J Clin Pharmacol* 2016; **81**: 538–52.
70. Bäckman P, Tehler U, Olsson B. Predicting Exposure after Oral Inhalation of the Selective Glucocorticoid Receptor Modulator, AZD5423, Based on Dose, Deposition Pattern, and Mechanistic Modeling of Pulmonary Disposition. *J Aerosol Med Pulm D* 2017; **30**: 108–17.
71. Melin J, Prothon S, Kloft C, *et al.* Pharmacokinetics of the Inhaled Selective Glucocorticoid Receptor Modulator AZD5423 Following Inhalation Using Different Devices. *AAPS J* 2017; **19**: 865–74.
72. Olsson B, Bäckman P. Mimetikos Preludium™: A New Pharma-friendly Aerosol Drug Deposition Calculator. *Respiratory Drug Delivery* 2018 2018; **1**: 103–12.
73. Yu JY, Rosania GR. Cell-based multiscale computational modeling of small molecule absorption and retention in the lungs. *Pharmaceut Res* 2010; **27**: 457–67.
74. Cabal A, Mehta K, Guo P, Przekwas A. In-silico lung modeling platform for inhaled drug delivery. *Proceedings Drug Delivery to the Lungs* 2016; **27**: 82–6.
75. Caniga M, Cabal A, Mehta K, *et al.* Preclinical Experimental and Mathematical Approaches for Assessing Effective Doses of Inhaled Drugs, Using Mometasone to Support Human Dose Predictions. *J Aerosol Med Pulm D* 2016; **29**: 362–77.
76. Gaz C, Cremona G, Panunzi S, Patterson B, Gaetano AD. A geometrical approach to the PKPD modelling of inhaled bronchodilators. *J Pharmacokinet Phar* 2012; **39**: 415–28.
77. Hofmann W. Modelling inhaled particle deposition in the human lung—A review. *J Aerosol Sci* 2011; **42**: 693–724.
78. (RIVM) National Institute for Public Health and the Environment. *Multiple Path Particle Dosimetry Model (MPPD v 1.0): A Model for Human and Rat Airway Particle Dosimetry*. Bilthoven, The Netherlands; 2002.
79. Bosquillon C. Drug transporters in the lung--do they play a role in the biopharmaceutics of inhaled drugs? *J Pharm Sci* 2010; **99**: 2240–55.

6 Appendix

6.1 Hazardous material

Not applicable.

6.2 Supplementary material publication I

1. Structures and key properties of model drugs

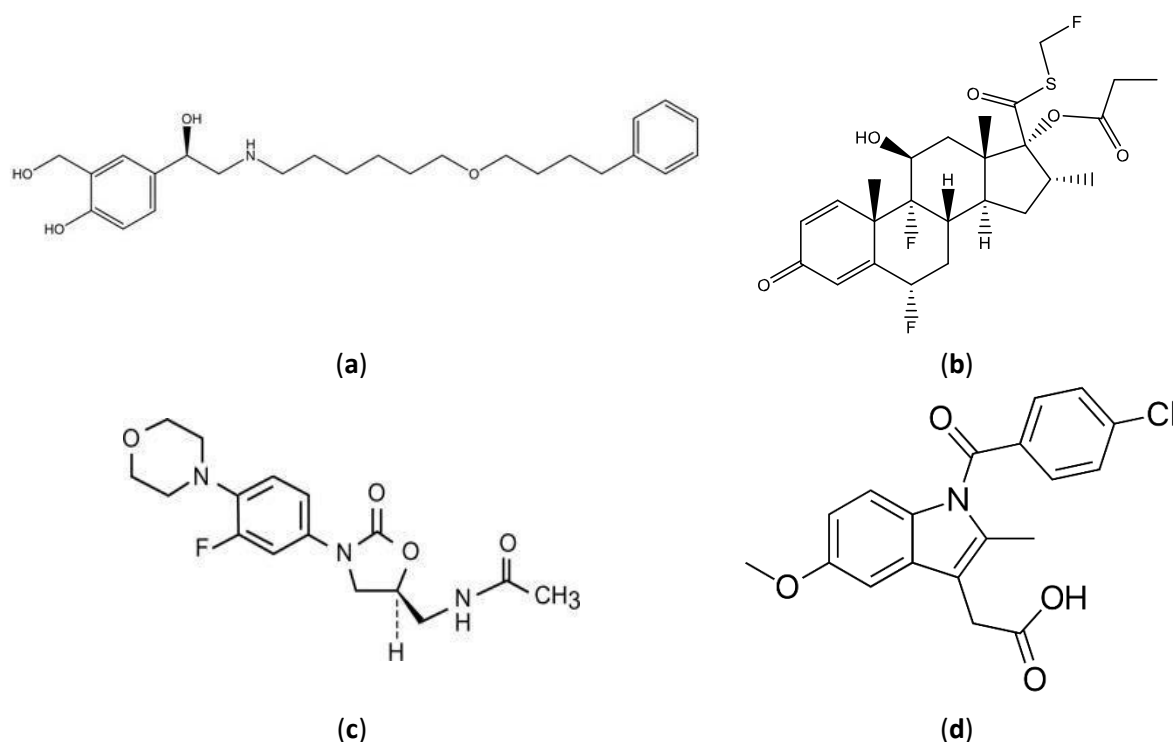


Figure S1. Chemical structures of the four model drugs. (a) Salmeterol; (b) fluticasone propionate; (c) linezolid; (d) indomethacin.

Table S1. Physicochemical characteristics of the model drugs.

Drug	Molecular weight [g/mol]	LogP	pKa	PPB rat	B:P	Permeability [10 ⁻⁶ cm/s]
SAL	604 (Base: 416)	2.5	9.8 (basic)	98.6%	1.70	14.0
FP	501	4.37	NA	98.5%	0.90	49.4
LIN	337	0.59	1.8 (basic) ^{b,c}	26.8%	0.93	20.4
IND	358	4.08 ^a	4.5 ^d	97.6%	NA	22.0

SAL: salmeterol, FP: fluticasone propionate, LIN: linezolid, IND: indomethacin, LogP: octanol/water partition coefficient, PPB: plasma protein binding, B:P: blood-to-plasma ratio. ^a Inagi et al. [1], ^b Taylor et al. [2], ^c Chiang et al. [3], ^d Budavari et al. [4]. All other values were measured in-house. Permeability was measured in a Caco-2 cell assay. The methods for the protein binding and permeability assays can be found elsewhere [5].

2. Study planning – Stochastic simulation-estimation (SSE) study

2.1. Methods

A stochastic simulation and estimation approach (SSE) was performed in R (Version 3.3.2) to optimize the design of the intravenous lung distribution studies for the simultaneous

estimation of pulmonary blood flows and K_p values. The pharmacokinetic (PK) model used for this analysis consisted of two systemic compartments and one tissue compartment representing the trachea (Figure S2).

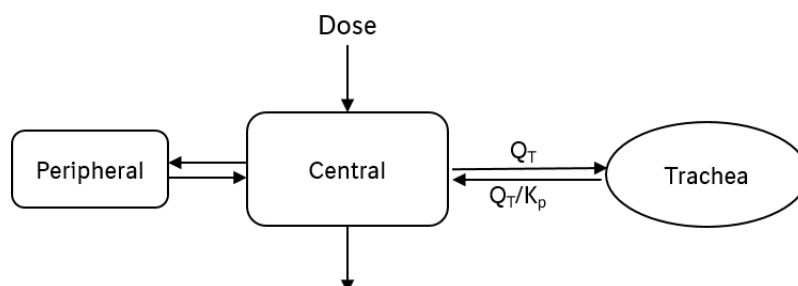


Figure S2. Structure of the model used in the SSE study. Q_T : tracheal blood flow; K_p : tissue-to-plasma partition coefficient.

PK parameters were derived from a preliminary cocktail PK study and can be found in Table S2. The weight of the trachea was based on measured weights from previous studies (0.0002 kg/kg bodyweight) the initial value for tracheal blood flow was scaled from literature data (bronchial circulation adjusted for trachea weight: 0.06 L/h/kg)⁹. The K_p was set to 70, assuming that at least one drug with high tissue affinity would be included in the study, facilitating the estimation of blood flow.

Table S2. Parameters used for the simulation of concentration-time profiles.

Parameter	CL	V	Q	V2	Q_T	K_p	Prop. error
Unit	$\frac{L}{h \cdot kg}$	$\frac{L}{kg}$	$\frac{L}{h \cdot kg}$	$\frac{L}{kg}$	$\frac{L}{h \cdot kg}$	-	-
Value	8.69	4.95	3.68	9.49	0.06	70	0.112

CL: systemic clearance, V: central volume of distribution (Vd), Q: intercompartmental clearance, V2: peripheral Vd; Q_T : blood flow to the trachea; K_p : tissue-to-plasma partition coefficient, Prop. error: proportional residual variability.

One thousand sets of simulated plasma and tissue concentration-time profiles were generated for two different sampling schemes. The first sampling scheme matched the one employed in the first study, with tissue samples taken after 1, 2, and 3 hours after start of the one-hour infusion (Study design I, 3 samples per time point). The second design included four time points of tissue samples (0.25 h, 0.75 h, 2 h, and 4 h after start of the one-hour infusion; study design II, 4 samples per time point). Each of these simulated datasets was used again as the basis for the simultaneous estimation of systemic and tissue-specific parameters. The distribution of resulting parameter estimates was further evaluated to assess identifiability, bias and imprecision of the model parameters.

Relative bias of the mean and the coefficient of variation were calculated as follows:

$$\text{Bias} = \frac{\mu_{\text{estimates}} - \text{true}}{\text{true}} \cdot 100\%, \quad (\text{S1})$$

with $\mu_{\text{estimates}}$ being the mean value of all 1000 estimates for a given parameter and true as the true value used for data simulation. The coefficient of variation (CV) was calculated by dividing the standard deviation of estimates ($\sigma_{\text{estimates}}$, $n=1000$)

$$\sigma_{\text{estimates}} = \sqrt{\frac{\sum(\text{estimate} - \text{true})^2}{n-1}}, \quad (\text{S2})$$

by the underlying true value and multiplying the result with 100:

$$\text{CV} = \frac{\sigma_{\text{estimates}}}{\text{true}} \cdot 100\%. \quad (\text{S3})$$

2.2. Results

The SSE studies indicated an adequate estimation of K_p (24.5 % CV, bias 0.113%), whereas an accurate estimation of lung tissue perfusion was not possible (1117% CV, bias 369%) with study design I, see Supplementary table 3. With study design II, the accuracy and bias of the blood flow estimation was much better (37.0% CV, bias 6.33%) without losing any precision regarding the K_p .

Table S3. Bias (mean) and coefficient of variation (CV) of the parameter estimates from the SSE study.

Study design	Parameter	CL	V	Q	V2	Q _T	K _p
		$\frac{L}{h \cdot \text{kg}}$	$\frac{L}{\text{kg}}$	$\frac{L}{h \cdot \text{kg}}$	$\frac{L}{\text{kg}}$	$\frac{L}{h \cdot \text{kg}}$	-
I	Bias, %	-0.677	-0.470	-1.86	4.63	369	0.113
	CV, %	7.87	16.7	20.0	30.5	1117	24.5
II	Bias, %	-0.310	-0.264	0.696	4.08	6.33	0.133
	CV, %	6.18	12.7	14.4	30.7	37.0	9.64

CL: systemic clearance, V: central volume of distribution (V_d), Q: intercompartmental clearance, V2: peripheral V_d; Q_T: blood flow to the trachea; K_p: tissue-to-plasma partition coefficient.

A boxplot of the parameter estimate distribution around the true value can be found in Figure S3.

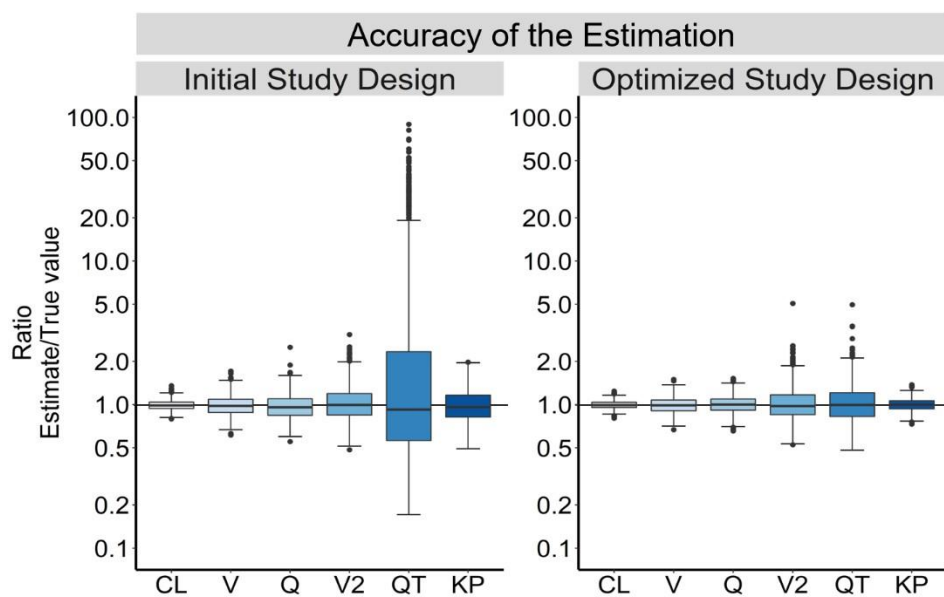


Figure S3. Parameter estimate distribution for the initial and optimized study designs (Study design I and II, respectively). The values are normalized to the true value used for the simulation of PK data. CL: systemic clearance, V: central volume of distribution (Vd), Q: intercompartmental clearance, V2: peripheral Vd; QT: blood flow to the trachea; KP: tissue-to-plasma partitioning coefficient.

Based on these results, estimation of localized pulmonary blood flow was deemed possible with the new study design II. However, the coefficient of variation of 37% was still quite high. This was addressed by the decision to estimate the blood flow simultaneously across all four model drugs to provide a richer dataset. Due to this, the number of tissue samples per time point could be reduced to three again.

3. Sampling scheme & Sample weights

Drug	Study	Bodyweight (BW)		N	Dose		Infusion		Sampling time points (min)		Mean sample weights (g)								
		mean (g)	%CV		(mg/kg/h)	(mg/kg/h)	duration (min)	rate (mL/kg/h)	tissue (min)	plasma (min)	lung (g)	%CV	trachea (g)	%CV	bronchi (g)	%CV	parenchyma (g)	%CV	rest lung (g)
Salmeterol ¹	1A	252	2.6	2	2	15	10	15	5, 15	15	5.05	0.0477	15.5	0.133	7.99	0.0493	21.6	0.590	16.4
	1B	264	3.0	3	2	45	10	45	" , 30, 45	45	0.70	0.0420	7.01	0.130	12.0	0.0527	29.7	0.627	2.11
	1C	257	1.8	3	2	60	10	120	" , 60, 120	120	3.44	0.0533	0.884	0.151	8.19	0.0523	23.7	0.633	8.93
	1D	251	2.6	3	2	60	10	240	" , 240	240	4.96	0.0490	18.6	0.127	16.0	0.0530	38.3	0.648	10.2
Fluticasone Propionate ¹	2A	321	3.0	2	2	15	10	15	5, 15	15	0.739	0.0647	19.1	0.167	25.79	0.109	39.6	0.744	14.1
	2B	329	6.7	3	2	45	10	45	" , 30, 45	45	9.87	0.0687	5.36	0.194	9.67	0.131	14.3	0.604	30.5
	2C	332	5.6	3	2	60	10	120	" , 60, 70, 90, 120	120	1.80	0.0703	8.15	0.159	9.80	0.0717	21.7	0.759	11.4
	2D	297	2.7	3	2	60	10	240	" , 180, 240	240	2.07	0.0660	21.4	0.125	67.9	0.186	45.7	0.492	31.9
Linezolid	3A	280	3.9	3	4	15	10	15	5, 15	15	2.97	0.0540	12.1	0.123	19.5	0.0730	32.8	0.640	10.2
	3B	280	1.9	3	4	45	10	45	" , 30, 45	45	1.50	0.0470	4.60	0.139	33.9	0.101	46.7	0.637	10.2
	3C	280	1.2	3	4	60	10	120	" , 60, 70, 90, 120	120	9.00	0.0400	7.36	0.143	34.7	0.0640	77.6	0.598	14.0
	3D	279	2.5	3	4	60	10	240	" , 240	240	10.4	0.0483	32.7	0.132	27.3	0.104	34.7	0.606	26.6
Indomethacin	4A	250	1.1	3	0.5	15	10	15	5, 15	15	0.197	0.0423	34.6	0.0960	11.4	0.0387	11.6	0.495	14.1
	4B	277	1.8	3	0.5	45	10	45	" , 30, 45	45	6.50	0.0480	2.95	0.150	11.9	0.119	55.8	0.720	8.60
	4C	290	3.7	3	0.5	60	10	120	" , 60, 70, 90, 120	120	10.1	0.0443	26.1	0.149	3.56	0.0600	40.3	0.786	17.7
	4D	259	5.2	3	0.5	60	10	240	" , 240	240	18.0	0.0413	8.91	0.118	18.5	0.112	46.7	0.660	12.0
Total	mean	281								1.29	0.0517		0.140			0.0860		0.640	
	%CV	9.3								12.5	25.5		20.6			63.9		20.4	

¹For both salmeterol and fluticasone propionate, results from one rat designated for tissue sampling after 0.25 h had to be excluded due to para-venous administration.

4. Additional PK study for salmeterol

The additional PK study used for the estimation of systemic PK of salmeterol was performed under the same overall conditions as the other *in vivo* studies. Four rats received salmeterol as part of a cocktail as an intravenous bolus dose of 4.81 $\mu\text{mol}/\text{kg}$. Blood samples (volume 100 μL) were collected at 0.083 h, 0.25 h, 0.5 h, 1.0 h, 2.0 h, 3.0 h, and 4.0 h.

5. Bioanalysis

5.1. Sample Preparation

Internal standards BI-1052 (internal source, 100 nM), indomethacin-d4 (Biomol GmbH, 500 nM), fluticasone propionate-d5 (Santa Cruz Biotechnology Inc, 100 nM), and linezolid-d3 (Biomol GmbH, 10 nM) were used for salmeterol (SAL), indomethacin (IND), fluticasone propionate (FP) and linezolid (LIN), respectively. After protein precipitation was performed by addition of acetonitrile, the samples were centrifuged at 50000 g for 10 minutes and the supernatant was injected into the LC system.

5.2. LC-MS Analysis

SAL was analysed using a Prodigy 5u ODS3 100A, 50 x 2 mm (Phenomenex, Torrance, CA, USA) at room temperature. Solvent A was consisting of 0.02% formic acid and solvent B of acetonitrile. The LC gradient started at 5% solvent B and increased from 0.5 – 2.0 min to 90% at a flow rate of 500 $\mu\text{L}/\text{min}$. From 2.0 to 3.5 min it was maintained at 90%. The column was conditioned for 0.5 min at 5% solvent B. The injection volume was 5 μL . FP, LIN and IND were analyzed using a YMC Hydrosphere C18, 2.1 x 33 mm, 3 μm (YMC Co. Ltd., Kyoto, Japan) at room temperature. Solvent A was consisting of 0.1% formic acid and solvent B of acetonitrile and methanol (1:1) supplemented with 0.1% formic acid. The

LC-gradient started at 5% solvent B and increased from 0.5 – 2.0 min to 50% at a flow rate of 500 $\mu\text{L}/\text{min}$. From 2.0 to 3.5 min it was maintained at 50%. The column was conditioned for 0.5 min at 5% solvent B. The injection volumes were 5 μL for FP and IND, and 2 μL for LIN.

A Thermo Scientific™ TSQ Altis™ triple quadrupole mass spectrometer was used for the analysis of SAL and IND, while a SCIEX QTRAP 6500 was used for FP and LIN. Both mass spectrometers were operated in positive mode.

Table S5. Mass spectrometry parameters.

Drug	Q1	Q3	CE
Salmeterol	416.3	91.1	55
BI-1052	453.1	275.1	27
Fluticasone propionate	501.2	313.2	19
Fluticasone propionate-d ₅	506.2	313.2	19
Linezolid	338.1	296.2	25
Linezolid-d ₃	341.1	297.2	25
Indomethacin	358.4	139.1	18
Indomethacin-d ₄	362.4	143.1	20

Multiple quality controls were carried out to assess the method robustness. Separate calibrations were performed for the investigated drugs and their respective internal standards. The concentrations used for calibration ranged from 1 to 15000 nM for SAL (several calibration batches), and 10 to 20000 nM for FP, LIN and IND. All measured samples fell within the calibration range. Quality controls were performed at 20, 200, and 10000 nM for SAL, and at 20, 200, and 15000 nM for the other drugs.

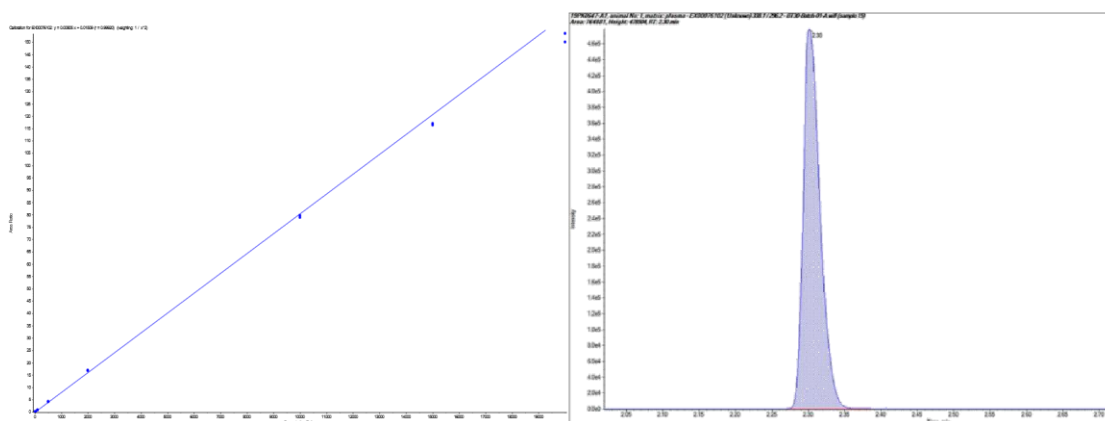


Figure S4. Calibration curve for LIN (left) and LC-MS chromatogram of an exemplary plasma sample (right).

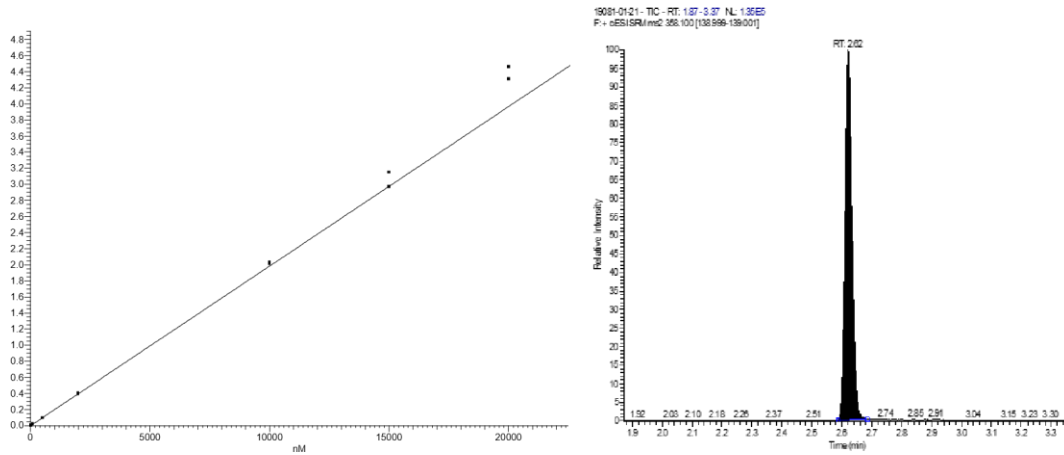


Figure S5. Calibration curve for IND (left) and LC-MS chromatogram of an exemplary plasma sample (right).

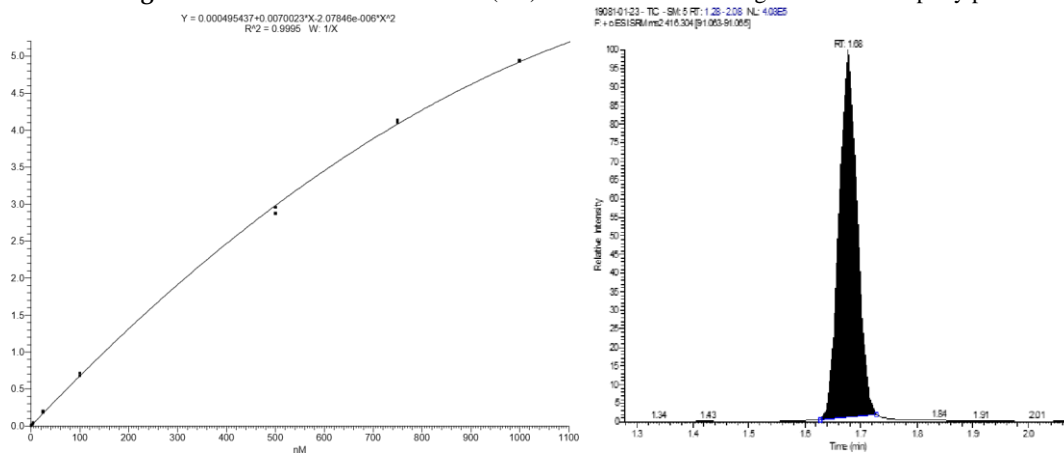


Figure S6. Calibration curve for SAL (left) and LC-MS chromatogram of an exemplary plasma sample (right).

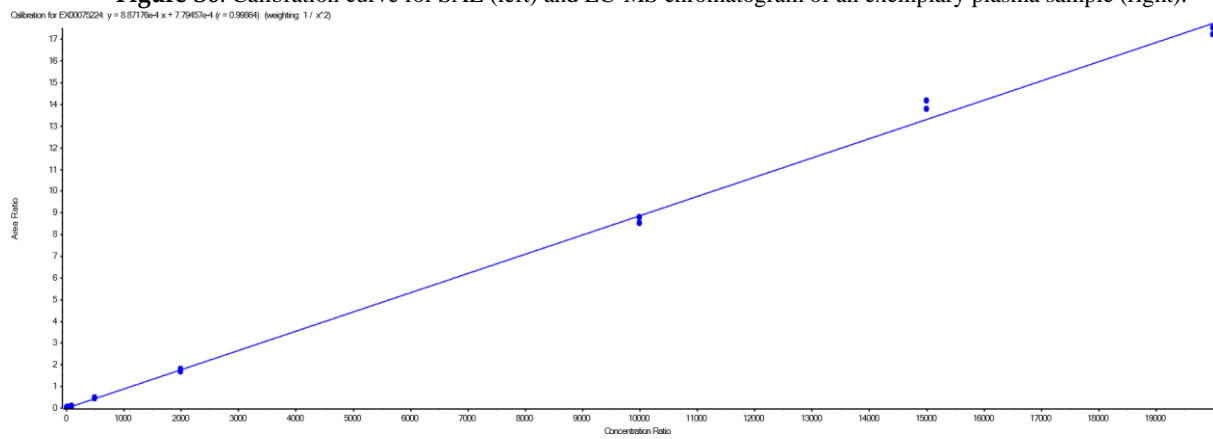


Figure S7. Calibration curve of FP.

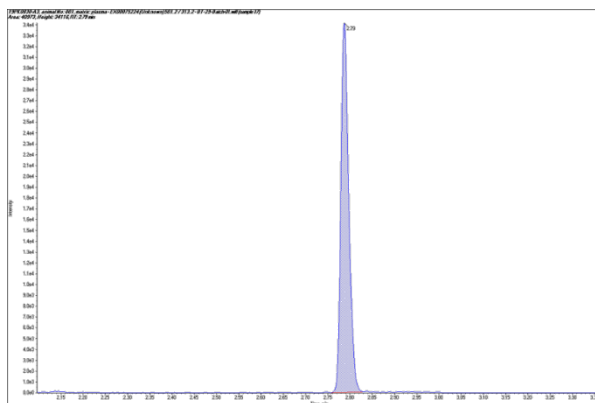


Figure S8. LC-MS chromatogram of an exemplary plasma sample containing FP.

6. Model code

```

test(){
  deriv(A1 = - C1 * C - C12 * (C - C2))
  deriv(A2 = C12 * (C - C2))

  deriv(Parenchyma = QP * (C - 1/KPP*CP))
  deriv(Bronchi   = QB * (C - 1/KPB*CB))
  deriv(Trachea   = QT * (C - 1/KPT*CT))

  dosepoint(A1)

  C = A1 / V
  C2 = A2 / V2

  Parenchyma_weight = 0.004 # kg parenchyme /kg bodyweight
  (assumption: 80% of total lung)
  Bronchi_weight   = 0.0008 # kg parenchyme /kg bodyweight
  (assumption: 20% of total lung - Trachea based on sample)
  Trachea_weight   = 0.0002 # Based on sample in the respective studies

  CP = Parenchyma / Parenchyma_weight # concentration in the alveolar parenchyma
  CB = Bronchi / Bronchi_weight # concentration in the bronchi
  CT = Trachea / Trachea_weight # concentration in the trachea

```



```

error(CEps = 0.1)          # residual variability plasma
error(CEps_t = 0.1)       # residual variability tissue

observe(CObs = C * (1 + CEps))

## Error model
observe(CObs_P = CP * (1 + CEps_t))
observe(CObs_B = CB * (1 + CEps_t))
observe(CObs_T = CT * (1 + CEps_t))

## Define covariate -> Compound; 1=FP, 2=Linezolid, 3=Indomethacin, 4=Salmeterol
fcovariate(CPD())

## Define systemic PK parameters
stparm(V      = tvVfp*(CPD==1)  + tvVlin*(CPD==2)  + tvVind*(CPD==3)  +
tvVsal*(CPD==4))
stparm(V2     = tvV2fp*(CPD==1) + tvV2lin*(CPD==2) + tvV2ind*(CPD==3) +
tvV2sal*(CPD==4))
stparm(Cl     = tvClfp*(CPD==1) + tvClin*(CPD==2) + tvClind*(CPD==3) +
tvClsal*(CPD==4))
stparm(Cl2    = tvCl2fp*(CPD==1) + tvCl2lin*(CPD==2) + tvCl2ind*(CPD==3) +
tvCl2sal*(CPD==4))

## Define the lung partition coefficients
stparm(KPP    = tvKPPfp*(CPD==1) + tvKPPlin*(CPD==2) + tvKPPind*(CPD==3) +
tvKPPsal*(CPD==4)) # Kp of the alveolar parenchyma
stparm(KPB    = tvKPBfp*(CPD==1) + tvKPBlin*(CPD==2) + tvKPBind*(CPD==3) +
tvKPBsal*(CPD==4)) # Kp of the bronchi
stparm(KPT    = tvKPTfp*(CPD==1) + tvKPTlin*(CPD==2) + tvKPTind*(CPD==3) +
tvKPTsal*(CPD==4)) # Kp of the trachea

## Define the perfusion rates
stparm(QP     = tvQP * (Ff_fp*(CPD==1) + Ff_lin*(CPD==2) + Ff_ind*(CPD==3) +
Ff_sal*(CPD==4))) # alveolar blood flow

```

```
stparm(QB = tvQB * (Ff_fp*(CPD==1) + Ff_lin*(CPD==2) + Ff_ind*(CPD==3) +  
Ff_sal*(CPD==4))) # bronchial blood flow
```

```
stparm(QT = tvQT * (Ff_fp*(CPD==1) + Ff_lin*(CPD==2) + Ff_ind*(CPD==3) +  
Ff_sal*(CPD==4))) # tracheal blood flow
```

```
fixef(tvQP = c(0, 21, ))
```

```
fixef(tvQB = c(0, 2, ))
```

```
fixef(tvQT = c(0, 0.5, ))
```

```
## Initial compound-specific values
```

```
# fluticasone propionate
```

```
Ff_fp = 0.0153 # fraction unbound in plasma
```

```
fixef(tvKPPfp = c(0, 6, ))
```

```
fixef(tvKPBfp = c(0, 6, ))
```

```
fixef(tvKPTfp = c(0, 6, ))
```

```
fixef(tvVfp(freeze) = c(0, 0.223336, ))
```

```
fixef(tvV2fp(freeze) = c(0, 2.40999, ))
```

```
fixef(tvClfp(freeze) = c(0, 3.37369, ))
```

```
fixef(tvCl2fp(freeze) = c(0, 4.71991, ))
```

```
# linezolid
```

```
Ff_lin = 0.732 # fraction unbound in plasma
```

```
fixef(tvKPPlin = c(0, 0.9, ))
```

```
fixef(tvKPBlin = c(0, 0.6, ))
```

```
fixef(tvKPTlin = c(0, 0.5, ))
```

```
fixef(tvVlin(freeze) = c(0, 0.32044, ))
```

```
fixef(tvV2lin(freeze) = c(0, 0.627917, ))
```

```
fixef(tvCllin(freeze) = c(0, 0.279411, ))
```

```
fixef(tvCl2lin(freeze) = c(0, 2.79208, ))
```

```

# indomethacin
Ff_ind = 0.024 # fraction unbound in plasma
fixef(tvKPPind = c(0, 0.3, ))
fixef(tvKPBind = c(0, 0.3, ))
fixef(tvKPTind = c(0, 0.3, ))

fixef(tvVind(freeze) = c(0, 0.153778, ))
fixef(tvV2ind(freeze) = c(0, 1, ))
fixef(tvClind(freeze) = c(0, 0.0691472, ))
fixef(tvCl2ind(freeze) = c(, 0, ))

# salmeterol
Ff_sal = 0.0139 # fraction unbound in plasma
fixef(tvKPPsal = c(0, 45, ))
fixef(tvKPBsal = c(0, 20, ))
fixef(tvKPTsal = c(0, 7, ))

fixef(tvVsal(freeze) = c(0, 0.12328, ))
fixef(tvV2sal(freeze) = c(0, 3.76907, ))
fixef(tvClsal(freeze) = c(0, 3.86488, ))
fixef(tvCl2sal(freeze) = c(0, 3.24267, ))
}

```

7. Calculation of total lung concentrations

Total lung concentrations were calculated based on the concentrations in the individual tissue samples of the upper bronchial tree, the alveolar parenchyma and the remaining lung tissue (see Materials and Methods, 2.4). The concentrations were converted to amounts using the respective sample weights (see Table S4). The total amount in all samples was then divided by the sum of all sample weights. These concentrations were then used for the estimation of PK model parameters. The resulting model predictions can be seen in Figure S9.

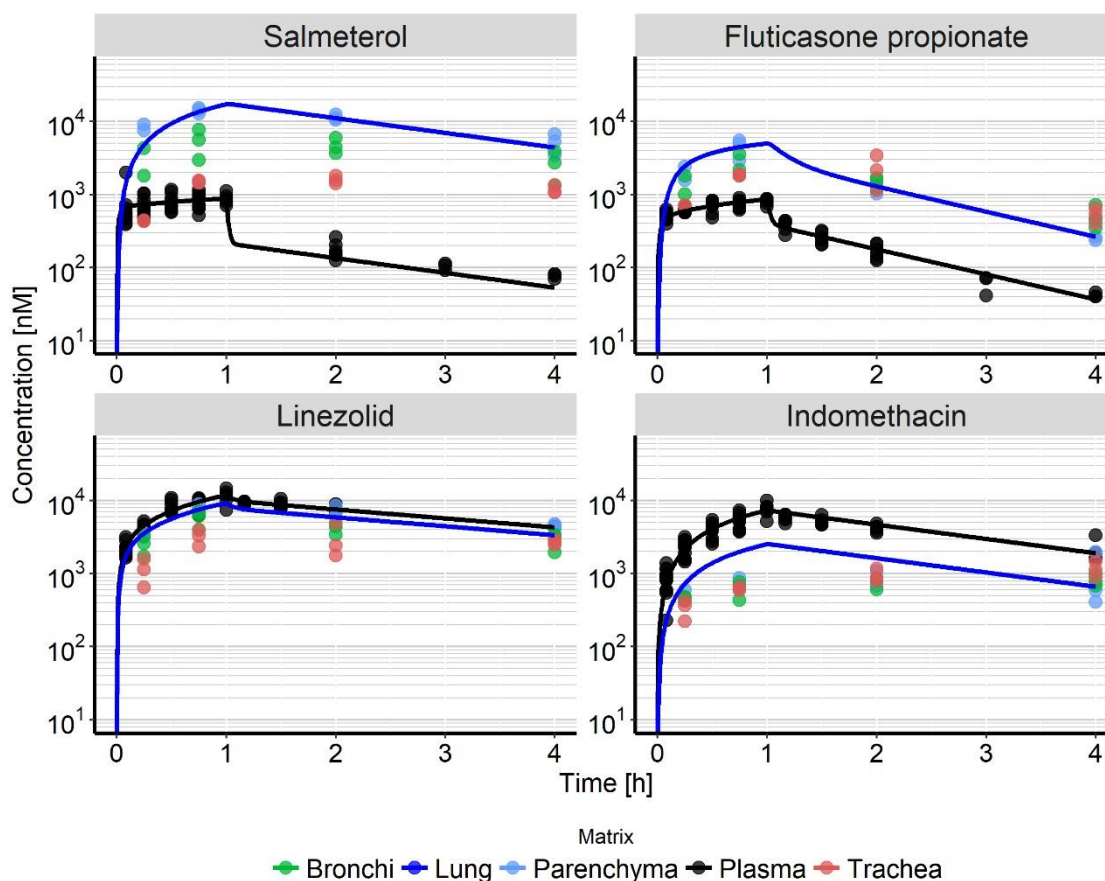


Figure S9. Concentration-time profiles predicted for plasma (black) and total lung in comparison to the observed concentrations in the separate lung tissues.

References:

1. Inagi, T.; MURAMATSU, T.; NAGAI, H.; TERADA, H. Mechanism of indomethacin partition between n-octanol and water. *Chemical and Pharmaceutical Bulletin* **1981**, *29*, 2330-2337.
2. Taylor, R.; Sunderland, B.; Luna, G.; Czarniak, P. Evaluation of the stability of linezolid in aqueous solution and commonly used intravenous fluids. *Drug design, development and therapy* **2017**, *11*, 2087.
3. Chiang, P.-C.; Hu, Y. Simultaneous determination of $\log d$, $\log p$, and $p_k a$ of drugs by using a reverse phase hplc coupled with a 96-well plate auto injector. *Combinatorial chemistry & high throughput screening* **2009**, *12*, 250-257.
4. Budavari, S.; O'Neil, M.J.; Smith, A.; Heckelman, P.E. *The merck index*. Merck Rahway, NJ: 1989; Vol. 11.
5. Cui, Y.; Lotz, R.; Rapp, H.; Klinder, K.; Himstedt, A.; Sauer, A. Muscle to brain partitioning as measure of transporter-mediated efflux at the rat blood–brain barrier and its implementation into compound optimization in drug discovery. *Pharmaceutics* **2019**, *11*, 595.

6.3 Supplementary material publication II

1. Animal experiments

The rats were anesthetized via whole body exposure to anaesthetic gas (2%–5% Isoflurane, 2.5 L/min Oxygen). Following anaesthetization, rats were intubated, placed in supine position on a heated device (39 °C), and the spontaneously breathing rats were connected to an anaesthetic gas supply (1.5%–2.5% Isoflurane, 2–2.5 L/min oxygen). Thereafter, a subcutaneous bolus of metamizole (100 mg/kg) was administered to the rats. The carotid artery and the jugular vein were prepared unilaterally, and catheters were placed after a body temperature of at least 36.5 °C was reached. The jugular catheter was used for infusing a cassette of ciprofloxacin, rifampicin, meropenem, and tigecycline over one hour (up to 5 mg/kg for each drug, infusion rate 5 mL/h/kg) using a standard infusion pump. The carotid catheter was used for blood pressure monitoring to adjust anaesthesia by changing isoflurane concentration as well as for collection of blood samples (volume 100 µL), which were collected in EDTA-tubes at the assigned time points. Plasma samples were prepared and subsequently stored at –20 °C. At the end of the in-life part, rats were exsanguinated, and lung tissue and epithelial lining fluid (ELF) samples were taken at 0.25, 0.75, 1.5, and 4 h (N = 3 rats/time-point) after start of the infusion, resulting in 12 samples per tissue and drug. Plasma was sampled until the end of the respective experiment (see Table S1).

Table S1. Study design and sampling time points of the animal experiments.

Study	N	Dose (mg/kg/h)	Infusion		Sampling time points (min)	
			Duration (min)	Rate (mL/kg/h)	Tissue (min)	Plasma (min)
1A	3	5	15	5	15	5, 15
1B	3	5	45	5	45	", 30, 45
1C	3	5	60	5	90	", 60, 70, 90
1D	3	5	60	5	240	", 120, 180, 240

2. Sample preparation

The lungs including trachea and larynx were removed *en bloc* immediately after exsanguination, rinsed in saline, blotted dry, and weighed. As a first step, the left lobe was cut directly after the first bifurcation and lavaged twice with 2 mL of phosphate buffered saline (PBS) at room temperature. The BALF was collected and stored at –20 °C. A 30–60 mg piece of the accessory lobe (parenchyma) was collected. For preparation of the bronchial sample, the remaining lung was held in place with forceps and the parenchyma was squished and carefully

stripped from the bronchi up to the third airway generation (1). After being flushed three times with the same 0.5 mL PBS sample, the trachea including the larynx was cut just above the first airway bifurcation and transferred to a weighed vial. Lavage fluid was collected and stored at $-20\text{ }^{\circ}\text{C}$ for the determination of ELF concentrations. The collected tissue samples were weighed, transferred to 7 mL Precellys® tubes (Bertin Instruments, Montigny-le-Bretonneux, France), and four parts of acetonitrile/methanol (1:1) solution were added. A Precellys® homogenizer was used to homogenize the samples. After centrifugation, supernatants were stored at $-20\text{ }^{\circ}\text{C}$.

3. Bioanalysis

3.1 Sample Preparation

A 5 μL plasma, lavage fluid, or supernatant sample from tissue homogenates was added to precipitation plates containing H₂O:acetonitrile (ACN):MeOH and spiked with internal standard solution (0.5 mM). 5 μL of 10 mM NH₄-acetate (pH7) was added to tigecycline samples. 70 μL of 5 mM ascorbic acid in ACN:methanol (MeOH) was added for protein precipitation. Composition of reagents used can be found in Table S2. The samples were placed in the freezer for 15 minutes, followed by centrifugation at 4000 rpm for four minutes. 30 μL of the supernatant were transferred onto a measuring plate containing 150 μL of 0.1% formic acid for tigecycline, and 150 μL of 0.1% formic acid for all other drugs. The plates were again centrifuged at 4000 rpm for one minute, and 20 μL of the supernatant were injected into the LC system.

Table S2. Concentration and composition of reagents.

Solutions	Concentration/composition
H ₂ O:ACN:MeOH	25:37.5:37.5
5 mM ascorbic acid in MeOH/ACN	1:1
Formic acid	0.1%
0.1% formic acid in MeOH:ACN	1:1
10 mM NH ₄ -acetate, pH7	

3.2 LC-MS Analysis

HPLC was performed with the Agilent 1290 Infinity II LC system (Agilent, Santa Clara, CA, USA). The column used for analysing was a Triart, C18, 30x2 mm, 3 μm , (YMC Co. Ltd.,

Kyoto, Japan) at 40°C. Solvent A was consisting of 0.1% formic acid and solvent B of 0.1% formic acid in MeOH/ACN. The LC-gradient started at 10% solvent B and increased from 0.1 – 2.3 min to 95% solvent B at a flow rate of 400 µL/min. From 2.3 to 3.2 min, it was maintained at 95% solvent B. The column was conditioned for 0.5 min at 10% solvent B. The injection volume was 20 µL.

A SCIEX Triple Quad™ 6500+ (AB Sciex, Darmstadt, Germany) mass spectrometer was used for the analysis. The mass spectrometer was operated in positive mode. The following MRM transitions were recorded:

Table S3. Mass spectrometry parameters (MRM transitions).

Drug	Q1	Q3	CE
Ciprofloxacin	332.1	288.0	25
Ciprofloxacin-d8	340.1	296.0	25
Rifampicin	823.4	791.4	19
2H8-rifampicin	831.4	799.2	19
Meropenem	384.1	141.0	25
Meropenem-d6	390.1	147.0	21
Tigecycline	586.2	513.2	33
Tetracycline	445.2	410.0	17

Multiple quality controls were carried out to assess the method robustness. Separate calibrations were performed for the investigated drugs and their respective internal standards. The concentrations used for calibration ranged from 1 to 20000 nM. All measured samples fell within the calibration range. Quality controls were performed at 20, 200, and 2000 nM.

3.3 Determination of urea concentrations in plasma and epithelial lining fluid

Urea concentrations in serum and lavage fluid (trachea and alveolar) were measured by an enzymatic rate method. Urea was hydrolysed by urease in the presence of water to ammonia and carbon dioxide. In the presence of glutamate dehydrogenase, the ammonia combines with α -ketoglutarate to produce L-glutamate with the concomitant equimolar oxidation of NADH to NAD. The removal of NADH was measured spectrophotometrically at 340 nm.

The measurements were performed using a Konelab 60i from Thermo Fisher Scientific (Vantaa, Finland). The test kit was supplied by Thermo Electron Corporation OY (Vantaa,

Finland). The analyses and methodologies were performed following the Konelab Chemistry Information Manual 12A/2003 March 2003.

4. Overview and ordinary differential equations of the model for oral inhalation

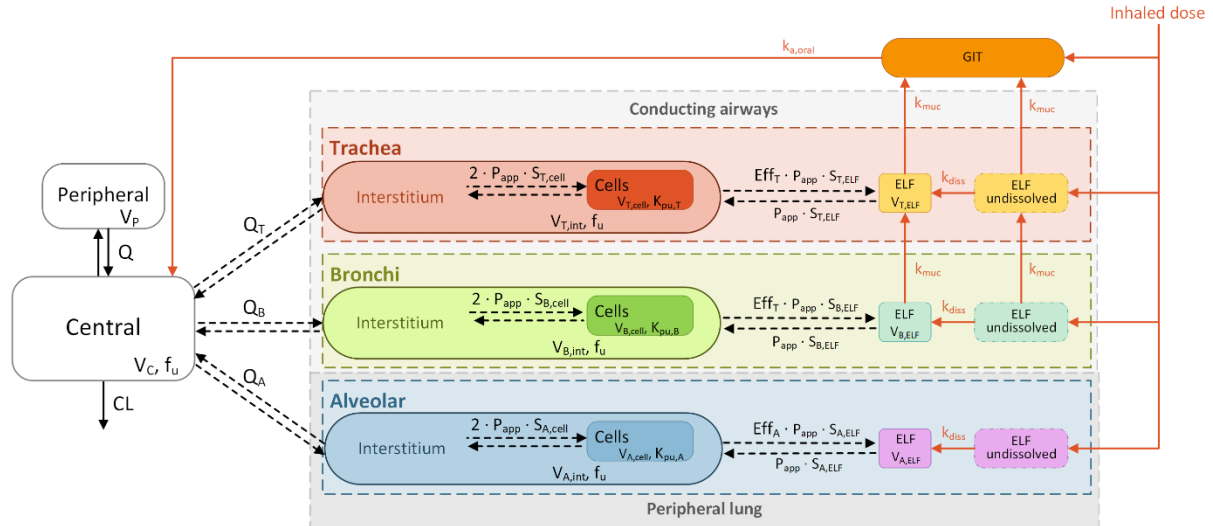


Figure S1. Structure of the pharmacokinetic model with added processes for the simulation of oral inhalation (orange arrows). Parameters of the pharmacokinetic model: CL : Systemic clearance, Q : intercompartmental clearance, $Q_{T/B/A}$: Perfusion rates of the trachea, bronchi, and alveolar region, respectively. V : Volume of distribution, f_u : fraction unbound, P_{app} : apparent permeability, S : Surface areas, Eff : Efflux ratio, K_{pu} : partition coefficients. Subscripts: C: Central compartment (CMT), P: Peripheral CMT, A: Alveolar, B: Bronchi, T: Trachea, Int: Interstitial, Cell: Cellular, ELF: Epithelial lining fluid. GIT: Gastrointestinal tract CMT, $k_{a,oral}$: first-order oral absorption rate constant, k_{muc} : first-order mucociliary clearance rate constant, k_{diss} : first-order dissolution rate constant.

Systemic compartments

$$dMT = -k_a \cdot MT + k_{muc} \cdot T_{undissolved} + k_{muc} \cdot T_{ELF} \quad \# \text{ Mouth-throat area and oral absorption}$$

$$dCentral = - (CL/V_C) \cdot Central - (Q/V_C) \cdot Central + (Q_1/V_{P1}) \cdot Peripheral1 + (Q_2/V_{P2}) \cdot Central + (Q_2/V_{P2}) \cdot Peripheral2 - (Q_T \cdot f_u / V_C) \cdot Central + (Q_T \cdot f_u / V_{T,int}) \cdot T_{int} - (Q_B \cdot f_u / V_C) \cdot Central + (Q_B \cdot f_u / V_{B,int}) \cdot B_{int} - (Q_A \cdot f_u / V_C) \cdot Central + (Q_A \cdot f_u / V_{A,int}) \cdot A_{int} + k_a \cdot MT$$

$$dPeripheral1 = (Q/V_C) \cdot Central - (Q_1/V_{P1}) \cdot Peripheral1$$

$$dPeripheral2 = (Q_2/V_C) \cdot Central - (Q_2/V_{P2}) \cdot Peripheral2$$

$$dInfs = 0 \quad \# \text{ Infusion rate dummy line}$$

$$dElim = (CL/V_C) \cdot Central$$

Trachea

$$dT_{undissolved} = -k_{diss} \cdot T_{undissolved} - k_{muc} \cdot T_{undissolved} + k_{muc} \cdot B_{undissolved}$$

$$dT_{ELF} = k_{diss} \cdot T_{undissolved} + k_{muc} \cdot B_{ELF} - k_{muc} \cdot T_{ELF} + f_u \cdot Eff_T \cdot P_{app} \cdot (SA_{T,ELF}/V_{T,int}) \cdot T_{int} - P_{app} \cdot (SA_{T,ELF}/V_{T,ELF}) \cdot T_{ELF}$$

$$\mathbf{dT}_{\text{int}} = (Q_T \cdot f_u/V_C) \cdot \text{Central} - (Q_T \cdot f_u/V_{T,\text{int}}) \cdot T_{\text{int}} - f_u \cdot 2 \cdot P_{\text{app}} \cdot (SA_{T,\text{cell}}/V_{T,\text{int}}) \cdot T_{\text{int}} + 2 \cdot P_{\text{app}} \cdot (SA_{T,\text{cell}}/V_{T,\text{cell}}) \cdot T_{\text{cell}}/K_{\text{pu},T} - f_u \cdot \text{Eff}_T \cdot P_{\text{app}} \cdot (SA_{T,\text{ELF}}/V_{T,\text{int}}) \cdot T_{\text{int}} + P_{\text{app}} \cdot (SA_{T,\text{ELF}}/V_{T,\text{ELF}}) \cdot T_{\text{ELF}}$$

$$\mathbf{dT}_{\text{cell}} = f_u \cdot 2 \cdot P_{\text{app}} \cdot (SA_{T,\text{cell}}/V_{T,\text{int}}) \cdot T_{\text{int}} - 2 \cdot P_{\text{app}} \cdot (SA_{T,\text{cell}}/V_{T,\text{cell}}) \cdot T_{\text{cell}}/K_{\text{pu},T}$$

Bronchi

$$\mathbf{dB}_{\text{undissolved}} = -k_{\text{diss}} \cdot B_{\text{undissolved}} - k_{\text{muc}} \cdot B_{\text{undissolved}}$$

$$\mathbf{dB}_{\text{ELF}} = k_{\text{diss}} \cdot B_{\text{undissolved}} - k_{\text{muc}} \cdot B_{\text{ELF}} + f_u \cdot \text{Eff}_T \cdot P_{\text{app}} \cdot (SA_{B,\text{ELF}}/V_{B,\text{int}}) \cdot B_{\text{int}} - P_{\text{app}} \cdot (SA_{B,\text{ELF}}/V_{B,\text{ELF}}) \cdot B_{\text{ELF}}$$

$$\mathbf{dB}_{\text{int}} = (Q_B \cdot f_u/V_C) \cdot \text{Central} - (Q_B \cdot f_u/V_{B,\text{int}}) \cdot B_{\text{int}} - f_u \cdot 2 \cdot P_{\text{app}} \cdot (SA_{B,\text{cell}}/V_{B,\text{int}}) \cdot B_{\text{int}} + 2 \cdot P_{\text{app}} \cdot (SA_{B,\text{cell}}/V_{B,\text{cell}}) \cdot B_{\text{cell}}/K_{\text{pu},B} - f_u \cdot \text{Eff}_T \cdot P_{\text{app}} \cdot (SA_{B,\text{ELF}}/V_{B,\text{int}}) \cdot B_{\text{int}} + P_{\text{app}} \cdot (SA_{B,\text{ELF}}/V_{B,\text{ELF}}) \cdot B_{\text{ELF}}$$

$$\mathbf{dB}_{\text{cell}} = f_u \cdot 2 \cdot P_{\text{app}} \cdot (SA_{B,\text{cell}}/V_{B,\text{int}}) \cdot B_{\text{int}} - 2 \cdot P_{\text{app}} \cdot (SA_{B,\text{cell}}/V_{B,\text{cell}}) \cdot B_{\text{cell}}/K_{\text{pu},B}$$

Alveolar region

$$\mathbf{dA}_{\text{undissolved}} = -k_{\text{diss}} \cdot A_{\text{undissolved}}$$

$$\mathbf{dA}_{\text{ELF}} = k_{\text{diss}} \cdot A_{\text{undissolved}} + f_u \cdot \text{Eff}_A \cdot P_{\text{app}} \cdot (SA_{A,\text{ELF}}/V_{A,\text{int}}) \cdot A_{\text{int}} - P_{\text{app}} \cdot (SA_{A,\text{ELF}}/V_{A,\text{ELF}}) \cdot A_{\text{ELF}}$$

$$\mathbf{dA}_{\text{int}} = (Q_A \cdot f_u/V_C) \cdot \text{Central} - (Q_A \cdot f_u/V_{A,\text{int}}) \cdot A_{\text{int}} - f_u \cdot 2 \cdot P_{\text{app}} \cdot (SA_{A,\text{cell}}/V_{A,\text{int}}) \cdot A_{\text{int}} + 2 \cdot P_{\text{app}} \cdot (SA_{A,\text{cell}}/V_{A,\text{cell}}) \cdot A_{\text{cell}}/K_{\text{pu},A} - f_u \cdot \text{Eff}_A \cdot P_{\text{app}} \cdot (SA_{A,\text{ELF}}/V_{A,\text{int}}) \cdot A_{\text{int}} + P_{\text{app}} \cdot (SA_{A,\text{ELF}}/V_{A,\text{ELF}}) \cdot A_{\text{ELF}}$$

$$\mathbf{dA}_{\text{cell}} = f_u \cdot 2 \cdot P_{\text{app}} \cdot (SA_{A,\text{cell}}/V_{A,\text{int}}) \cdot A_{\text{int}} - 2 \cdot P_{\text{app}} \cdot (SA_{A,\text{cell}}/V_{A,\text{cell}}) \cdot A_{\text{cell}}/K_{\text{pu},A}$$

Effect compartments (plasma and bronchi)

$$\mathbf{dEff}_P = k_{e0} \cdot \text{Central} \cdot f_u/V_C - k_{e0} \cdot \text{Eff}_P$$

$$\mathbf{dEff}_{B,\text{cell}} = k_{e0} \cdot (B_{\text{cell}}/K_{\text{pu},B}/V_{B,\text{cell}}) - k_{e0} \cdot \text{Eff}_{B,\text{cell}}$$

$$\mathbf{dEff}_{B,\text{ELF}} = k_{e0} \cdot B_{\text{ELF}}/V_{B,\text{ELF}} - k_{e0} \cdot \text{Eff}_{B,\text{ELF}}$$

Bacteria compartments (plasma and bronchi)

$$\mathbf{dP}_{\text{bac}} = k_{\text{growth}} \cdot P_{\text{bac}} \cdot (1 - P_{\text{bac}}/B_{\text{max}}) - (k_{\text{max}} \cdot \text{Eff}_P/(EC_{50} + \text{Eff}_P)) \cdot P_{\text{bac}}$$

$$\mathbf{dB}_{\text{bac},\text{cell}} = k_{\text{growth}} \cdot B_{\text{bac},\text{cell}} \cdot (1 - B_{\text{bac},\text{cell}}/B_{\text{max}}) - (k_{\text{max}} \cdot \text{Eff}_{B,\text{cell}}/(EC_{50} + \text{Eff}_{B,\text{cell}})) \cdot B_{\text{bac},\text{cell}}$$

$$\mathbf{dB}_{\text{bac},\text{ELF}} = k_{\text{growth}} \cdot B_{\text{bac},\text{ELF}} \cdot (1 - B_{\text{bac},\text{ELF}}/B_{\text{max}}) - (k_{\text{max}} \cdot \text{Eff}_{B,\text{ELF}}/(EC_{50} + \text{Eff}_{B,\text{ELF}})) \cdot B_{\text{bac},\text{ELF}}$$

5. Atypical plasma protein binding of tigecycline

Based on reported protein-binding measurements^{2,3} (see Figure S2), the concentration-dependent unbound fraction was calculated as follows,

$$\%f_u = b \cdot C_{total}^{-a} \quad (1)$$

with $a = 0.25$, $b = 100$, and C_{total} as the total concentration (mg/L) in a given compartment. To prevent unreasonably high f_u at low concentrations, in case of concentrations below 2 nM, a f_u of 100% was fixed.

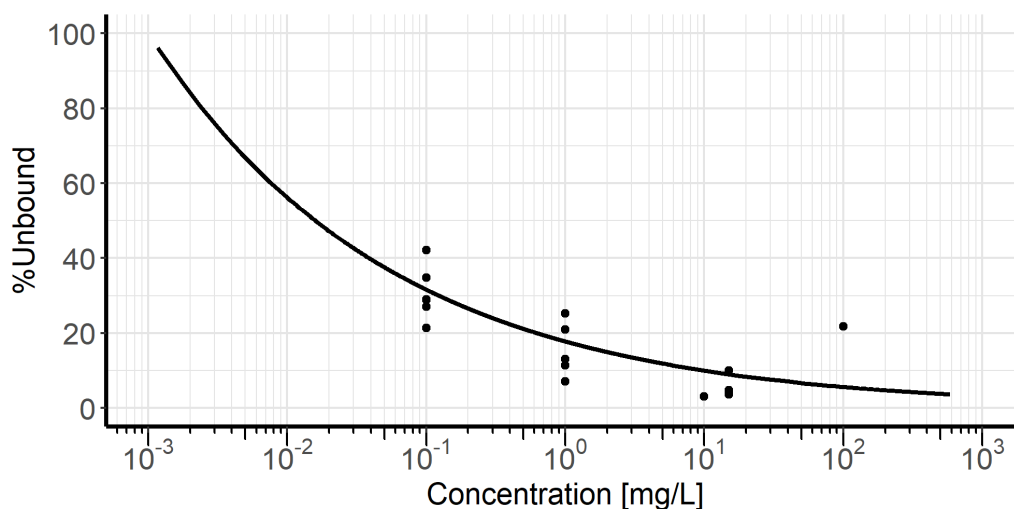


Figure S2. Observed fraction unbound of tigecycline in plasma (circles) and model prediction (line).

Even though the observed PK data was better described when the atypical binding was considered (compare Figures S3 and S4), the concentration range where it has been reliably measured is limited. After translation to humans, the PBPK model with the fixed fraction was also able to describe tigecycline concentrations in plasma and pulmonary biopsy samples⁴⁰ reasonably well without further adjustment of parameters (see Figure S6). Therefore, the simpler model was deemed sufficient for the sensitivity analysis.

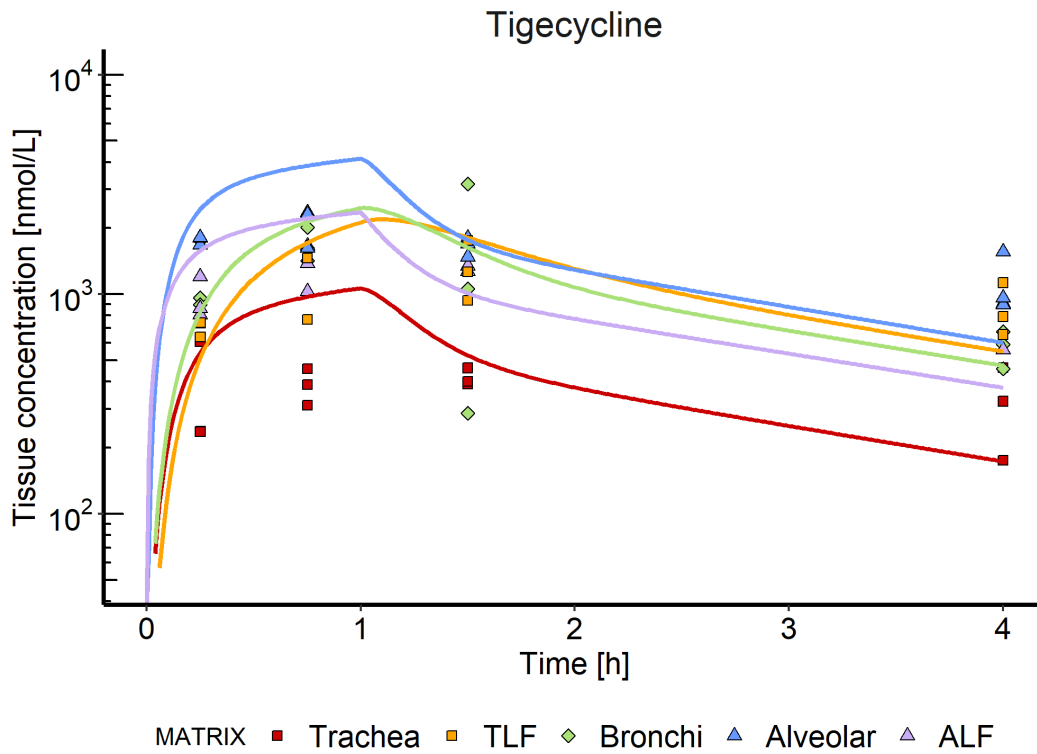


Figure S3. Predicted and observed tigecycline concentrations in homogenized pulmonary tissues and epithelial lining fluids, assuming atypical plasma protein binding. TLF: tracheal lining fluid, ALF: Alveolar lining fluid.

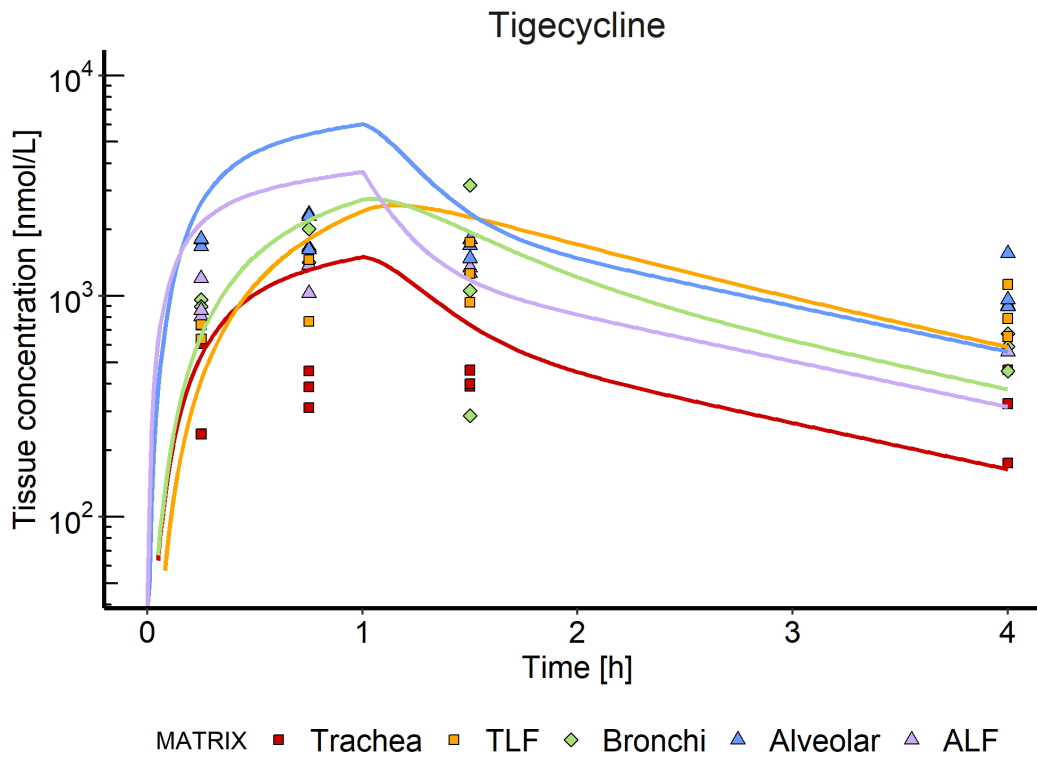


Figure S4. Predicted and observed tigecycline concentrations in homogenized pulmonary tissues and epithelial lining fluids, assuming a fixed fraction unbound of 20%. TLF: tracheal lining fluid, ALF: Alveolar lining fluid.

6. Additional figures

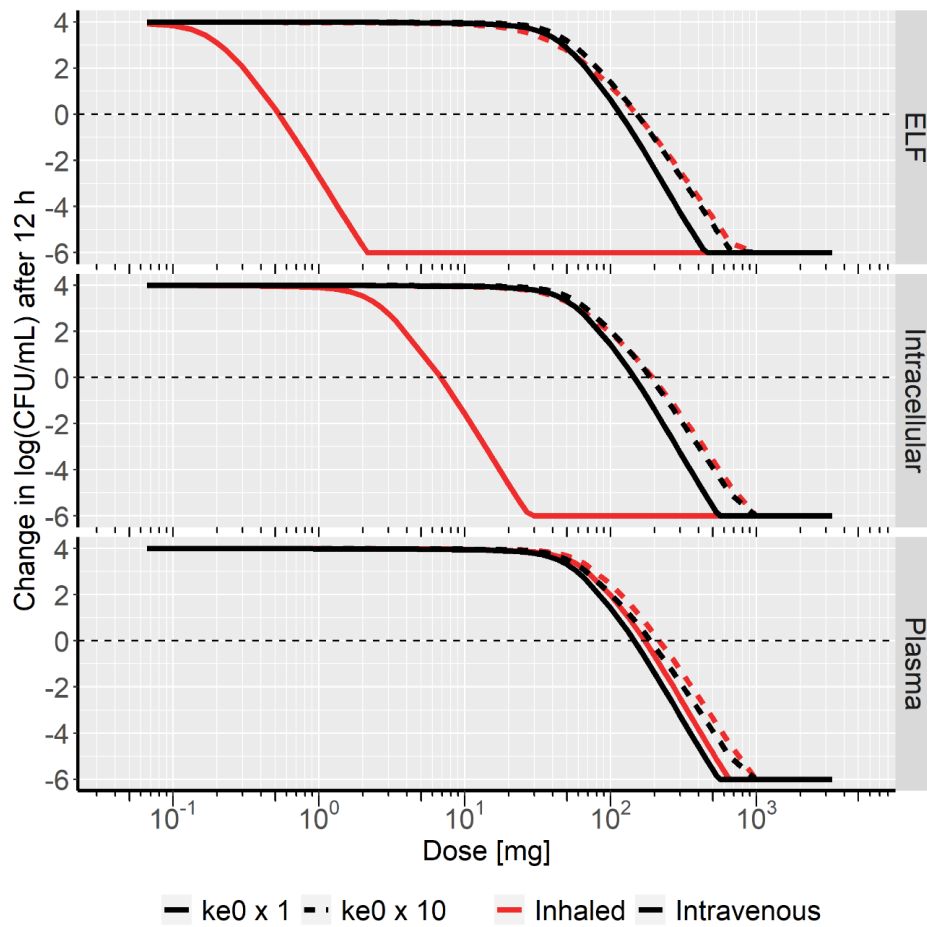


Figure S5. Dose-response curves for ciprofloxacin with unchanged (solid lines) and increased k_{e0} (ten-fold higher, dashed lines).

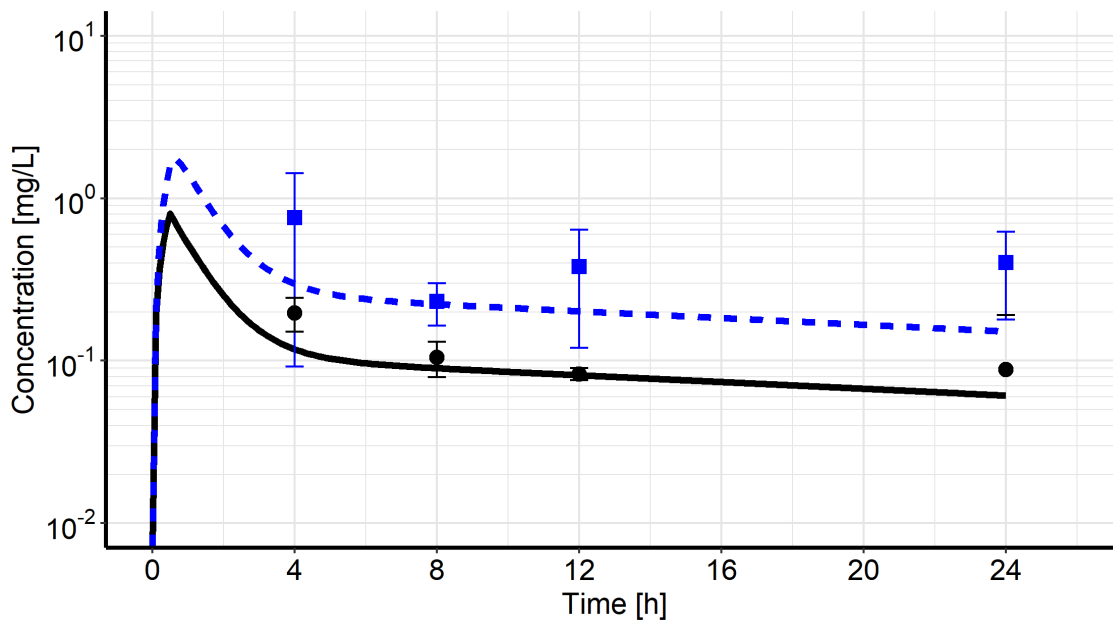


Figure S6. Tigecycline concentrations in humans after intravenous infusion. Observed concentrations were taken from Rovold et al. (2). Blue rectangles: Observed pulmonary concentrations (mean) from lung biopsies, black circles: observed serum concentrations. Error bars represent the standard deviation. Dashed blue line: predicted alveolar concentrations (total tissue), black line: predicted plasma concentrations.

7. Comparison of cellular and whole tissue partition coefficients

Table S4. Comparison of cellular and whole tissue unbound partition coefficients (K_{pu}).

Parameter	Drug-specific parameters								
	Unit	Ciprofloxacin		Rifampicin		Tigecycline		Tigecycline Salmeterol PK	
		Cellular	Tissue*	Cellular	Tissue*	Cellular	Tissue*	Cellular	Tissue*
$K_{pu,Trachea}$	-	4.22	3.60	14.0	12.0	2.73	2.33	362	309
$K_{pu,Bronchi}$	-	3.69	3.16	32.5	27.8	8.23	7.04	1030	881
$K_{pu,Alveolar}$	-	5.70	3.00	51.9	27.3	19.2	10.1	2180	1150

* The K_{pu} of the respective tissues is calculated as follows $K_{pu,tissue} = K_{pu,cellular} * \frac{V_{cell}}{V_{tissue}}$

8. References

1. Himstedt A, Braun C, Wicha SG, Borghardt JM. 2020. Towards a Quantitative Mechanistic Understanding of Localized Pulmonary Tissue Retention—A Combined In Vivo/In Silico Approach Based on Four Model Drugs. *Pharm* 12:408.
2. Mukker JK, Singh RP, Derendorf H. Determination of Atypical Nonlinear Plasma–Protein-Binding Behavior of Tigecycline Using an In Vitro Microdialysis Technique. *J Pharm Sci* 2014; 103: 1013–9.
3. Muralidharan G, Micalizzi M, Speth J et al. Pharmacokinetics of Tigecycline after Single and Multiple Doses in Healthy Subjects. *Antimicrob Agents Ch* 2005; 49: 220–9.
4. Rodvold KA, Gotfried MH, Cwik M, Korth-Bradley JM, Dukart G, Ellis-Grosse EJ. 2006. Serum, tissue and body fluid concentrations of tigecycline after a single 100 mg dose. *J Antimicrob Chemoth* 58:1221–1229.

6.4 Supplementary material publication III

S1. Abbreviations

Table S1. Abbreviations of PK parameters.

CL	Systemic clearance
V _n	Volume of distribution of the n th compartment
Q _n	Intercompartmental clearance to the n th compartment
F _{pul}	Pulmonary bioavailability/Lung deposited dose (Model NaL)
PF1	First proportionality factor
PF2	Second proportionality factor
K _{slow}	Slow pulmonary absorption rate constant
K _{med}	Intermediate pulmonary absorption rate constant
K _{fast}	Fast pulmonary absorption rate constant
K _{NaL}	Non-absorptive loss rate constant
K _{Transit}	Transit rate constant
IIV	Interindividual variability
Prop _{iv}	Proportional residual variability after intravenous administration
Prop _{inh}	Proportional residual variability after inhalation
PPP	Sequential estimation of systemic and absorption PK parameters (based on intravenous PK and inhalation PK, respectively), estimation of absorption parameters on top of the fixed systemic typical population parameters (thetas) and their variance (omega matrix)
IPP	Sequential estimation of systemic and absorption PK parameters (based on intravenous PK and inhalation PK, respectively), estimation of absorption parameters on top of the fixed individual PK parameters (empiric Bayesian estimates, thetas + etas)
ALL	Simultaneous estimation of systemic and absorption PK parameters on a combined dataset of intravenous and inhalation PK data

S2. Model Parameterization

Parameterization of the fractions of the dose absorbed with a slow, intermediate and fast rate constant ($F_{slow/med/fast}$):

$$F_{slow} = nDose \cdot PF1 \cdot F_{Pul} \quad (S1)$$

$$F_{med} = nDose \cdot PF2 \cdot (1 - PF1) \cdot F_{Pul} \quad (S2)$$

$$F_{fast} = nDose \cdot (1 - PF2 \cdot (1 - PF1) - PF1) \cdot F_{Pul} \quad (S3)$$

With $nDose$ being the nominal dose, F_{Pul} being the pulmonary bioavailability, and $PF1$ and 2 as the proportionality factors (Parameterization from Borghardt et al. (1)).

S2.1. Ordinary differential equations

Model_IIIa (Olodaterol, Borghardt et al. (1))

$$\begin{aligned} dCentral &= - (CL/V1 \cdot Central) + (Kfast \cdot Abs.fast) + (Kmed \cdot Abs.med) + (Kslow \cdot \\ &Abs.slow) - \\ &(Q2/V1 \cdot Central) + (Q2/V2 \cdot Peripheral.1) - (Q3/V1 \cdot Central) + (Q3/V3 \cdot \\ &Peripheral.2) - (Q4/V1 \cdot Central) + (Q4/V4 \cdot Peripheral.3) \end{aligned}$$

$$dPeripheral.1 = (Q2/V1 \cdot Central) - (Q2/V2 \cdot Peripheral.1)$$

$$dPeripheral.2 = (Q3/V1 \cdot Central) - (Q3/V3 \cdot Peripheral.2)$$

$$dPeripheral.3 = (Q4/V1 \cdot Central) - (Q4/V4 \cdot Peripheral.3)$$

$$dAbs.fast = - (Kfast \cdot Abs.fast)$$

$$dAbs.med = - (Kmed \cdot Abs.med)$$

$$dAbs.slow = - (Kslow \cdot Abs.slow)$$

$$dElim = (CL/V1 \cdot Central)$$

Model_II (AZD5423, Melin et al. (2))

$$\begin{aligned} dCentral &= -(CL/V1 \cdot Central) + (Kfast \cdot Abs.fast) + (Kslow \cdot Abs.slow) - (Q2/V1 \cdot \\ &Central) + (Q2/V2 \cdot Peripheral.1) - (Q3/V1 \cdot Central) + (Q3/V3 \cdot Peripheral.2) - \\ &(Q4/V1 \cdot Central) + (Q4/V4 \cdot Peripheral.3) \end{aligned}$$

$$dPeripheral.1 = (Q2/V1 \cdot Central) - (Q2/V2 \cdot Peripheral.1)$$

$$dPeripheral.2 = (Q3/V1 \cdot Central) - (Q3/V3 \cdot Peripheral.2)$$

$$dPeripheral.3 = (Q4/V1 \cdot Central) - (Q4/V4 \cdot Peripheral.3)$$

$$dAbs.fast = - (Kfast \cdot Abs.fast)$$

$$dAbs.slow = - (Kslow \cdot Abs.slow)$$

$$dElim = (CL/V1 \cdot Central)$$

Model_I (Fluticasone propionate, Krishnaswami et al. (3))

$$\begin{aligned} dCentral &= -(CL/V1 \cdot Central) + (Kmed \cdot Abs.med) - (Q2/V1 \cdot Central) + (Q2/V2 \cdot \\ &\quad Peripheral.1) - \\ &\quad (Q3/V1 \cdot Central) + (Q3/V3 \cdot Peripheral.2) - (Q4/V1 \cdot Central) + (Q4/V4 \cdot \\ &\quad Peripheral.3) \end{aligned}$$

$$dPeripheral.1 = (Q2/V1 \cdot Central) - (Q2/V2 \cdot Peripheral.1)$$

$$dPeripheral.2 = (Q3/V1 \cdot Central) - (Q3/V3 \cdot Peripheral.2)$$

$$dPeripheral.3 = (Q4/V1 \cdot Central) - (Q4/V4 \cdot Peripheral.3)$$

$$dAbs.med = - (Kmed \cdot Abs.med)$$

$$dElim = (CL/V1 \cdot Central)$$

Model_NaL (inhaled insulin, Sakagami et al. (4))

$$\begin{aligned} dCentral &= -(CL/V1 \cdot Central) + (Kmed \cdot Abs.med) - (Q2/V1 \cdot Central) + (Q2/V2 \cdot \\ &\quad Peripheral.1) - (Q3/V1 \cdot Central) + (Q3/V3 \cdot Peripheral.2) - (Q4/V1 \cdot Central) + \\ &\quad (Q4/V4 \cdot Peripheral.3) \end{aligned}$$

$$dPeripheral.1 = (Q2/V1 \cdot Central) - (Q2/V2 \cdot Peripheral.1)$$

$$dPeripheral.2 = (Q3/V1 \cdot Central) - (Q3/V3 \cdot Peripheral.2)$$

$$dPeripheral.3 = (Q4/V1 \cdot Central) - (Q4/V4 \cdot Peripheral.3)$$

$$dAbs.med = - (Kmed \cdot Abs.med) - (Knal \cdot Abs.med)$$

$$dElim = (CL/V1 \cdot Central) + (Knal \cdot Abs.med)$$

Model_Transit (PF-00610355, Diderichsen et al. (5))

$$\begin{aligned} d\text{Central} &= -(CL/V1 \cdot \text{Central}) + (K_{\text{med}} \cdot \text{Abs.med}) - (Q2/V1 \cdot \text{Central}) + (Q2/V2 \cdot \\ &\text{Peripheral.1}) - (Q3/V1 \cdot \text{Central}) + (Q3/V3 \cdot \text{Peripheral.2}) - (Q4/V1 \cdot \text{Central}) \\ &+ (Q4/V4 \cdot \text{Peripheral.3}) \end{aligned}$$

$$d\text{Peripheral.1} = (Q2/V1 \cdot \text{Central}) - (Q2/V2 \cdot \text{Peripheral.1})$$

$$d\text{Peripheral.2} = (Q3/V1 \cdot \text{Central}) - (Q3/V3 \cdot \text{Peripheral.2})$$

$$d\text{Peripheral.3} = (Q4/V1 \cdot \text{Central}) - (Q4/V4 \cdot \text{Peripheral.3})$$

$$d\text{Abs.fast} = - (K_{\text{transit}} \cdot \text{Abs.fast})$$

$$d\text{Abs.med} = (K_{\text{transit}} \cdot \text{Abs.fast}) - (K_{\text{med}} \cdot \text{Abs.med})$$

$$d\text{Elim} = (CL/V1 \cdot \text{Central})$$

For 'Model Transit', dosing was performed into the 'Abs.fast' compartment, with transition from 'Abs.fast' to 'Abs.med' representing the transit process rather than parallel absorption.

S2.2. Parameter values used for simulation

Table S2. Parameter values used for data simulation. For abbreviations, see Table S1.

Parameter	Unit	I	Transit	NaL	II	IIIa
CL	[L/h]	46.0	1.40	24.6	44.7	74.2*
V1	[L]	15.0	17.8	4.40	11.8	23.5
Q2	[L/h]	17.4	16.0	81.8	9.97	31.7
V2	[L]	245	221	11.4	707	2590
Q3	[L/h]	0	0	0	55.0	65.7
V3	[L]	1 [#]	1 [#]	1 [#]	40.4	473
Q4	[L/h]	0	0	0	12.5	22.5
V4	[L]	1 [#]	1 [#]	1 [#]	103	16.1
F _{pul}	%	10.0%	77.2%	10.0%	49.0%	49.5%
PF1		-	-	-	0.383	0.701
PF2		-	-	-	-	0.889
K _{slow}	[h ⁻¹]	-	-	-	1.18	0.0318
K _{med}	[h ⁻¹]	0.180	0.852	0.0230	-	0.347
K _{fast}	[h ⁻¹]	-	-	-	49.6	2.59
K _{NaL}	[h ⁻¹]	-	-	1.09	-	-
K _{Transit}	[h ⁻¹]	-	1.08	-	-	-
ADDITIONAL PARAMETERS FOR EVALUATION OF PERFORMANCE ON CLINICAL DATASETS						
Prop _{iv,plasma}	%CV	-	-	-	15.1	15.8
Prop _{iv,urine}	%CV	-	-	-	-	37.7
Prop _{inh,plasma}	%CV	-	-	-	15.5	15.8
Prop _{inh,urine}	%CV	-	-	-	-	37.7
IIV F _{Pul}	%CV	-	-	-	44.1	32.2 (IOV)
IIV CL	%CV	-	-	-	15.1	26.8 (CL _{NR})*
IIV V1	%CV	-	-	-	53.3	26.2
IIV Q2	%CV	-	-	-	18.9	25.7

* The original Model IIIa included two separate clearance values (renal and non-renal clearance, CL_R and CL_{NR}). The naïve-pooled analysis did not distinguish between these clearances; however, as interindividual variability (IIV) was put on the non-renal part, both clearances were implemented as separate processes in the population PK analysis. The respective values for CL_R and CL_{NR} were 10.5 and 63.7 L/h, respectively.

[#] For models with less than four systemic PK compartments originally (Models I, NaL, and Transit), Q values for the missing compartments (3 and 4) were set to 0 to remove drug transfer to these compartments while still allowing for automation of the simulation/re-estimation process. The corresponding Volumes of distribution were set to 1 to avoid division by 0.

Table S3. Initial base parameters used for estimation in the naïve-pooled analysis.

Parameter	Unit	I	Transit	NaL	II	IIIa
F _{pul}	%	50.0	50.0	50.0	50.0	50.0
PF1		-	-	-	0.500	0.500
PF2		-	-	-	-	0.500
K _{slow}	[h ⁻¹]	-	-	-	0.100	0.0100
K _{med}	[h ⁻¹]	0.100	0.100	0.100	-	0.100
K _{fast}	[h ⁻¹]	-	-	-	1.00	1.00
K _{NaL}	[h ⁻¹]	-	-	0.100	-	-
K _{Transit}	[h ⁻¹]	-	0.100	-	-	-

Initial parameters for parallel retries were varied randomly using the *rnorm* function in R (random sampling from a specified normal distribution) as follows, resulting in a lognormal distribution of parameters:

$$\text{Initial parameter} = \text{Initial base parameter} \cdot e^{\text{rnorm}(n=1, \text{mean}=0, \text{sd}=1)} \quad (\text{S4})$$

F_{Pul}, PF1 and PF2 were logit transformed beforehand to constrain the values between 0 and 1.

S2.3. Semi-mechanistic model

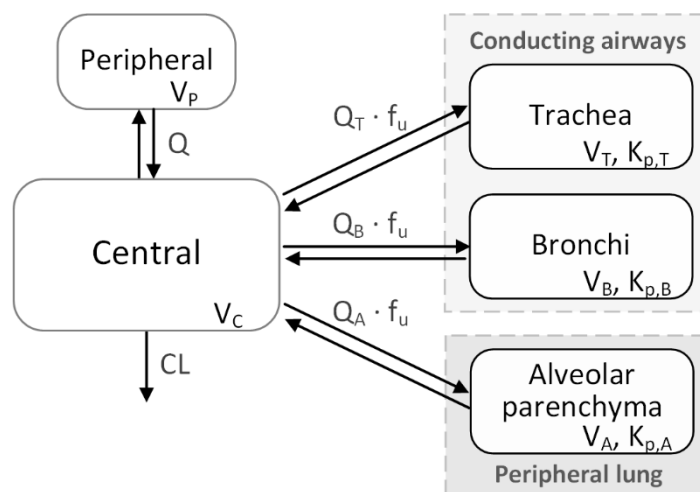


Figure S1. Structure of the semi-mechanistic model. CL : systemic clearance, V_C : central volume of distribution (V_d), Q : intercompartmental clearance, V_P : peripheral V_d ; Q_T , Q_B , and Q_A represent the blood flow to the trachea, bronchi and alveolar parenchyma, respectively. f_u : fraction unbound in plasma, V_T : weight of the trachea, V_B : weight of the bronchi, V_A : weight of the alveolar parenchyma. $K_{p,T}$, $K_{p,B}$, and $K_{p,A}$ denote the tissue-to-plasma partition coefficients for the respective tissues. Adapted from Himstedt et al. (6).

The semi-mechanistic model was adapted to oral inhalation. The assumed pulmonary availability was 50%, with 80% of the lung dose depositing in the peripheral lung (alveolar parenchyma). The remaining 20% were equally distributed between the trachea and bronchi.

Table S4. Parameters used for simulation with the semi-mechanistic model. Abbreviations: see the caption of Figure S1.

Parameter	Unit	Value
CL	L/h/kg	0.971
V_C	L/kg	0.123
Q	L/h/kg	0.815
V_P	L/kg	3.77
f_u		0.014
K_T		6.52
K_B		18.6
K_A		39.3
Q_T	L/h/kg	0.0227
V_T	L/kg	0.0002
Q_B	L/h/kg	0.326
V_B	L/kg	0.000800
Q_A	L/h/kg	4.45
V_A	L/kg	0.00400

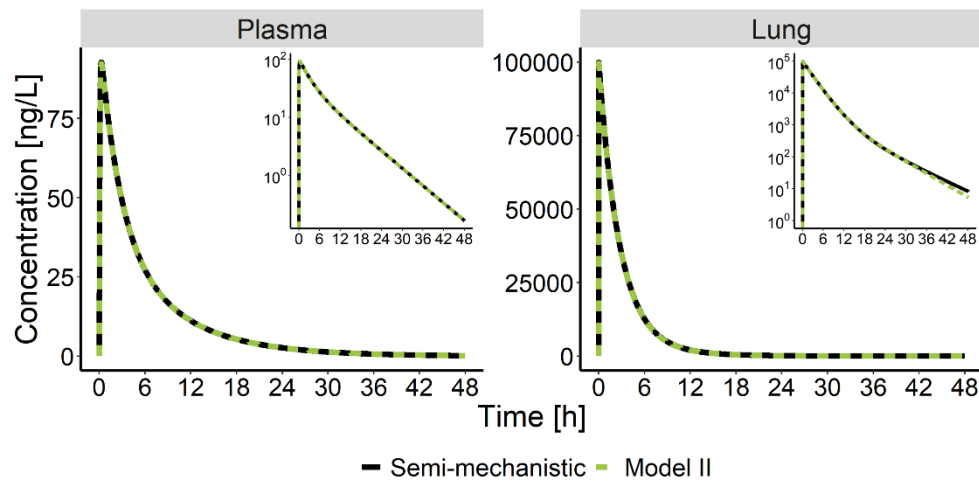


Figure S2. Plasma and lung concentration-time profiles. Simulation model: Semi-mechanistic lung distribution model (solid line). Estimation model: Model II (dashed line).

S3. Exemplary Figures: Scenarios 1 and 3

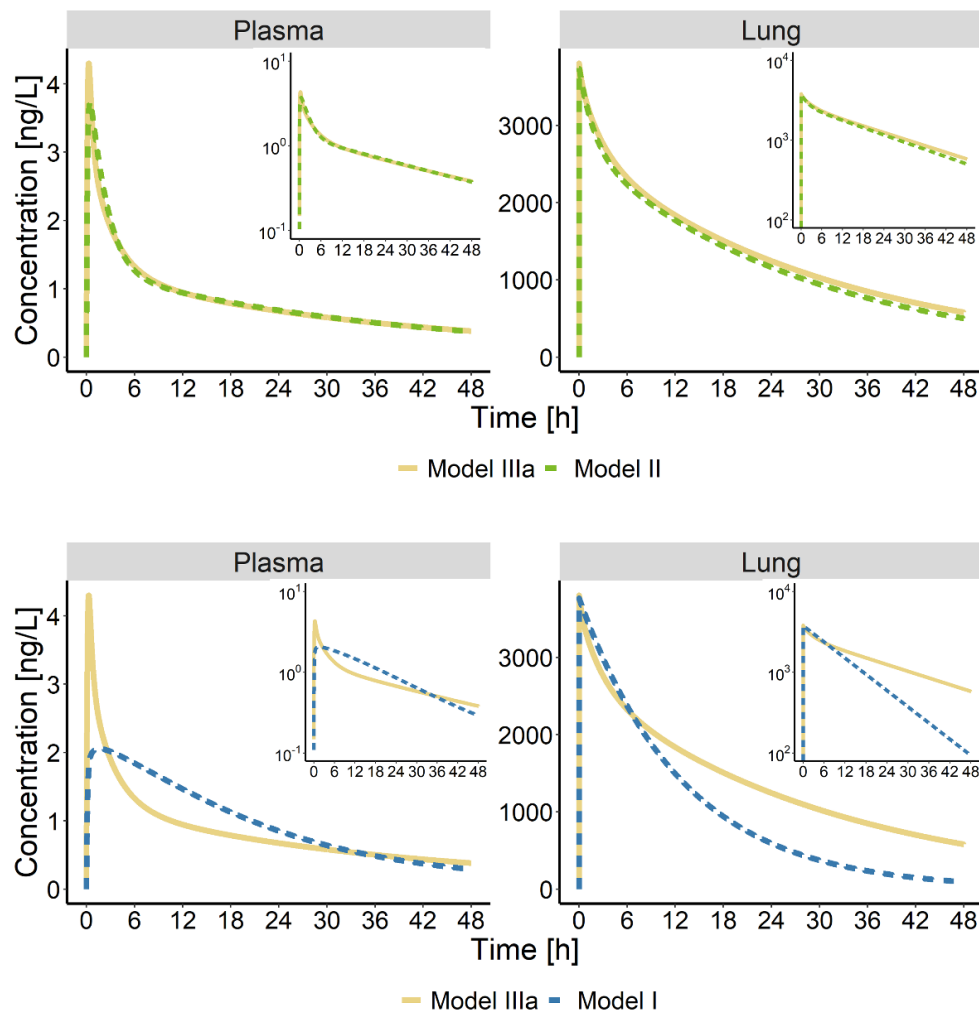


Figure S3. Exemplary plasma (left) and lung (right) concentration-time profiles for scenarios 1 (top) and 3 (bottom). Solid lines: Model used for simulation. Dashed lines: Predictions based on estimated model parameters and the respective model used for re-estimation.

S4. Non-compartmental analysis

The AUC_{0-last} in plasma, as well as the area under the first moment curve ($AUMC_{0-last}$), were calculated via the log-linear trapezoidal method after both intravenous administration and oral inhalation. Extrapolation of the AUC to infinity was performed by addition of the last observed concentration divided by the terminal slope of log-transformed concentration data (C_{last}/λ_z). λ_z was determined by linear regression over the last three observations. The $AUMC_{0-last}$ was extrapolated to infinity by addition of the term $((C_{last} \cdot t_{last})/\lambda_z + C_{last}/\lambda_z^2)$, t_{last} denoting the time of the last observed concentration. Pulmonary bioavailability (F_{Pul}) was calculated as shown in Eq. S5:

$$F_{Pul} = \frac{AUC_{inhaled}}{AUC_{i.v.}} \cdot \frac{Dose_{i.v.}}{Dose_{inhaled}} \quad (S5)$$

Inferring on pulmonary AUC ($AUC_{0-inf,Lung}$) was performed as follows: The $AUC_{0-inf,plasma}$ and $AUMC_{0-inf,plasma}$ were used to determine the mean residence time (MRT) for both administration routes:

$$MRT_{i.v.} = \frac{AUMC_{i.v.}}{AUC_{i.v.}} - \frac{T_{inf}}{2} \quad (S6)$$

$$MRT_{inhaled} = \frac{AUMC_{inhaled}}{AUC_{inhaled}} \quad (S7)$$

T_{inf} denotes the duration of the intravenous infusion.

The mean absorption time (MAT) was calculated by subtracting the mean residence time (MRT) after inhalation from the MRT after intravenous administration:

$$MAT = MRT_{inhaled} - MRT_{i.v.} \quad (S8)$$

The MAT was then used to infer on the pulmonary absorption rate constant k_a :

$$k_a = \frac{1}{MAT} \quad (S9)$$

To infer on the pulmonary AUC_{0-inf} , the equation for AUC calculation in plasma (Eq. S11) was adjusted to the lung, inserting F_{Pul} as the bioavailability (F) and the pulmonary absorption rate k_a as the elimination rate from the lung:

$$AUC_{0-Inf} = \frac{Dose \cdot F}{CL} \quad (S10)$$

$$AUC_{0-inf,Lung} = \frac{Dose_{inhaled} \cdot F_{Pul}}{k_a \cdot V_{Lung}} \quad (S11)$$

V_{Lung} was set to 0.840 L based on literature values for lung weight (7).

These analyses, performed in parallel to the population PK analyses, yielded ambivalent results for both scenarios. While the NCA performed on the dataset simulated with ‘Model IIIa’ resulted in plausible, yet biased values, the simulation with ‘Model II’ could not be analyzed with an NCA, as for some individuals the MRT after inhalation was shorter than after i.v. administration. In depth evaluation of the data indicated that this was due to biased $AUMC_{t_z-Inf}$ values, i.e., the extrapolated area of the AUMC was underestimated compared to the true area. In agreement, analysis of inhalation PK data from individuals with negative MAT values showed that the terminal slope λ_z was overestimated (i.e. a steeper terminal profile was assumed, Figure S4) compared to the true value. For this reason, and as this specific terminal part of the AUMC often constitutes a substantial part of the $AUMC_{0-Inf}$ (33), these individuals were characterized by an underestimated $AUMC_{inhaled}$. Combined with sometimes overestimated $AUMC_{0-inf,i.v.}$ values, this can explain the finding of negative MAT values. Thus, NCA for drugs with long terminal half-lives may necessitate even longer observation times or more accurate bioanalysis to adequately capture the terminal phase of the concentration-time profiles. This however might not always be feasible. Even for individuals with a positive MAT, the mean predicted $AUC_{0-inf,lung}$ was over tenfold higher than the true value. Furthermore, an NCA is only applicable if the same assumptions hold true as for the parallel absorption models, i.e. MCC and pulmonary metabolism being negligible (26). This leads to the conclusion that, the PK modeling approaches are more robust towards non-optimally designed sampling schemes, as well as providing more reliable estimates for the duration of pulmonary retention.

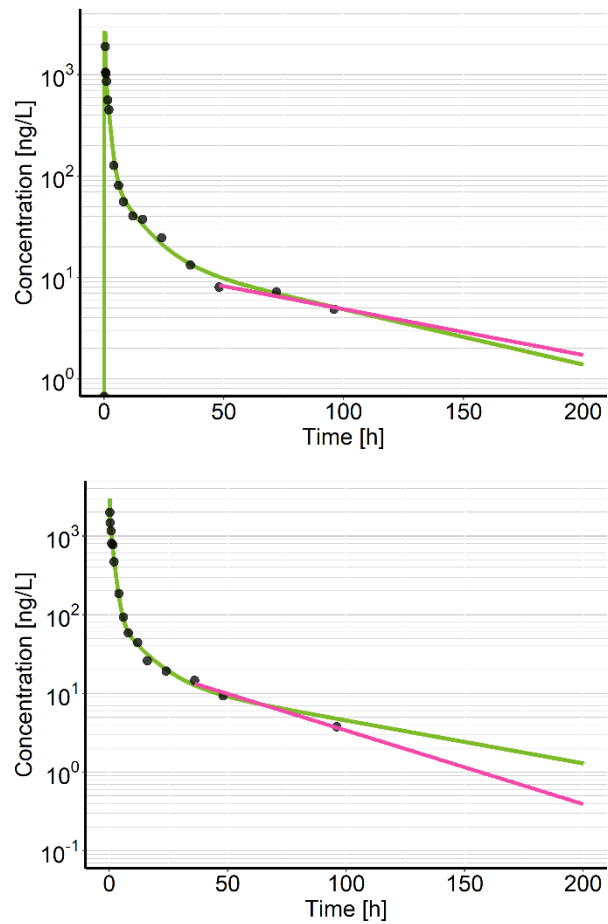


Figure S4. Deviation of true and calculated terminal slopes for an example individual after intravenous administration (left panel), and oral inhalation (right panel). Green line: true plasma concentration-time profile simulated with 'Model II'; Black dots: simulated "observed" data; Pink line: Extrapolation from the last three data points by linear regression. The combination of calculated slopes (too flat after intravenous dosing and too steep after inhalation) leads to negative MAT values for this individual, when calculated as described above.

S6. Comparison of parameter estimates between PPP, IPP, and ALL

Table S5. Median and 2.5th and 97.5th percentiles of PK parameters estimated the true model using three methods (PPP, IPP, and ALL). Simulation model: Model II/4CMT. For abbreviations, see Table S1

Parameter	Unit	Simulation	Estimation method		
			PPP	IPP	ALL
CL	[L/h]	44.7	44.7 [41.0, 48.7]	44.7 [41.1, 48.4]	44.8 [41.2, 48.7]
V1	[L]	11.8	11.7 [8.58, 16]	11.7 [8.74, 15.8]	11.6 [8.65, 15.8]
Q2	[L/h]	9.97	10.1 [8.77, 11.4]	10 [8.78, 11.4]	9.99 [8.9, 11.4]
V2	[L]	707	710 [575, 990]	706 [568, 999]	709 [614, 877]
Q3	[L/h]	55	55.4 [50.9, 61.1]	55.5 [50.9, 61.3]	55.3 [51.4, 60.1]
V3	[L]	40.4	40.5 [36.7, 44.3]	40.6 [36.7, 44.7]	40.4 [37.2, 44]
Q4	[L/h]	12.5	12.7 [11.4, 14.2]	12.7 [11.3, 14.1]	12.7 [11.8, 13.7]
V4	[L]	103	104 [85.8, 127]	104 [85.5, 126]	105 [90.8, 119]
Prop _{iv}	%CV	15.1	15.3 [14, 16.8]	15.3 [14, 16.7]	-
F _{pul}	%	49.0%	48.1% [41.5%, 56.3%]	48.9% [42.2%, 56.2%]	48.6% [42.3%, 55.9%]
PF1		0.383	0.399 [0.269, 0.536]	0.397 [0.301, 0.473]	0.405 [0.319, 0.484]
K _{slow}	[h ⁻¹]	1.18	1.18 [0.964, 1.47]	1.19 [0.975, 1.49]	1.19 [0.985, 1.47]
K _{fast}	[h ⁻¹]	49.6	63.3 [17.1, 98600]	45.4 [26.1, 207]	43.6 [24.6, 163]
Prop _{inh}	%CV	15.5	15.5 [13.8, 17.5]	15.5 [13.9, 17.1]	15.2 [13.9, 16.7]
IIV F _{Pul}	%CV	44.1	40.6 [18.8, 63.2]	40.9 [24.9, 57.7]	40.5 [25, 57.6]
IIV CL	%CV	15.1	13.9 [8.5, 19.6]	14.0 [8.7, 20.3]	13.9 [8.2, 19.6]
IIV V1	%CV	53.3	50.8 [29.3, 75.8]	50.6 [29.3, 74.1]	50.1 [29.6, 76.6]
IIV Q2	%CV	18.9	17.2 [7, 26.5]	17.7 [7.4, 26.8]	17.9 [9.2, 26.6]

1. Borghardt JM, Weber B, Staab A, Kunz C, Formella S, Kloft C. Investigating pulmonary and systemic pharmacokinetics of inhaled olodaterol in healthy volunteers using a population pharmacokinetic approach. *British Journal of Clinical Pharmacology*. 2016;81(3):538-52.
2. Melin J, Prothon S, Kloft C, Cleton A, Amilon C, Jorup C, et al. Pharmacokinetics of the Inhaled Selective Glucocorticoid Receptor Modulator AZD5423 Following Inhalation Using Different Devices. *AAPS Journal*. 2017;19(3):865-74.
3. Krishnaswami S, Hochhaus G, Möllmann H, Barth J, Derendorf H. Interpretation of absorption rate data for inhaled fluticasone propionate obtained in compartmental pharmacokinetic modeling. *International Journal of Clinical Pharmacology and Therapeutics*. 2005;43(3):117-22.
4. Sakagami M. Insulin disposition in the lung following oral inhalation in humans: A meta-analysis of its pharmacokinetics. *Clinical Pharmacokinetics*. 2004;43(8):539-52.
5. Diderichsen PM, Cox E, Martin SW, Cleton A, Ribbing J. Characterizing systemic exposure of inhaled drugs: application to the long-acting beta2-agonist PF-00610355. *Clin Pharmacokinet*. 2013;52(6):443-52.
6. Himstedt A, Braun C, Wicha SG, Borghardt JM. Towards a Quantitative Mechanistic Understanding of Localized Pulmonary Tissue Retention—A Combined In Vivo/In Silico Approach Based on Four Model Drugs. *Pharmaceutics*. 2020;12(5):408.
7. Molina DK, DiMaio VJM. Normal Organ Weights in Men: Part II—The Brain, Lungs, Liver, Spleen, and Kidneys. *The American Journal of Forensic Medicine and Pathology*. 2012;33(4).

Acknowledgements

First of all, I would like to express my gratitude to Prof. Sebastian Wicha, for the wonderful supervision and support during the last years. Despite the complications that come with supervising a PhD student working halfway across the country, as well as in a pandemic, you always made sure that there was enough time to be able to discuss and provide help along the way.

Special mention goes to Jens Borghardt, for the supervision from the industry perspective. Thank you for all the valuable input, great working environment, and of course for always pushing me to take on new challenges.

Another huge thanks goes to my direct colleagues from DDS, former and current, who not only supported my work with knowledge and data, and were available for fruitful discussions and proofreading, but also provided further insights into the industry. Special mention goes to Clemens Braun, Hermann Rapp, and Achim Sauer.

I also want to thank the entire working group in Hamburg for providing a great atmosphere to work in, and especially Astrid Bröker for letting me sleep on her couch during my sporadic stays up north.

Finally, I would like to thank my family and friends, who pulled me out of the world of pharmacy from time to time and for giving me whole-hearted support all the way.

Eidesstattliche Versicherung

Hiermit versichere ich an Eides statt, die vorliegende Dissertation selbst verfasst und keine anderen als die angegebenen Hilfsmittel benutzt zu haben. Die eingereichte schriftliche Fassung entspricht der auf dem elektronischen Speichermedium. Ich versichere, dass diese Dissertation nicht in einem früheren Promotionsverfahren eingereicht wurde.

Weyhe, den 13.11.2023

Anneke Himstedt